

UNIVERSITA' DEGLI STUDI DI PAVIA

FACOLTA' DI INGEGNERIA
DIPARTIMENTO DI INGEGNERIA INDUSTRIALE E DELL'INFORMAZIONE

DOTTORATO DI RICERCA IN BIOINGEGNERIA E BIOINFORMATICA
XXIX CICLO -2016

KERATIN-BASED 3D SCAFFOLD DESIGN FOR BONE TISSUE ENGINEERING

PhD Thesis by
ALESSIA PATRUCCO

Advisors:
Prof. Lorenzo Fassina
Prof. Claudio Tonin

PhD Program Chair:
Prof. Riccardo Bellazzi



UNIVERSITA' DEGLI STUDI DI PAVIA

FACOLTA' DI INGEGNERIA
DIPARTIMENTO DI INGEGNERIA INDUSTRIALE E DELL'INFORMAZIONE

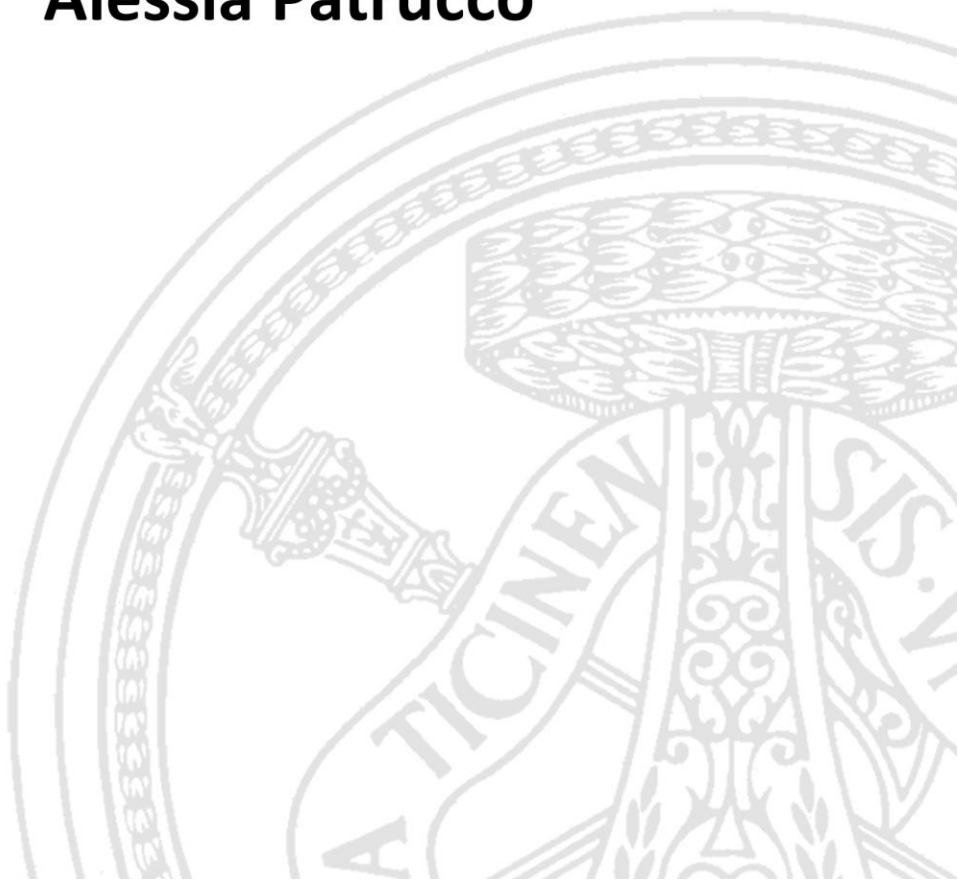
DOTTORATO DI RICERCA IN BIOINGEGNERIA E BIOINFORMATICA
XXIX CICLO - 2016

KERATIN-BASED 3D SCAFFOLD DESIGN FOR BONE TISSUE ENGINEERING

PhD Thesis by
Alessia Patrucco

Advisors:
Prof. Lorenzo Fassina
Prof. Claudio Tonin

PhD Program Chair:
Prof. Riccardo Bellazzi



A mio figlio Lorenzo,
meraviglia del mio mondo.

Lo studio e la ricerca della verità e della
bellezza rappresentano una sfera di
attività in cui è permesso di rimanere
bambini per tutta la vita.

A. Einstein

Acknowledgments

I owe much gratitude to my supervisor Prof. Fassina who gave me the important opportunity to do this wonderful PhD project and for his precious advices.

Thank you to Prof. Visai for her valuable help during the PhD experiments. I would like to express my special thanks of gratitude to my supervisor Prof. Tonin, a font of knowledge and patience, who teaches the researchers to search the knowledge and highlight the benefit and remind us that certain standards must always be maintained.

I would obviously like to thank my parents always loving, supportive and willing.

Many thanks to my lovely cool friends who are pleased when I am happy.

And to my son Lorenzo, I said: “thanks for being!”

Abstract (Italiano)

In questo lavoro di tesi è stato progettato e caratterizzato uno scaffold 3D di cheratina innovativo tramite un approccio bio-ingegneristico integrato che unisce anche lo stimolo bio-meccanico generato da un campo elettromagnetico pulsato (PEMF).

Lo scaffold è stato preparato mediante la fibrillazione di fibre di lana (cheratina) sfruttando i componenti istologici che le compongono (fibrille o cellule corticali), al fine di ottenere una struttura adatta alla rigenerazione ossea. È stato quindi progettato uno scaffold di cheratina (spugna di fibrille di lana) con micro e macro-porosità interconnesse di dimensione controllata, al fine di ospitare le cellule, favorendone l'adesione e guidando opportunamente la formazione di nuovo tessuto.

Crosslinks aggiuntivi impartiti alle catene cheratiniche hanno permesso di ottenere uno scaffold con eccellente stabilità in acqua nonostante l'elevato rigonfiamento, resilienza alla compressione e stabilità alla degradazione. La cheratina contiene sequenze di adesione cellulare che facilitano la crescita delle cellule. Infatti, cellule SAOS-2 coltivate sulle spugne di fibrille di lana in condizioni proliferative (PM) e osteoinduttive (OM), hanno mostrato rispettivamente una crescita e un differenziamento ottimali. Il differenziamento, in termini di aumento della mineralizzazione e deposizione di proteine della matrice è stimolato dall'applicazione del PEMF. Lo stimolo bio-meccanico velocizza il processo di differenziamento in condizioni osteoinduttive, mostrando una perfetta sinergia tra gli stimoli biochimici e meccanici nell'accelerazione del processo differenziativo.

La valutazione della crescita di cellule staminali da midollo osseo su scaffold di cheratina 2D e 3D (film di fibrille di lana e idrogeli di cheratina) ha mostrato la loro efficacia nel supportare le cellule staminali; in particolare, i sistemi 3D, grazie al loro diverso tempo di degradazione, possono funzionare da cell-delivery system o da impalcatura a lungo termine.

L'elevato tempo di degradazione mostrato dalla spugna di fibrille di lana suggerisce che questo scaffold possa essere promettente come supporto a lungo termine per la formazione ossea *in vivo*.

Abstract (English)

Novel keratin-based 3D scaffold for bone tissue engineering have been produced, characterized and tested, applying the bio-mechanical stimuli generated by a pulsed electromagnetic field (PEMF). Controlled-size, interconnected porosity, tailored to match the natural bone tissue features, has been designed for cell guesting, proliferation and guided tissue formation, exploiting the natural histological structure of the wool fibers. Additional crosslinking of the keratin chains allowed obtaining excellent water stability and significant swelling due to the synergic contribution of hydrophilicity and porosity, associated to increased compression resilience and ageing resistance. Keratin contains cellular-binding motifs for cell attachment, found in the native extra-cellular matrix, which facilitate better growth, providing proliferation signals and minimising apoptotic cell death. Viability and consistent proliferation were observed for SAOS-2 human osteoblast cells cultured both in proliferative (PM) and osteogenic (OM) media, that were highlighted by PEMF application, especially in the osteogenic conditions, with increased mineralization and higher ECM proteins deposition. PEMF stimulated an earlier differentiation in osteogenic conditions, showing a perfect synergy between biochemical and mechanical stimuli in the acceleration of the differentiation process.

Evaluation of the attachment and growth of human bone marrow mesenchymal cells on different 2D and 3D keratin-based scaffolds, made with wool fibril films, sponges and hydrogels, showed that keratin-based materials are an effective support for stem cell growth. In particular, 3D systems gave the best results and, thanks to the different ageing time, they can be proposed as cell delivery system or for long-term scaffolding.

The longer degradation rate suggests that wool fibril sponges can be promising candidates for long-term support of bone formation *in vivo*.

List of abbreviations

ALP	alkaline phosphatase
BCA	bicinchoninic acid
BM	bone marrow
BM-MSCs	bone marrow mesenchymal stromal cells
BMP-2	bone morphogenetic protein-2
cAMP	cyclic adenosine monophosphate
c-fos	proto-oncogene
CFU-F	fibroblast colony-forming units
CLSM	confocal laser scanning microscopy
COL-I	type I collagen
COL-III	type III collagen
COX-2	cyclooxygenase 2
DEC	decorin
DSC	differential scanning calorimetry
DTT	dithiothreitol
ECM	extracellular matrix
EDS	glutamic acid-aspartic acid-serine motif
EDTA	ethylenediaminetetraacetic acid
EDX	energy dispersive x-ray spectroscopy
EGDE	ethylene glycol diglycidyl ether
ELISA	enzyme-linked immunosorbent assay
FACS	fluorescence activating cell sorting
FDA	fluorescein diacetate
FN	fibronectin
GDE	glycerol diglycidyl ether
HPLC	high-performance liquid chromatography
LDV	leucine-aspartic acid-valine motif
MC3T3-E1	murine pre-osteoblasts cell line
MTT 3	[4,5-dimethylthiazol-2-yl]-2,5 diphenyl tetrazolium bromide
OC	osteocalcin
OM	osteogenic medium
OP	osteopontin
OSN	osteonectin
PBS	phosphate-buffered saline
PEG	polyethylene glycol
PEMF	pulsed electromagnetic field
PGA	polyglycolic acid
PGE ₂	prostaglandin E2
PLA	polylactic acid
PLGA	poly lactic-co-glycolic acid
PM	proliferative medium

PMMA	polymethylmethacrylate
PNPP	p-nitrophenol phosphate
PVA	polyvinyl alcohol
RGD	arginine-glycine- aspartic acid motif
RH	relative humidity
rhBMP-2	recombinant human bone morphogenetic protein-2
rhIGF-1	recombinant insulin-like growth factor type 1
RT	room temperature
SAOS-2	human osteosarcoma cell line
SDS	sodium dodecyl sulfate
SDS-PAGE	sodium dodecyl sulfate polyacrylamide gel electrophoresis
SEM	scanning electron microscopy
VEGF-C	vascular endothelial growth factor
TBS	tris-buffered saline
TRITC	tetramethylrhodamine B isothiocyanate

Contents

1	Introduction	1
1.1.	<i>Biomaterials in bone tissue engineering</i>	1
1.2.	<i>Keratin</i>	5
1.3.	<i>Keratin in the biomedical field</i>	8
1.4.	<i>Wool fibres</i>	14
1.5.	<i>Motivation and novelty of the research</i>	17
2	Wool fibrils sponges	18
2.1.	<i>Aim of the work</i>	18
2.2.	<i>Materials and methods</i>	18
2.2.1.	Preparation of the bio-composite sponges.....	18
2.2.2.	Characterization methods.....	19
2.3.	<i>Results and discussion</i>	24
2.3.1.	Morphological characterization.....	24
2.3.2.	Degree of crosslinking.....	25
2.3.3.	Amino acid composition.....	26
2.3.4.	SDS-PAGE.....	27
2.3.5.	PH of the water extract.....	28
2.3.6.	Thermal analysis (DSC).....	28
2.3.7.	Water swelling.....	30
2.3.8.	Tensile behavior.....	30
2.3.9.	Compression behavior.....	31
2.3.10.	3-(4,5-dimethylthiazole-2yl)-2,5-diphenyl tetrazolium bromide (MTT) test.....	32
2.3.11.	Fluorescein diacetate (FDA) assay.....	33
2.3.12.	Scanning Electron Microscopy (SEM) investigation.....	34
2.3.13.	Ageing of wool fibril sponges vs commercial collagen sponges.....	35
2.4.	<i>Conclusions</i>	38
3	Wool fibrils sponges and Pulsed Electromagnetic Field (PEMF)	39
3.1.	<i>Aim of the work</i>	39
3.2.	<i>Bone remodeling</i>	39
3.3.	<i>Models and numerical dosimetry inside an electromagnetic bioreactor</i>	44
3.4.	<i>Materials and methods</i>	47
3.4.1.	Characterization methods.....	47
3.5.	<i>Results and discussion</i>	51
3.5.1.	3-(4,5-dimethylthiazole-2yl)-2,5-diphenyl tetrazolium bromide (MTT) test.....	51
3.5.2.	Cytoskeleton organization.....	52
3.5.3.	Fluorescein diacetate (FDA) assay.....	53
3.5.4.	Phosphate determination.....	54
3.5.5.	Calcium quantification.....	55
3.5.6.	SEM and EDX.....	56
3.5.7.	Protein Matrix analysis.....	60

3.5.8. Alkaline Phosphatase (ALP) activity.....	61
3.5.9. Compression behavior.....	62
3.6. <i>Conclusions</i>	68
4 Keratin fibrils 3D sponges, keratin hydrogels and 2D keratin fibrils films in stem cell attachment	69
4.1. <i>Aim of the work</i>	69
4.2. <i>Materials and methods</i>	69
4.2.1. Preparation of keratin hydrogels	69
4.2.2. Preparation of 2D keratin fibrils films	70
4.2.3. Characterization methods.....	70
4.3. <i>Results and discussion</i>	73
4.3.1. Morphological characterization	73
4.3.2. Amino acid composition	75
4.3.3. SDS-PAGE	76
4.3.4. PH of the water extract.....	77
4.3.5. Thermal analysis (DSC).....	77
4.3.6. Water swelling.....	79
4.3.7. Tensile behavior	79
4.3.8. Compression behavior	80
4.3.9. Cell viability.....	81
4.3.10. Ageing of the wool fibril films and the keratin hydrogels.....	82
4.4. <i>Conclusions</i>	84
5 Conclusions	85
References	87

Chapter 1

Introduction

1.1. Biomaterials in bone tissue engineering

Bone is a composite tissue made of 30% matrix, 60% mineral and 10% water [1].

The bone matrix is mainly composed by collagen which is responsible for the tensile strength. Calcium phosphate is the mineral component of bone which imparts compressive strength.

Bone tissues are classified in cortical (compact), and cancellous (trabecular) tissues. Compact bone shows compressive Young's modulus of elasticity ranging from 17 to 20 GPa and compressive strength from 131 to 224 MPa, while Young's modulus and compressive strength for trabecular bones range from 50 to 100 MPa and 5 to 10 MPa, respectively [2-4].

Bone tissue is susceptible to fracture as a result of traumatic injury, pathology and resorption [1], and the market for materials in orthopedics is continuously growing. Many bone substitute materials have been produced and studied over the last two decades. In general, they consist in metals, ceramics, bioactive glasses, natural or synthetic polymers, and composites of these [5-7]. Stainless steel, titanium and its alloys, are employed for the majority of fracture fixation treatments [8-9]. These devices and implants are not resorbable and often require a second surgery in order to be removed them from the patient [10-11]. This increases infection risks, complications and health care costs. In addition, thanks to the difference in mechanical properties of these devices in compared to the natural bone, mechanical forces are not transferred to the healing bone resulting in unwanted bone resorption and implant loosening [12-15].

Bone defects management can alternatively involve the use of a procedure called autografting, which involves the harvesting of patient bone from a non-load-bearing site (usually an easily accessible site like the iliac crest) and transplantation into the defect site [16-18]. This represents the gold standard treatment because it possesses all the necessary characteristics for new bone growth, namely osteoconductivity (the physical property of the graft to serve as a scaffold for viable bone healing), osteogenicity (the ability

of the graft to produce new bone) and osteoinductivity (the ability of the graft material to induce stem cells to differentiate into mature bone cells) [1].

Autologous bone has the best clinical outcome, since it integrates dependably with the patient bone without immune complications of allogeneic (i.e. from a human cadaver) or xenogeneic bone (i.e. from an animal source). Unfortunately, there are some drawbacks such as limited bone supply, donor site morbidity, anatomical, structural and surgical limitations, and increased bone resorption [19-20]. Hence, all the drawbacks associated with the use of these bioengineering solutions, including a lack of biodegradability for metals and for some ceramics, limited supply and donor site morbidity with autologous bone tissue, and the potential for disease transmission with allogeneic and xenogeneic tissue [21-22], targeted the scientific community toward development of novel materials and bioengineering approaches development.

Currently bone defects management is addressed to develop resorbable materials with properties tailored to match the biochemical and biomechanical requirements of bone tissue engineering [23-26]. The scaffold must support and guide cells and tissue allowing their growth towards new bone formation [27-30]. Scaffold removal *via in vivo* degradation to non-toxic products is desirable once bone repair and healing has occurred.

Therefore, absorbable materials are sought, since they can be used as an implant and do not require a second surgical event for removal. Ideally, the reabsorption should have a similar rate as the physiological bone remodeling. In this way, the material is replaced with normal bone, and bone restoration is not hampered by the physical presence of foreign materials [31].

Inorganic biomaterials

There are many inorganic materials of clinical interest similar in composition to the mineral part of the bone, for example tricalcium phosphate, hydroxyapatite, bioactive glasses or their combinations [5-7] [32].

Bioactive glasses (Ca- and possibly P-containing silica glasses), for example, when inserted in a biological environment, produce a bioactive hydroxycarbonated apatite layer that can bond biological tissue. Hence, they can be tailored to deliver ions, such as Si, in order to activate gene transduction pathways, leading to cell differentiation and osteogenesis promotion [5, 34].

The resorption rate of bioactive glasses and bioceramics depends on material, for instance, hydroxyapatite persists for years following implantation, while other calcium phosphates have a greater capacity to be resorbed but less strength for sustaining loads [35]. Bioactive inorganic materials show a brittle behavior resulting in a mismatch in mechanical properties compared to bone, for this reason they are not good for load-bearing applications [36].

Polymers

Polymer materials display a large versatility in biomedical applications compared to metals and ceramics, and extensive interdisciplinary research is in

progress with the aim of improving their performances associated with better biocompatibility [37].

Synthetic polymers such as polylactic acid (PLA), polyglycolic acid (PGA), copolymers of PLA and PGA (PLGA), and polycaprolactone have been used in a number of clinical applications.

Synthetic polymer materials can be synthesized to give various properties predictable lot of uniformity.

Moreover, natural polymers generally show higher tolerability, no cytotoxic effect on cells and, in some cases, additional useful properties; for instance, chitosan has hemostatic and antibacterial properties. Natural polymers are interesting candidates for tissue engineering and provide innate biological informational guidance to cells that favors cell attachment and promotes chemotactic responses.

Several natural polymers such as collagen, gelatin, alginate, silk fibroin, chitosan, fibrin, fibronectin, elastin and hyaluronic acid have been widely studied in a broad spectrum of biomedical applications.

In particular, proteins are kept in high consideration for biomaterials production due to their ability to function as the ECM [38].

The most important and essential feature to qualify a material as a biomaterial is the biocompatibility over time.

There are also other important properties in addition to biocompatibility: the material should have an acceptable shelf life, its degradation time should match the regeneration process, it should have suitable mechanical properties suitable for the indicated application, variation of mechanical properties subsequent to degradation should be compatible with the regeneration process, and the degradation products should be non-toxic and easy-removed from the body [39].

Biomaterials properties for bone reconstruction

In addition to the above mentioned properties, mechanical properties, geometry, porosity, and interconnection between pores are some of the most important properties in bone scaffolding. In regenerative medicine approaches, porous scaffolds or implants are often used for supporting the regeneration of bone tissue. The role of such porous devices is particularly important in the treatment of segmental bone defects [40-43], in which the defect size is so large that the natural healing process cannot occur without a scaffold guide supporting the bone replacement.

For example, a minimum pore size of around 100 μm is required for bone restoration process. A porous structure with smaller pore size and/or low interconnection between pores may not be able to provide the required space for bone ingrowth or for physiological angiogenesis [44].

However, the requirements regarding the pore size are different when *in vitro* studies are compared with *in vivo* studies. Pore sizes $>300 \mu\text{m}$ are recommended for scaffolds, but a study suggested that lower porosity may be advantageous *in vitro* because cell proliferation will be better controlled and cell aggregation could be forced when the porosity is lower. In comparison, higher

porosity and larger pore sizes may be advantageous *in vivo*, because they could stimulate bone regeneration [45].

The chemistry of the materials is equally important, affecting cell attachment and chemotactic responses [44].

In addition to scaffold porosity and mechanical properties, the shape of the material can be tailored also to provide a three-dimensional cellular microenvironment with high water content and cell or drug encapsulation and delivery [46-47]. All these performances can be satisfied for example by hydrogels (e.g. polyethylene glycol, alginate-based, protein-based etc.), currently popular materials that can often be delivered in a low invasive manner and prepared *in situ*. Their viscoelastic properties seem particularly suitable for instance for cartilage regeneration [48-51].

1.2. Keratin

Keratins refer to a group of insoluble proteins produced in certain epithelial cells of vertebrates, belonging to the superfamily of intermediate filament proteins, and form the bulk of the skin and the epidermal appendages such as wool, hairs, nails, horns, and feathers [52].

Keratins are naturally biocompatible and possess cell motifs binding residues of leucine-aspartic acid-valine (LDV), glutamic acid-aspartic acid-serine (EDS) and arginine-glycine- aspartic acid (RGD) supporting cellular attachment [53-54], that is the first step of the tissue engineering replacement process.

Recent literature shows that keratin-based biomaterials have the capacity to specifically interact with cells leading propagation of the intracellular signalling pathway specifically contributing to haemostasis. Through application of biochemical and molecular tools, they contribute to haemostasis through two probable mechanisms: integrin mediated platelet adhesion and increased fibrin polymerization [55-59].

Keratins have been utilized as biomaterials for decades, and are currently under investigation for a variety of tissue regeneration and trauma applications. It has been suggested that certain keratins may have the capacity to act as a colloid in fluid resuscitation applications, providing viscosity and oncotic properties that may be beneficial during acute ischemic events. More especially, some oxidized keratin derivatives, also known as keratoses, have shown good blood and cardiovascular compatibility associated with the capability to induce vasodilatation. Administration of certain keratose derivatives resulted in significant changes in the microvasculature of the cremaster muscle of rats, and their effect on the mechanism of vasodilatation is the object of further investigation [60].

Keratin from different sources

Keratin-based materials are characterised by the highest content of cysteine compared with other proteins; cysteine residues give rise spontaneously to cysteine crosslinks; as a result, keratins are tough and resistant to the natural environment and to many chemicals [61].

Keratins are commonly classified by X-ray diffraction where they can show α -pattern, β -pattern, and amorphous pattern.

Alpha-keratin is found in mammals and it is the primary constituent of wool, hair, nails, hooves, horns and the *stratum corneum* of skin.

The β -form is the major component of hard avian and reptilian tissues, such as feathers, claws and beaks of birds, and scales and claws of reptiles.

Also, keratins can be classified as soft keratins (e.g. *stratum corneum*) usually weakly consolidated and with a lower amount of sulfur and lipids, and hard keratins found in hair, nails, claws, beaks and quills, which have a more coherent structure and a higher amount of sulfur [52].

Both α - and β -keratinous materials are organised in a fine filament-matrix structure at the nanoscale, namely, for α -keratins, the ‘intermediate filaments (IF)’ and for β -keratins the ‘beta-keratin filaments’ [62]. In α -keratins several kinds of low-sulfur proteins compose the IFs [63] and the matrix consists of high-sulfur and high-glycine–tyrosine proteins; on the contrary, there are no different types of proteins in β -keratins [64].

Keratin extraction

Although extraction of keratins from different sources has been conducted in various ways, a preliminary scouring with warm water and surfactants must be generally carried out to remove soluble and insoluble dirt, such as soil, salts and fatty matters (grease and waxes such as lanolin from wool). Wool, hair, horn and feather are then defatted with organic solvents (petrol ether, dichlorometane or acetone) in order to completely remove all external lipids and other impurities.

The primary concern for extraction is the breakage of disulfide bonds, to enable solubilization of keratins without breaking peptide bonds. In fact, extraction processes involve the presence of reducing or oxidating agents, more especially when wool and hair, which contain the highest amount of cystine, are involved.

Nevertheless, most of the literature data on keratin extraction refer to reduced keratins [65].

Keratins extracted *via* reduction are named kerateines; during this process cystine bonds are broken and converted in two cysteine residues. Reductive extraction usually involve treatments with thiols such as 2-mercaptoethanol, thiourea [66], dithiothreitol (DTT) [67] or thioglycolic acid [68], in addition with denaturing agents, such as urea or sodium dodecyl sulfate (SDS), and sometimes chelating agents such as ethylenediaminetetraacetic acid (EDTA).

One of the most widely used reagents in recent years is the Shindai solution, established by Nakamura *et al.* [69], which is composed of 25 mM Tris-HCl, 2.6 M thiourea, 5 M urea, and 5% (v/v) 2-mercaptoethanol (pH 8.5). Urea and thiourea mainly account for the disruption of hydrogen bonds, and eventually facilitate easy access of the reducing reagents to the disulfide bonds of the keratin molecules, 2-Mercaptoethanol is added to break disulfide linkages *via* reaction of its thiolate anion, and Tris-HCl is added to adjust to an optimal pH environment. In fact, despite the fact that disulfide bonds are easily hydrolyzed at a high pH in the presence of hydroxide ions, severe alkaline conditions above pH 10.0 give rise to the desruption of the peptide chains or deamidation of certain amino acids such as asparagine or glutamine [66].

Reductive extraction is followed by dialysis, to wash out chemicals and restore disulphide cystine bonds by re-oxidation of cysteine thiols, producing the regenerated keratin.

Different is the case of oxidised keratins, namely the keratoses, in which the cystine residues give irreversibly rise to cysteic acid residues. The oxidative extraction usually involves treatment with peracetic or performic acid to oxidise cystine to cysteic acid [70-72]. The oxidized proteins have been termed α -, β -,

and γ -keratases, corresponding to low-sulfur, membrane complex, and high-sulfur proteins, respectively [73].

In particular, Alexander and Earland reported the percentage of oxidized keratin fractions extracted from wool, that are (60%) α -, (30%) γ -, and (10%) β -keratase. Anywhere, there is a loss of several amino acid components, keratins are only partially oxidized, and sulfidryl groups remain un-modified [74].

Conversion of cystine residues to sulfonic acid derivatives was reported to be irreversible in peracetic acid-mediated oxidation. The breakage of peptide bonds that frequently occurs in the treatment with peracetic acid, hardly occurs when keratins are treated with performic acid, resulting in a higher extraction yield [75].

While keratases are readily soluble in water, kerateines are water-insoluble but they are soluble in formic acid, allowing blending with fibroin or synthetic polyamides, for instance.

In addition, hydrogen peroxide has been reported to be also effective in the oxidative extraction of keratins [76].

Sulphitolysis is another method to extract keratins. Disulphide cystine bonds are cleaved to give a thiol and an S-sulphonate anion (or Bunte salt) by the action of sulphites. In the end, only a part of the cystine groups of the native proteins are restored during the subsequent oxidation in air, but cysteine-S-sulfonate keratins are obtained [68-71] [73-74] [76-77].

For instance, aqueous solution containing urea, SDS and sodium metabisulfite have been used to extract keratin from wool and hair [78]. After extraction, the regenerated keratin solutions are dialyzed against water to remove chemicals.

Generally, the higher is the cystine content of the protein source, the harder is the extraction and dissolution of the related keratins.

Alternative methods

Keratin-based biomasses have been also exploited hydrolyzing the protein backbone, to obtain the corresponding peptides and amino acids. Hydrolysis can be carried out with different chemical agents, although boiling in alkali media represents the most common way to carry out a strong hydrolysis of keratin; alternatively, also strong acids can effectively disrupt the protein chains [79].

More recently, enzymatic treatments [80], sometimes along to mild chemical treatment (usually alkali pre-treatments) and treatments with steam and superheated water have been proposed for the hydrolysis of wool [81-85].

Steam explosion is a green technology based on short time steam cooking biomasses at a high temperature for several minutes, followed by explosive decompression. Using saturated steam at 220 °C (~22 bar) for 10 min followed by a rapid decompression, clean wool fibres were degraded producing a dark-yellow "wool sludge" made of water-soluble peptides and free amino acids, associated with insoluble fibre remains [86]. The wool sludge was submitted to phase separation by filtration, centrifugation, and precipitation of the soluble materials from the supernatant liquid. Characterisation of the liquid and solid phases revealed the disruption of the histology fiber structure and the reduction

of the protein molecular weight to water-soluble peptides and free amino acids, associated with breaking of disulfide bonds and decomposition of the high-sulfur-content protein fraction [86-87].

The hydrolysis conditions of wool fibres with superheated water were also studied in depth by a microwave-assisted laboratory-scale reactor, with the aim of tailoring the conversion extent of the protein chains into oligopeptides and amino acids in the temperature range 150-180 °C [88-90].

Keratin processing

Keratins for biomedical applications have been regenerated into various forms, such as films [91-120], sponges [53] [121-136], hydrogels [137-154], fibres [155-171], nanoparticles/microcapsules [172-173] alone or blended with other natural and man-made polymers [174] or with bio-glasses [175].

Yamauchi *et al.* [105] prepared keratein films permeable to glucose, urea, and sodium chloride, and tested their biodegradability *in vitro* and *in vivo*. Since films of pure keratein resulted brittle and fragile, glycerol in different concentrations was added to improve processability. Many works were focused on the improvement of the mechanical properties of regenerated keratin films, including the addition of natural polymers and crosslinking agents. For example, keratein films crosslinked by ethylene glycol diglycidyl ether (EGDE) and glycerol diglycidyl ether (GDE) were produced resulting in tenacious and flexible films [102]; also, excellent mechanical performances have been obtained blending regenerated keratin with chitosan [106].

Keratein was demonstrated to be suitable for modifications of the abundantly present cysteine residues, making it versatile. The cysteine residues are indeed easily modified; for instance, keratein films have been modified with the cell adhesion peptide Arg-Gly-Asp-Ser (RGDS) at the free cysteine residues [107] improving fibroblast cell growth and adhesion.

Moreover, due to their high amount of cystine, regenerated keratins are resistant to many chemicals, hence processing require solubilization with formic acid [176] or with the same reducing or oxidizing agents used for extraction.

1.3. Keratin in the biomedical field

Wound dressing

Wound healing is a very complex process involving several correlated biological events that include coagulation, inflammation, removal of damaged matrix, cellular proliferation and migration, angiogenesis, matrix synthesis and deposition, re-epithelization and remodelling [177].

A wound can be described as a defect or a break in the skin, which could be due to an external damage or as a result of a defect in physiological conditions which would then result in a pathological disruption of the structure and function of the skin [178].

The prerequisite for complete lesion repair is the rapid restoration of physiological conditions. Incorrect repair may result in serious damages including the loss of skin, hair and glands, onset of infection, occurrence of skin diseases, injuries to the circulatory system, and, in severe cases, death of the tissue.

Some types of keratins play a key role in skin morphogenesis and in the hair cycle processes. In addition, the onset of re-epithelialization after skin injury is related to the re-organization of keratin filaments in keratinocytes around the wound site [179]. Hence, since keratin is an active skin building block which is naturally bio-compatible also when it comes from animal sources, keratin-based materials have been proposed in many studies for wound repair applications.

Pechter *et al.* [180] demonstrated that keratin dressings, in both liquid and solid form, may stimulate epithelialization by enhancing activation of keratinocytes. Tang *et al.* suggested a positive effects on re-epithelialization *via* stimulating keratinocyte migration and production of basement membrane proteins of collagens, at the base of this activation [181].

Keratin biomaterials demonstrated high biocompatibility and enhanced fibroblasts cell adhesion [107] [119] [129] and there are many papers [78] [117] [121-124] [146], and patents [182-185] on keratin-based materials, in solid or liquid form, for wound dressing applications.

Keratin has been proposed alone, or blended with chitosan, for instance, which is a natural polymer that shows an antibacterial properties [120] [124]. Gelatin, fibrin and collagen have been also used along keratin to prepare material for wound management [122-123] [146] and, in some cases, the blends have been filled with drugs for drug delivery too [121].

The application of keratin-based products in burns healing was evaluated by Loan *et al.*, comparing their effectiveness against current standard care in the management of superficial (where only the epidermis is damaged) and partial thickness burns (where the epidermis and part, but not all, of the dermis is damaged). The keratin products were found to facilitate healing with minimal scarring, be well tolerated with minimal pain and itch, be easy to use for the health professional and be cost effective for the health care provider [186].

Obviously, the biggest challenge consists in the treatment of chronic wounds, including amputations, diabetic and leg ulcers, pressure sores and surgical and traumatic wounds (e.g. accidents and burns), where patient immunity is low and the risk of infections and complications are high [179].

About the venous leg ulcers, caused by chronic venous hypertension, compression therapy is the current fundamental treatment [187]; nevertheless, many new wound care products tailored to facilitate healing processes in the wound site have been studied and developed in the past years.

The clinical work carried out by Than *et al.* demonstrated improvement in different patients with recalcitrant, venous and mixed venous and arterial leg ulcers treated with keratin-based dressings.

Three forms of keratin wound dressing products have been developed: a hygroscopic gel for minimally exudative wounds, a matrix for moderately

exuding wounds and an absorbent foam laminated with a perforated keratin film on the wound contact side, for highly exuding wounds [188].

Hammond *et al.* have examined the patient acceptability of three new types of keratin wound dressings during development. A sample of 23 patients, with leg ulcers of differing aetiology, were recruited: 77% showed improvements in their wounds and 18% healed completely [187]. Another clinical study was carried out by Than *et al.* that observed a significant improvement in the robustness of the skin, consisting in a reduced propensity to blister, and improved healing of blisters in wounds from patients with epidermolysis bullosa [145].

Peripheral nerve regeneration

Peripheral nerve injuries damage the ability to feel normal sensations and exercise muscle movements, due to denervation of adjacent tissues and muscles bringing about loss of sensory and motor functions. Peripheral nerve injuries result in paralysis, chronic pain, and neuropathies leading to severe disability [155]. The gold standard treatment is the nerve autograft that shows many limits such as lengthy or multiple surgical procedures as well, the donor tissue availability, the resulting morbidities and the additional injuries and scarring. In addition, only about 50% patients significantly regain useful function after autograft surgery [156].

So, as in other biomedical applications, modern strategies are focused on the design of a biocompatible structure to support the damages repair.

In the field of nerve tissue engineering, many hydrogels, serving as luminal fillers for tubular nerve conduits, have been developed to guide peripheral nerve regeneration. There has been significant progress in the development of hydrogels with naturally derived biomaterials such as collagen, hyaluronic acid, chitosan, and alginate for guided nerve regeneration [147] [189], but the potentiality of keratin hydrogels has been evaluated by many studies too [148] [152].

Sierpinski *et al.* demonstrated the neuroconductivity of a hair keratin gel, showing mediation of a significant nerve regeneration response, in part through activation of Schwann cells, probably by a chemotactic mechanism, thanks to the intrinsic RGD motif increasing their attachment and proliferation, and up-regulate expression of important genes [149]. The Schwann cells activation is also evidenced in another study by Pace *et al.* [152].

Van Dyke *et al.*, showed the long-term effects of keratin hydrogels on peripheral nerve regeneration, for up to 6 months of implantation in a peripheral nerve injury mouse model. After this time, accelerated peripheral nerve regeneration was found in the nerve conduits filled with keratin hydrogel, as evidenced by increased axon density and improved electrophysiological recovery, similarly to nerve autografts transplanted in mice [150].

Another study showed that the neuroinductive activity of biomaterials was enhanced combining a keratin hydrogel with a neurotrophic factor. In detail, Lin *et al.* developed polycaprolactone nerve conduits containing a glial cell line-derived neurotrophic factor loaded with microspheres and a keratin hydrogel.

This biomaterial was implanted in a rat model with a sciatic nerve defect. After 6 months, a higher density of Schwann cells and axon development within the transplanted nerve conduit were found, demonstrating the high potentiality of advanced keratin material in peripheral nerve repair [151].

Keratin for bone reconstruction

Autologous bone grafting is the gold standard of bone replacement because it provides osteogenic cells and osteoinductive factors needed for regeneration. The bone graft usually consists in the trabecular bone from the patient's iliac crest, but cortical bone can be used as well. Nevertheless, polymers, ceramics and metals, have been proposed as biological support [190].

Scaffolds play a key role in bone tissue engineering providing a 3D environment for cell seeding, attachment and proliferation, while providing mechanical signals during bone regeneration [191].

Keratin in different form, such as sponges [127] [131] [135], hydrogel [135], nanofibers [116] [159] and nanoparticles [191] have also been proposed in bone tissue engineering applications. Tachibana *et al.* produced keratin carboxyl-sponges, using calcium phosphate, with the aim to mimic the matrix gamma-carboxyglutamic acid protein, which is responsible for osteoblast calcification, later, hydroxyapatite particles suspensions were added onto the carboxyl-sponges to fabricate trapped sponges. These materials supported osteoblast cultivation and altered their differentiation pattern based on the expression pattern of alkaline phosphatase [127].

Modified keratin sponges were also produced by the alkylation of a large amount of active SH group on keratins by iodoacetic acid and 2-bromoethylamine, obtaining carboxyl and amino sponges respectively. Keratin carboxy-sponges have also been functionalized with the bone morphogenetic protein-2 (BMP-2). The authors found that cells outside the BMP-2-loaded structure did not differentiate, but differentiation was confined inside the scaffold. This approach is promising for in vivo applications because external heterotopic ossification may be avoided [131].

Similar remarks came from another study in which regenerative bone capacity of rhBMP-2 on keratin hydrogels and sponges, and collagen sponges, have been compared in a critically sized rat mandibular defect model. It was found that both keratin hydrogels and keratin sponges resulted in significantly less ectopic bone growth than collagen sponges at both 8 and 16 weeks post-operatively. These studies demonstrate the regenerative capacity of keratins with reduced ectopic growth compared to collagen sponges [135].

De Guzman *et al.* evaluated keratose-based biomaterials added with BMP-2 as a new carrier/scaffold by implantation into a critical-size rat femoral defect. Compared to the normal cortical bone, the regenerated tissue had greater volume and mineral content but less density and ultimate shear stress values. Moreover, experimental data showed that regeneration was similar to a commercial crosslinked collagen material used for control. Surprisingly, treatment with keratose only led to deposition of more bone outgrowth than the untreated negative control at the 8-week time point. The application of keratose

also demonstrated a notable reduction of adipose tissues within the gap. While not able to induce osteogenesis on its own, the authors suggested that keratose may be the first biomaterial capable of suppressing adipose tissue formation, thereby indirectly enhancing bone regeneration [192].

Dias *et al.* investigated the *in vivo* biocompatibility and osseointegration of keratin materials in an ovine model. They used six different keratin scaffolds inserting them into drilled round defects in the femur and tibia of sheep. All keratin implants showed similar histological profiles up to 24 weeks postsurgery, which included granulation tissue surrounding and infiltrating the implants, followed by new bone formation radiating from the existing bone [193].

Controlled release

Keratin-based materials in different forms like films [95] [119] [194-195], hydrogels, sponges [121] [196] and nanoparticles [197-198] have been proposed for drug-delivery too.

Different processing methods to obtain 3D structure keratins capable to entrap active molecules are reported in literature. De Guzman *et al.* produced crosslinked sponges made of PEG and keratin and investigated the diffusion release profiles of the scaffold-absorbed soluble proteins with varying pI (charges) and sizes in physiological and acid pH (4).

They also tested the functional bioactivity through endothelial cell culture onto keratin substrates with absorbed VEGF-C.

The results showed keratin-PEG materials can potentially be used as a slowly degradable sponge-like material for burst-release of high amount of growth factors in acidic environment. At the same time, they attract endogenous positively charged growth factors in neutral to basic pH media, suggesting a feasible strategy with potential applications for selective proteins delivery [196].

With the aim to prevent postoperative abdominopelvic adhesion, a significant surgical complication, Peyton *et al.* evaluated the effectiveness of a halofuginone infused keratin hydrogel in a rat cecal abrasion model. They produced keratin hydrogels infused with halofuginone, a type-1 collagen synthesis inhibitor, founding that the drug release from the hydrogel in phosphate-buffered solution was sustained over 7 days and correlated with keratin degradation [143].

Modifications of keratins have been carried out by Han *et al.* in order to modulate the drug delivery rate. They prepared modified keratin hydrogels by alkylation (capping) with iodoacetamide of cysteine thiol groups of kerateines, providing tunable rates of gel degradation and drug delivery speed. The alkylated keratins did not lead to toxicity in MC3T3-E1 pre-osteoblasts and the authors reported that alkylated kerateine gels eroded more rapidly than the non-alkylated ones. Controlled over erosion led to tunable rates of delivery of rhBMP-2, rhIGF-1, and ciprofloxacin [199].

In another study, the delivery rate of rhodamine B (dye used as a model drug) in keratin-PVA blend films has been modulated by crosslinking keratin with dialdehyde starch. Results showed that the release rate of rhodamine B

decreased with increasing the dialdehyde starch content, since cross-linking improves the water resistance of the films [200].

The degradation rate of keratins has been also tuned with the cystine crosslinks found in different proportion in the oxidated or reduced keratins. Hence, different amount of kerateines and keratoses have been blended by Ham *et al.* resulting in hydrogels with tunable control over the release rates of recombinant human insulin-like growth factors [201].

Along 3D matrices capable to entrap drugs in their physical structure, keratin nanoparticles also have been proposed for drug delivery. For instance, oxorubicin-loaded keratin nanoparticles have been developed as intracellular drug delivery for cancer therapy [197]. The *in vitro* cellular uptake experiments indicate that drug released from the doxorubicin-loaded keratin-g-PEG nanoparticles can be efficiently internalized into the cells, and the drug shows a faster release into the nuclei of the cells under higher glutathione concentrations.

Finally, as for drugs, keratin hydrogels have been proposed for encapsulation of living cells too [202].

Other biomedical applications

Keratin-based biomaterials have been proposed also for other biomedical purposes in addition to the above reported applications. XianGuo *et al.* produced films of keratin/fibroin/gelatin that were applied in an animal study for repairing urinary tract defects [203].

Noishiki *et al.* proposed the application of keratin as antithrombogenic biomaterial, preparing a vascular graft coated with heparinized keratin derivatives [204].

It was also found that keratin biomaterials attenuate hypoxia-mediated cell toxicity [205] and the application of keratin to the myocardial infarction was proposed by Shen *et al.* Myocardial infarction occurs when a coronary artery becomes occluded; in this state the heart cannot adequately deliver oxygen to tissues within the body. Shen *et al.* treated umbilical vein endothelial cells exposed to long-term hypoxia with keratin, showing that keratin provides a protective effect to cells in hypoxia, which proliferate in response [206].

Keratins have been also proposed for ocular surface reconstruction [207-208] and for antithrombogenic applications [110], and have demonstrated efficacy as a hemostatic agent in several animal models, including a rabbit haemorrhage model in which a keratin hydrogel performed better than the commercialized hemostatic agents in controlling blood loss [209-210] [57]. Poly(ϵ -caprolactone)/keratin nanofibrous mats have been proposed as scaffold in vascular tissue engineering [210]. Finally, keratin films offer a possibility as a human nail plate substitute [108] [109]. Data of permeation coefficients of keratin films and bovine hoof plates (a well-accepted nail model) were comparable; therefore keratin films are suggested as an artificial nail model for *in vitro* permeation studies [211].

1.4. Wool fibres

Wool is a noteworthy example of hard keratin. A clean wool fibre contains approximately 82% keratinous proteins with a high concentration of cystine. About 17% is protein material of low cystine content, namely “non-keratinous material” mainly present in the cell membrane complex, and about 1% is non-proteinaceous material consisting of waxy lipids, plus a small amount of polysaccharide material [72].

Wool fibres consist of flattened cuticle cells, disposed like tiles on a roof that make up the external layer surrounding the cortex, composed by spindle shaped cells, namely the cortical cells (or fibrils), and embedded in intercellular materials (the cell membrane complex).

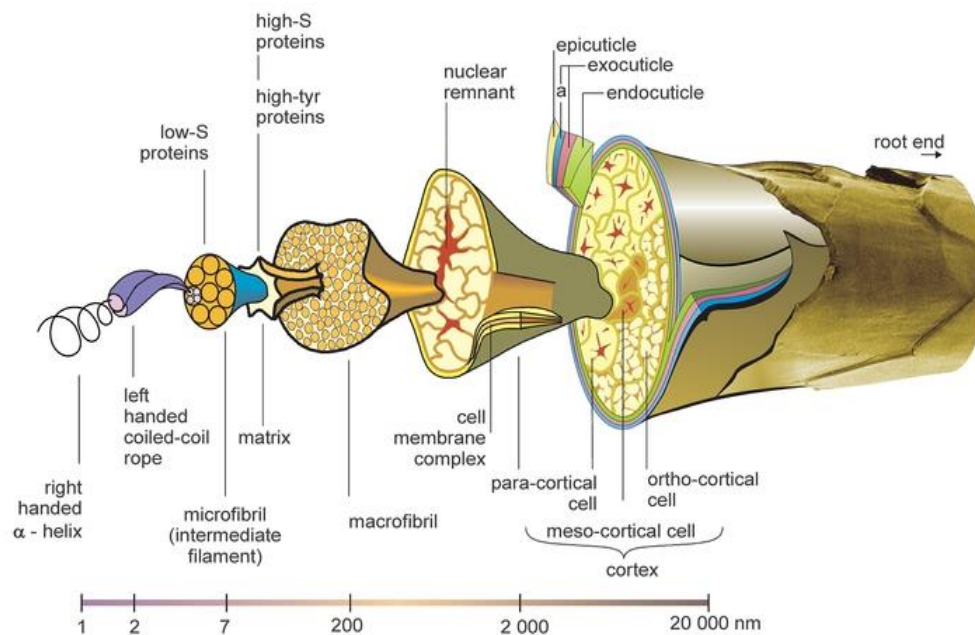


Figure 1.1: The structure of a wool fibre [212]

Moreover, each cortical cell is composed of microfibrils, made of multiple α -helical, closely packed, low sulphur subunits, embedded in a matrix containing two non-filamentous protein types, namely the high-sulphur proteins and the glycine- and tyrosine-rich proteins [213] [52].

When wool is submitted to mechanical forces in certain conditions can fibrillate: the fibre structure integrity goes lost and the cortical cells come out from the bulk of the fibre (Fig. 1.2).

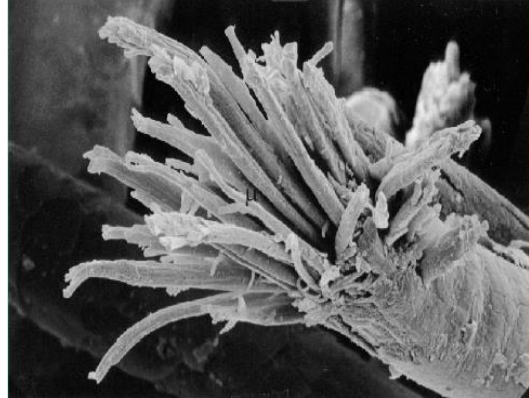


Figure 1.2: Fibrillated wool fibre

The molecular weight distribution of wool keratins shows two protein fractions between 60000 and 45000 Da, related to the low-sulphur keratin from the intermediate filaments of fibre cortex with typical α -helix secondary structure, and a series of low molecular weight fractions between 28000 and 11000 Da, from the high-sulphur protein of the matrix embedding the intermediate filament and from the fibre cuticle [214].

Amino acid analysis of wool and hair keratins shows a higher content in cystine (detected as cysteine: $\frac{1}{2}$ CYS) compared to feather and horn keratins (Tab. 1.1).

The higher cysteine amount found in wool and hair is probably due to the high amount of high-sulphur proteins correlated with an increase of cystine in the high-sulphur protein domain [214]. Glutamic acid, aspartic acid, leucine, lysine and arginine, which are the amino acids that contribute to the α -helix assembling of the low-sulphur proteins, are most abundant in horn–hoof, while feather keratins contain the lowest amount of the same [217]. Moreover, wool and hair show the higher amount of cystine compared to horn, while feather keratin shows the lowest one.

Table 1.1: Amino acid composition of keratins from different sources
¹ [214]; ² [215]; ³ [216].

Amino acids	Wool (mol%) ¹	Horn-hoof (mol%) ¹	Hair (mol%) ²	Feather (mol%) ³
CYA	0,20	0,00	0,1	-
ASP	7,00	8,70	5,1	6,25
SER	8,50	7,20	11,5	10,38
GLU	13,80	16,30	13	9,91
GLY	4,60	4,00	5,8	6,77
HIS	1,30	1,30	0,9	0,58
ARG	10,20	10,80	6,5	5,93
THR	6,60	5,10	7	4,58
ALA	3,30	3,70	4,5	4,06
PRO	5,70	4,40	8,4	10,36
½ CYS	10,80	7,10	16,1	1,02
TYR	5,90	4,50	2,1	2,88
VAL	5,10	5,30	5,5	7,04
MET	0,60	1,00	0,5	9,52
LYS	3,00	4,60	2,6	2,05
ILE	3,20	4,10	2,6	5,03
LEU	7,20	8,70	6,2	7,21
PHE	3,60	3,20	1,6	5,03

Only the arginine content was quite similar in the materials. Otherwise, cysteine, proline, serine and threonine, that constitute more than half of the amino acid residues of high-sulphur proteins, are most abundant in wool. Moreover, methionine, a sulphur amino acid that is not present in the high-sulphur protein domains, is most abundant in horn–hoof compared to wool [72].

On the other hand, the amount of glycine and tyrosine, that characterise the protein material between the cell structures of wool fibres, is higher in wool than in horn–hoof [214].

1.5. Motivation and novelty of the research

In this work novel 3D scaffold for bone tissue engineering have been produced, characterized and tested, using an integrated bio-engineering approach, applying the bio-mechanical stimuli generated by a pulsed electromagnetic field (PEMF) to study a novel approach for bone tissue engineering.

The novelty of this research mainly consisted in designing a biocompatible and absorbable keratin scaffold with associated micro- and macro-porosity, by an innovative method. The material selected was keratin from sheep's wool because of the interesting properties described above

On the contrary to conventional chemical processes described in literature, in this work neither strong reducing nor oxidizing agents and dialysis were used for extraction and processing of the proteins.

This processing method involves the exploitation of the wool cortical cells (fibrils), the main histological components of the wool fiber structure that were used as building block for novel 3D scaffolds.

The cortical cells were extracted from wool by ultra-sonication of wool fibres bathed in clean water; casting of the resulting suspension, produced a microporous solid network made of interconnected fibrils, suitable for cell nutrient feeding and signalling. Moreover, controlled-size salt-leaching gave to the network an additional 3D-tailored macro-porosity, matching native bone features for cell proliferation and cell guided tissue formation.

Despite the fact that keratin scaffold from human hair have been also studied for different biomedical applications because of the autologous origin, in this work the source of keratin was sheep's wool. This because human hair contain a pronounced medulla, the innermost layer of the hair shaft, and pigment granules. Moreover, the fineness and the structural features of wool fibers are more easily standardized, to produce homogeneous samples for research purposes. Nevertheless, in a second step a similar process could be hypothetically applied to human hair too, tailoring the process conditions to this kind of material.

Finally, the mechanical stimuli generated by a pulsed electromagnetic field (PEMF) was applied as an integrated bio-engineering approach, in order to evaluate the PEMF-mediated bone mechanotransduction when cells are cultured onto the novel keratin scaffold.

Chapter 2

Wool fibrils sponges

2.1. Aim of the work

The aim of this experimental part is the preparation of a novel keratin scaffold with integrated micro- and macro-porosity, the relative chemical-physical characterization, and the preliminary biological evaluation using SAOS-2 cells line for *in vitro* osteoblast studies.

2.2. Materials and methods

In this section the materials and the methods used are reported in detail. All analytical grade chemicals were purchased from Sigma-Aldrich, except otherwise specified.

2.2.1. Preparation of the bio-composite sponges

Botany wool, 20.3 μm mean fibre diameter, in the form of top (the fibre sliver obtained from raw wool by scouring, carding, and combing processes) was supplied by The Woolmark Co., Italy.

Procedure

8 g wool fibres weighed in standard atmosphere (20 °C and 65% RH), were cut into snippets of some millimetres and bathed in 400 ml 0.1 N NaOH (material to liquor ratio 1:50) for 24 h at 60 °C without stirring. The snippets were rinsed with tap water until neutral pH on a stainless steel sieve (120 mesh), then soaked in deionised water (total volume 150 ml) and submitted to ultrasonic treatment for 30 min with a Sonics Vibracell 750 (Cole Parmer) sonicator, equipped with a stainless steel 1/2 inch “solid” probe. Power was tuned to 600 W at 20 kHz frequency, with control temperature set at 50 °C. This treatment produces a suspension of cortical cells and fibre fragments in the

aqueous protein solution. Coarse fibre fragments were removed by filtration with a stainless steel, 120 mesh sieve. The permeate cell suspension was centrifuged at 12000 rpm for 15 min, and the supernatant was removed. The solid precipitate was added with 16 ml deionised water and kept on stirring until the complete suspension of the cortical cells that were arranged to 0.05 g/ml. This suspension was added with 1.17 g/ml controlled size NaCl (400–500 μm), then cast at 50 °C until dry. The resulting material was washed 5 times with deionised water in order to completely remove the salt, giving rise to a wool fibril sponge that was dried again at 50 °C. An additional thermal treatment at 180 °C for 2 h was carried out to improve the water stability of the sponge, increasing isopeptide bonding and other crosslinks through dehydration, as reported in literature [218].

Sponges were cut (0.8 mm diameter) in order to fit in the cell culture well plate.



Figure 2.1: Wool fibril sponges cut and placed in the cell culture well plate

2.2.2. Characterization methods

Morphological characterization

SEM investigation of the sponges was performed with a LEO (Leica Electron Optics) 135 VP SEM, at 15 kV acceleration voltage and 30 mm working distance. The samples were mounted on aluminium specimen stubs with double sided adhesive tape and sputter-coated with 20 nm thick gold layer in rarefied argon, using an Emitech K 550 Sputter Coater with 20 mA current for 180 s. Cross sections of the films were obtained by fragile fracture in liquid nitrogen.

Porosity was measured by an inert gas stereopycnometer Quantachrome, model SPY-3. Sponge samples were placed 24 h in standard atmosphere (20 °C, 65% RH) before being placed into the pycnometer cell, and fluxed with argon for 10 min to remove moisture and air. After that, the measurement of the

volume has been performed. Once the real volume has been measured, the samples were weighed in order to calculate the true density.

Degree of crosslinking

The crosslinking degree of the sponges before and after the thermal treatment was determined by the ninhydrin assay [219-220]. Sponges (10 mg) were heated in a ninhydrin solution (2% (w/v)) at 100 °C for 20 min. The optical absorbance of the resulting solution was read at a wavelength of 570 nm wavelength, using a Perkin Elmer Lambda 35 spectrometer.

The concentration of free amino groups in the sample was determined using a standard curve of glycine concentration vs absorbance. Non-crosslinked sponges (not submitted to thermal treatment) were used as a control materials. Triplicate samples were evaluated. The degree of crosslinking was determined by the following equation:

$$\text{Degree of crosslinking (\%)} = [(\text{NH}_2)_{\text{nc}} - (\text{NH}_2)_{\text{c}}] * 100 / (\text{NH}_2)_{\text{nc}}$$

Where $(\text{NH}_2)_{\text{nc}}$ and $(\text{NH}_2)_{\text{c}}$ are the mole fraction of free NH_2 in the non-crosslinked and crosslinked samples respectively.

Amino acid composition

The wool fibril sponges were submitted to amino acid analysis compared with the original wool. All samples (40 mg) were hydrolyzed with 15 ml HCl (6M) at 110 °C for 24 h in sealed tubes. Free amino acid residues were derivatized with hydroxysuccinimidyl carbamate (AQC-Waters) and eluted on a 15x0.39 cm reversed-phase column (Waters). An Alliance high-performance liquid chromatograph (HPLC-Waters) was used and the eluate was detected at 254 nm. The quantitative amino acid composition was determined by calibration with the Amino Acid Standard H (Pierce), cysteic acid and lanthionine (TCI Europe) as external standards and α -aminobutyric acid as internal standard.

SDS-PAGE

The samples (15 mg) were extracted in 1 ml solution containing Tris/HCl (550 mM, pH 8.6), DTT (140 mM), ethylenediaminetetraacetic acid (5 mM) and urea (8 M) for 4 h under nitrogen atmosphere, according to the Marshall method [221]. The protein concentration of the extract was determined with the Bradford protein assay method (Bio-Rad) using bovine serum albumin standard. Samples were dissolved into a buffer containing the NuPAGE LDS sample buffer and the NuPAGE sample reducing buffer as recommended by the Invitrogen protocol, to deliver 30 mg of sample to the gel (NuPAGE reducing agent contains 500 mM DTT at a ready-to-use 10 concentration in a stabilized liquid form; NuPAGE buffer contains lithium dodecyl sulphate at a pH of 8.4), which allow for maximal activity of the reducing agent. Sodium dodecyl sulphate-polyacrylamide gel electrophoresis

(SDS-PAGE) was performed using a Xcell SureLock Mini-Cell (Invitrogen) on Bis-Tris 4-12% polyacrylamide pre-cast gel (Invitrogen) using the NuPAGE MOPS SDS running buffer. This is suitable for proteins with molecular weights from 191 to 14 KDa, referring to myosin, phosphorylase, bovine serum albumin, glutamic dehydrogenase, alcohol dehydrogenase, carbonic anhydrase, myoglobin red and lysozyme as the molecular weight markers (blue prestained standard from Invitrogen).

PH of the water extract

In accordance with the International Wool Textile Organization standard IWTO-2-96, the wool fibril sponges were bathed in distilled water at 20 °C and stirred for an hour before the pH measurement.

Thermal analysis

Differential scanning calorimetry (DSC) was performed with a Mettler Toledo DSC 821 calorimeter, flushing the cells with 100 ml/min nitrogen. The temperature programme was set in the range from 30 to 400 °C, at 10 °C/min heating rate, and the instrument was calibrated with the indium standard. The data were collected on a computer using the Mettler Toledo Star System. About 1 mg conditioned sponges (20 °C, 65% RH) cut into snippets were used to optimise the heat transmission to the crucible. All tests were replicated three times.

Water swelling

Sponges were previously dried in a ventilate oven at 105 °C, then stored in standard conditions (20 °C and 65% RH) for 24 h. Small cylindrical samples (4 mm height × 2 mm diameter) were cut and bathed in distilled water at room temperature until constant size. Swelling ratio was calculated from both the height and diameter increase, according to the following equation: $[(V_{wet} - V_{dry}) / V_{dry}] \times 100$, where V_{dry} and V_{wet} are the volumes of the dry and the wet sponges, respectively. Measures were performed with a stereomicroscope at 12 x magnification.

Tensile behavior

Tensile properties were measured in conditioned standard atmosphere at 20 °C, 65% RH with an Instron 5500 R Series IX dynamometer, according to the EN-ISO 5079 standard [222]. Sponges were cut into strips 5 mm width × 20 mm length, and submitted to tensile stress at the constant rate elongation of 10 mm/min. Six samples were measured for tensile strength, modulus and deformation, reporting the average and the standard deviation of the results.

Compression behavior

Compression properties of the sponges were determined in conditioned standard atmosphere at 20 °C, 65% RH with an Instron 5500 R Series IX

dynamometer, according to the CNR standard developed for the evaluation of wool mattresses. Six samples (8 mm diameter, 4 mm thickness) in the conditioned and in the wet state (bathed in distilled water for 2 h, then drained for testing), were submitted to 10 compression cycles (maximum load of 5 N) at the constant deformation rate of 10 mm/min, in order to evaluate also the resilience. Every compression cycle was stopped on reaching 3 mm stroke, starting from the top of the sponge.

Samples were measured for compression force and deformation, reporting the average and the standard deviation of the results.

Cell culture

The human osteosarcoma cell line SAOS-2 was obtained from the American Type Culture Collection (HTB85, ATCC, Manassas, VA, USA). The cells were cultured in McCoy's 5A modified medium with 0.4% L-glutamine and HEPES (Cambrex Bio Science, Baltimore, Maryland), supplemented with 15% foetal bovine serum, 1% sodium pyruvate, 1% antibiotics and 0.2% amphotericin B. The cells were cultured at 37 °C with 5% CO₂, routinely trypsinized after confluency, counted and seeded onto keratin sponges. Before seeding keratin scaffolds were sterilised at 180 °C for 3 h, then equilibrated for 24 h in physiological solution and for three days in culture medium.

Cells were cultured on scaffold for 1, 3 and 7 days changing medium two times *per week*. Cells were cultured on a plastic support as control.

3-(4,5-dimethylthiazole-2-yl)-2,5-diphenyl tetrazolium bromide (MTT) test

The quantitative 3-[4,5-dimethylthiazol-2-yl]-2,5 diphenyl tetrazolium bromide (MTT) test was used to assess the cell viability in all experimental conditions. The MTT solution (0.5 mg/ml) was added to cells for 3 h. Absorbance was measured at 570 nm with a microplate reader (BioRad Laboratories, Hercules, California). The optical density value is directly proportional to the number of viable cells in the culture medium. A standard curve of the cell viability was used to express the results as the number of live cells.

Fluorescein diacetate (FDA) assay

FDA assay was performed at 1 and 7 days of culture on keratin scaffolds to evaluate cell viability. FDA (Invitrogen) is an esterase that freely diffuses into cells and is rapidly esterified to fluorescein once it enters into a viable cell. Briefly, 5 mg/ml FDA stock solution was prepared in acetone: 40 µl stock solution was diluted in 10 ml phosphate buffer solution (PBS) (137 mM NaCl, 2.7 mM KCl, 4.3 mM Na₂HPO₄, 1.4 mM NaH₂PO₄, pH 7.4) and 250 µl was mixed with 500 µl culture medium. Cells were incubated with working solution for ten minutes at room temperature and, before observation, propidium iodide was added to a final concentration of 2 µg/ml to stain dead cell nuclei. Finally, the cells were investigated by a Confocal Laser Scanning Microscope (CLSM) (Leica TCS SP2, Leica Instruments, Germany) acquiring images every 1.5 µm till 100 µm depth.

Scanning Electron Microscopy (SEM) observations

Morphology investigation of the cells supported on the keratin scaffolds was carried out after 1 and 7 days from seeding. Samples were fixed with 2.5% (v/v) glutaraldehyde solution in 0.1 M Na-cacodylate buffer (pH 7.2) for 1 h at 4 °C, washed with Na-cacodylate buffer, then dehydrated at room temperature in a gradient ethanol series up to 100%. Scaffolds were lyophilized 3 h for complete dehydration, then sputter coated with gold (300 nm) and investigated using a Zeiss EVO-MA10 scanning electron microscope (Carl Zeiss, Oberkochen, Germany).

Ageing of wool fibril sponges vs collagen commercial sponges

Wool fibril sponges, previously dried in a ventilate oven at 105 °C to constant mass, were bathed (0.02 g/ml) in the Ringer's solution.

The degradation rate was calculated according to the following equation, expressed as percentage, was determined measuring the weight loss versus time. Swelling ratio from both the height and diameter increase: $[(W_i - W_f) / W_i] \times 100$, where W_i and W_f are the weigh of the sponge samples before and after the ageing test, respectively.

Statistical analysis

Each test was repeated three time at least in the same experimental conditions. Differences between groups were tested by the one-way analysis of variance. The Tukey's test was used to correct for multiple comparisons and statistical relevance was established at two-tailed $p \leq 0.05$. All calculations were generated using the GraphPad Prism 5.0 software (GraphPad Inc., San Diego, California).

2.3. Results and discussion

In this section results and the relative discussion are reported.

2.3.1. Morphological characterization

Wool fibril sponges were prepared by ultrasonic irradiation of wool fibers soaked in clean water, previously swollen in mild alkali.

The disruption of the fiber histological structure produced a suspension of cortical cells (fibrils) into the aqueous protein medium resulting from degradation of the other histological components.

The obtained suspension was submitted to salt-leaching to prepare micro- and macro-porous keratin sponges with the aim of mimicking native tissues for cell proliferation and cell guided tissue formation.

Wool fibril sponges produced are opaque and homogeneous, resilient, and easy to handle (Fig. 2.2).



Figure 2.2: Visual appearance of the wool fibril sponge (in the wet state)

Yellowing of the sponge is due to the thermal stabilization treatment. Figure 2.3 shows the micro and macro porosity structure of the sponge under the scanning electron microscope (SEM). Macroporosity, given by the salt leaching process, shows an even distribution and interconnection both on the surface and in the bulk, as evidenced from the cut edge thickness. The diameter of the holes made by salt leaching ranges from 190 to 560 μm , with average diameter 290 μm and standard deviation 110 μm .

The microporosity is due to the randomly oriented cortical cells stuck to each other by the hydrolysed keratin matrix, is clearly visible in figure 2.3 (c). Cortical cell dimensions and shapes are comparable with literature data on the cortical cells in the original wool [223].

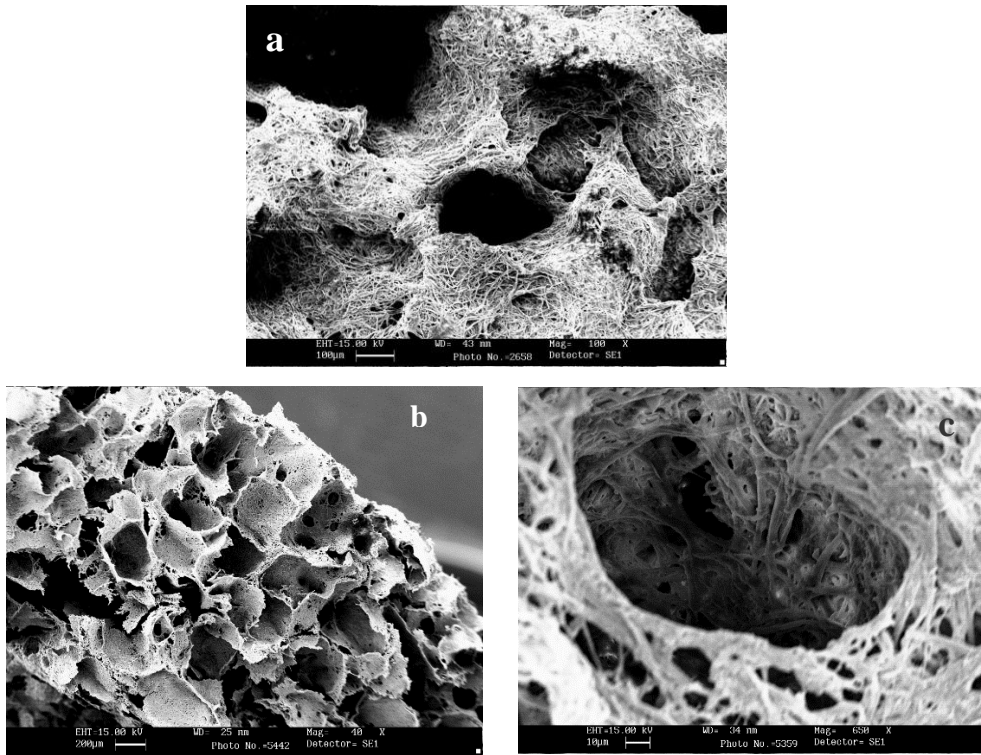


Figure 2.3: SEM images of the keratin wool fibril sponge: surface morphology 100 \times (a), 40 \times cross-section (b) and detail of a pore morphology 650 \times (c)

The cross-section of the sponge shows an even distribution of the macropores whose dimension is suitable for cell guesting, while the micropores should allow feeding of the nutrients and active molecules for cell growing and differentiation.

Wool fibril sponges showed 93% interconnected porosity, with a true density 1.32 g/cm³ (SD: 0.6 g/cm³), compared to the apparent density 0.09 g/cm³ (SD: 0.01 g/cm³).

Based on early studies, the minimum requirement for pore size is considered to be \sim 100 μ m due to cell size, migration requirements and transport. However, pore sizes $>$ 300 μ m are recommended, due to enhanced new bone formation and the formation of capillaries. Because of vascularization, pore size has been shown to affect the progression of osteogenesis. Small pores favored hypoxic conditions and induced osteochondral formation before osteogenesis, while large pores, that are well-vascularized, lead to direct osteogenesis without preceding cartilage formation [45].

2.3.2. Degree of crosslinking

Keratin naturally contains post-transcriptional cystine inter-chain crosslinks made of two cysteine residues; moreover keratin sponges were

submitted to an additional thermal treatment at 180 °C for 2 h, carried out to improve their water stability.

The resulting degree of crosslinking, due to free amino group bonding, was of 42.7 ± 2.1 .

This percentage, obtained by the ninhydrin assay, does not take in account additional crosslinks not involving amino groups.

2.3.3. Amino acid composition

The amino acid composition of the wool fibril sponges was investigated and compared with the amino acid composition of the original wool (Tab. 2.1).

During the preparative hydrolysis with HCl, several amino acid residues are converted or degraded. In particular, asparagines and glutamine are completely converted to aspartic and glutamic acids respectively, tryptophan residues are completely destroyed by the acidic conditions, while methionine, cystine, cysteine and tyrosine undergo partial degradation. Cystine and cysteine are conventionally reported as $\frac{1}{2}$ cystine [224].

Table 2.1: Amino acid composition of the wool fibril sponges compared with the original wool (* $p < 0.001$)

Amino acid	Wool (mol %)	Wool fibril sponges (mol %)
CYA	0,19	0,22
ASP	8,67	8,09
SER	10,49	8,49
GLU	14,89	16,99
GLY	6,26	5,59
HIS	0,58	0,77
ARG	5,99	5,73
THR	5,78	5,24
ALA	5,6	6,24
PRO	6,33	9,29
LANT	0,59*	6,59*
$\frac{1}{2}$ CYS	10,83*	2,39*
TYR	2,36	1,96
VAL	5,66	6,53
MET	0,41	0,5
LYS	3,53	3,94
ILE	3,02	3,22
LEU	6,93	6,8
PHE	1,89	1,41

The main differences in the amino acid composition of the sponges compared with the original wool were the loss of cystine and the formation of lanthionine. Formation of lanthionine (Cys-S-Cys) from cystine (Cys-S-S-Cys) was first reported by Horn *et al.* [225] when they isolated, from wool treated with sodium carbonate, a new amino acid-containing thioether. Indeed, disulfides are unstable under alkaline conditions, resulting in the formation of lanthionine-containing products.

Lanthionine, which results from cystine reaction with mild alkali [226], was found in small amount (0.59 mol%) in the original wool but its amount increased to 6.67 mol% in the wool fibril sponges. At the same time, the amount of 1/2 cystine decreased from 10.83 mol% in the original wool to 2.39 mol% in the sponges. The lanthionine present in the sponges, as well as the remaining cystine, is also responsible for the insolubility of these sponges in aqueous media.

No significant differences related to the other amino acids were detected between the original wool and the sponges.

2.3.4. SDS-PAGE

Evaluation of the molecular weight by SDS-PAGE is carried out in reducing condition to allow the separation of protein chains.

In spite of the attempts, the extraction of the proteins from the wool fibril sponges with the standard SDS-PAGE protocol for keratins was unsuccessful, because lanthionine (thioether) formation prevents solubilisation in reducing agents.

This unsuccessful result in the molecular weight determination is not so surprising, since it is consistent with thioether formation, although the presence of other non-reducible cross-linked species other than thioether linkage could not be excluded [227].

In fact thioether modifications on proteins were originally identified in wool and food proteins treated under alkaline conditions.

The SDS-PAGE was also performed on the suspension of cortical cell before casting that was partially soluble in the reducing buffer, since water evaporation results in additional lanthionine formation.

However, figure 2.4 shows that the suspension of cortical cells remained close to the loading point.

These results confirm the presence of crosslinks, affecting the shape and the molecular size of the proteins that constitute the sponges.

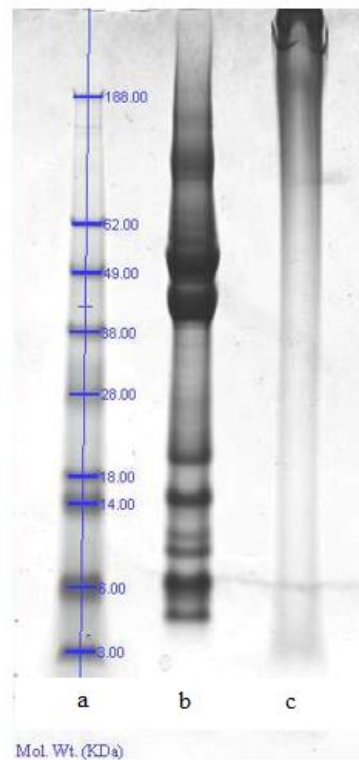


Figure 2.4: SDS-PAGE patterns of suspension of cortical cells immersed in a keratin matrix (c) compared to reference wool (b); (a) molecular marker

2.3.5. PH of the water extract

This test has been carried out in order to exclude the presence of sodium hydroxide traces in the wool fibril sponges, which may negatively affect the pH of the culture media.

The pH of the water extract was 7, confirming the absence of residual alkali released by the sponges to aqueous media.

2.3.6. Thermal analysis (DSC)

Figure 2.5 shows the DSC traces of the wool fibril sponges compared with that of the original wool fibres. Water evaporation results in the large first-order transitions below 100 °C, in both the traces of the original fibres and the sponges.

Moreover, the endothermic peaks between 230 °C and 240 °C are related to denaturation of the crystalline protein domains [226].

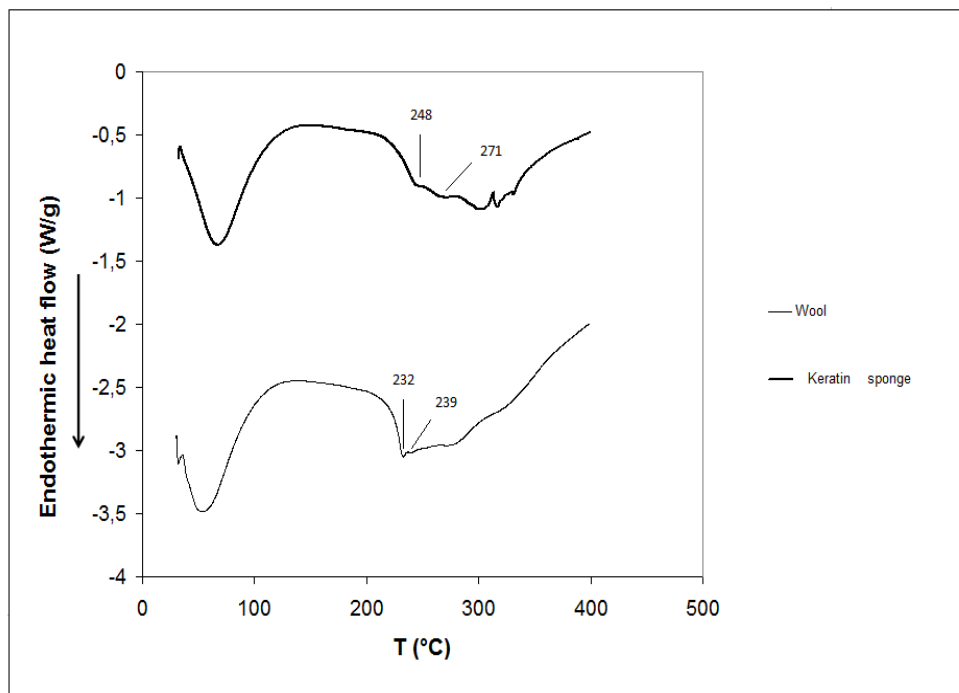


Figure 2.5: DSC thermograms of the wool fibril sponges compared with the original wool fibers

The presence of a bimodal endothermic peak in the denaturation trace of the original wool fiber (a shoulder on the higher temperature side of the trace) is attributed to differences in the transition enthalpy of the α -helical material in the domains of *ortho*- and *para*-cortical cells [228].

More in detail, the cortical cells are made of microfibrils composed of multiple α -helical, low sulphur crystalline subunits (referred to as intermediate filaments) embedded in a matrix containing two non-filamentous protein types, one cystine rich (high sulphur proteins) and the other rich in glycine and tyrosine.

Differences in the cystine (sulphur) content of the matrix lead to the identification of two types of cortical cells: *ortho*-cortical cells, containing a lower proportion of high sulphur matrix material, and *para*-cortical cells, with a higher concentration of disulphide linkages, belonging to two distinctive domains called respectively the *ortho*-cortex, more hydrophilic and the *para*-cortex, with a higher amount of sulphur [229].

As shown in figure 2.5, the thermal transition of the crystallites in the *para*-domains takes place at a higher temperature (239 °C) because of the higher thermal stability of the higher sulphur crosslinked matrix with respect to the *ortho*-domains that denature at 232 °C, resulting in a bimodal denaturation DSC trace. On the other hand, the figure shows that the denaturation of the sponge proteins results into different peaks, shifted to a higher temperature, not related to the bimodal denaturation of *ortho* and *para* domains anymore, but more likely due to the presence of different amounts of lanthionine and isopeptides cross-linked keratins, resulting from the alkali treatment and thermal stabilisation process respectively.

Finally, degradation of all the fibre components occurs at temperatures higher than 300 °C.

2.3.7. Water swelling

Wool fibril sponges significantly swell in water, because of the synergic contribution of hydrophilicity and porosity.

Water dipping caused a volume increase from 24% to 38%; nevertheless, sponges were stable in water for 1 month without structural changes and no weight loss.

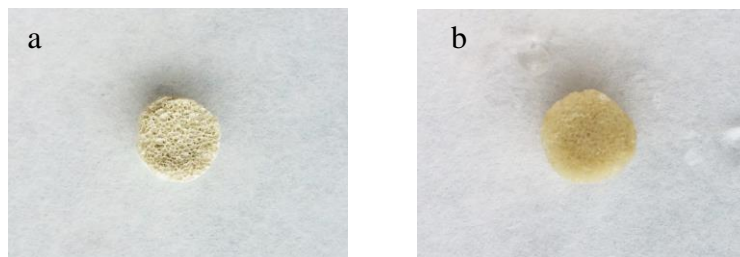


Figure 2.6: Visual appearance of the dry (a) and wet (b) sponge

2.3.8. Tensile behavior

Fig. 2.7 shows the tensile behavior of 6 samples cut from the wool fibril sponges, in terms of relative stress and strain.

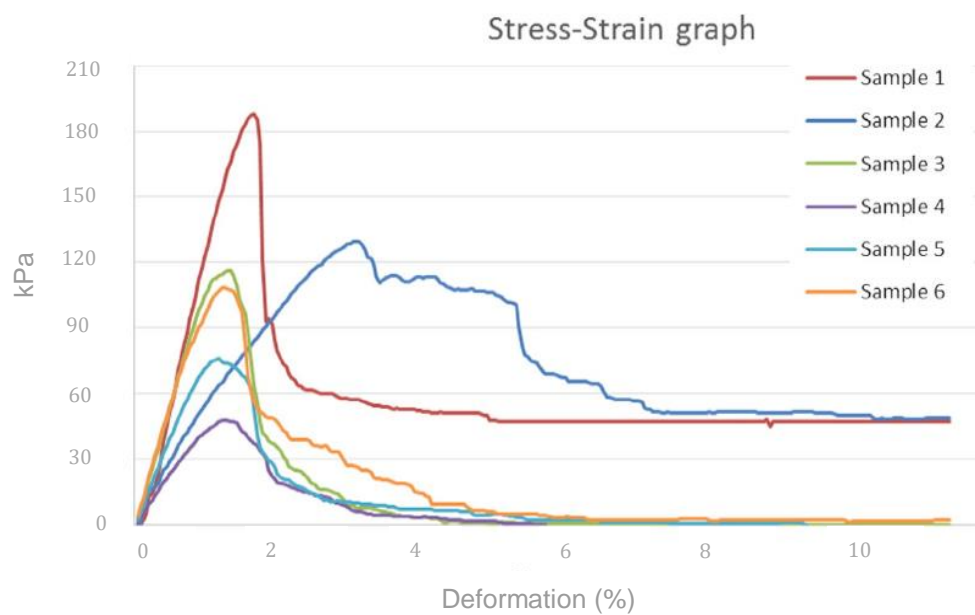


Figure 2.7: Stress-strain behavior of the wool fibril sponges

The average tensile strength calculated on 6 samples was 103 kPa (SD = 30.4 kPa), the average elongation at break was 1.480% (SD = 1.140%) and the average Young's Modulus was 4.420 MPa (SD = 2.760 MPa). There is a large variability among the ultimate tensile strength (force at break) modulus and elongation among the samples. This may be due to the random distribution of the macro-pores originated by salt-leaching.

2.3.9. Compression behavior

For the evaluation of the compression behavior, every sample was submitted to ten repeated compression cycles, in order to measure the resilience performances too.

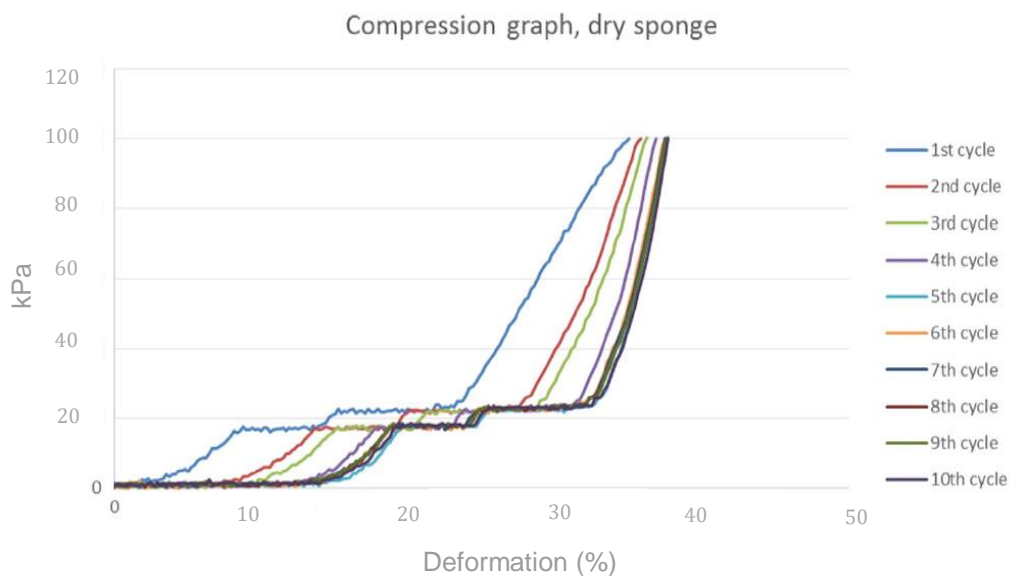


Figure 2.8: Compression behavior of the wool fibril sponges in the dry state.

Figures 2.8 and 2.9 show the compression behavior of samples cut from the wool fibril sponges in the dry state and in the wet state respectively, submitted to 10 repeated compression cycles as previously described. The compression behavior of both the dry and wet sponges is described by two different sloping segments joined by a horizontal line (Fig. 2.8). For the sponge in the dry state the compression moduli from the first to the tenth cycle increase from 19 kPa to 79 kPa (SD = 2.3 and 5.1 kPa respectively) in the compression range from 4 kPa to 14 kPa (first sloping segment), and from 49.7 kPa to 99.4 kPa (SD = 3.2 and 5.1 kPa respectively) in the load range from 30 kPa to 40 kPa (second sloping segment).

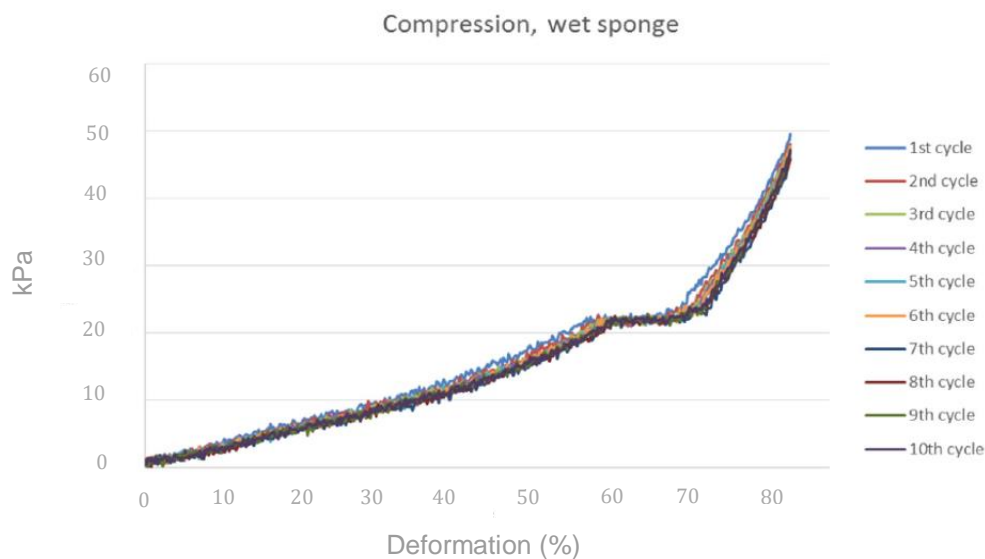


Figure 2.9: Compression behavior of the wool fibril sponges in the wet state.

For the sponges in the wet state the compression moduli in the load ranges from 4 kPa to 14 kPa (first sloping segment) and from 30 kPa to 40 kPa (second sloping segment) remained unchanged from the first to the tenth cycle (7.6 kPa and 25.5 kPa respectively) (SD = 0.2 and 7 kPa respectively), as shown in Fig. 2.9. Both the compression traces of the dry and the wet sponges display a horizontal line most likely due to reversible crushing deformation of the macropore structure, but the wet sponges are more deformable and more resilient since the compression traces are almost overlapping each other and no permanent deformation was detected. In other words, water molecules filled the macro- and micro-pores and also penetrated into the amorphous keratin domains, resulting in increased elasticity of the whole structure.

2.3.10. 3-(4,5-dimethylthiazole-2-yl)-2,5-diphenyl tetrazolium bromide (MTT) test

The SAOS-2 cell line was selected for biocompatibility-cell viability assay [230], since it represents a widely used and well-accepted model for in vitro osteoblast studies.

Fig. 2.10 shows the results of cell viability after 1, 3 and 7 days performed using the MTT assay. MTT is converted to its insoluble, purple, formazan salt by the mitochondrial esterase in live cells. The amount of formazan, photometrically measured, is proportional to the cellular metabolic activity, and therefore to the cell number.

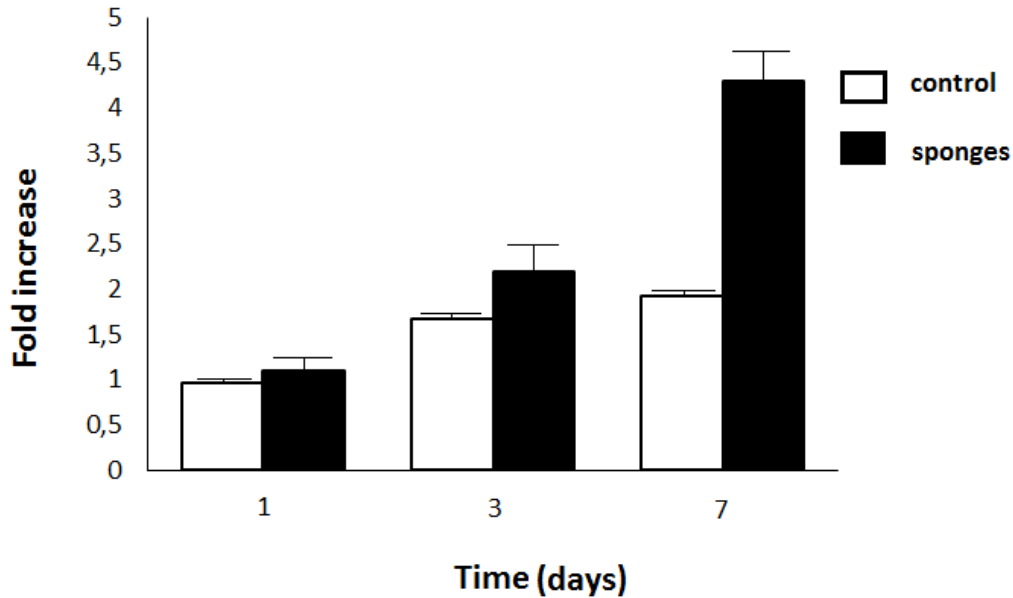


Figure 2.10: Viability of SAOS-2 cells cultured on wool fibril sponges. Viability is expressed as fold increase related to seeded cells for 1, 3 and 7 days, respectively

After 24 h, no significant difference in the cell viability was observed with respect to the seeded cells, suggesting a complete adhesion of the cells onto the wool fibril sponges. Consistent cell proliferation ($p \leq 0.05$) was reported for longer incubation times, showing a 2-fold and 4-fold increase after 3 and 7 days, respectively.

As can be seen in figure 2.10, cells seeded on the control plastic sheet showed a lower rate of proliferation compared to the wool fibril sponge. Both the cellular-binding motifs, that mimic the sites for cell attachment found in the native extra-cellular matrix, and the micro- and macro-porosity of the sponge, contributed to the good cell response.

2.3.11. Fluorescein diacetate (FDA) assay

Figure 2.11 shows representative CLSM images of SAOS-2 cells stained with FDA assay at 1, and 7 days culture.

Cells show the typical SAOS-2 cells morphology indicating that wool fibrils sponges did not affect the SAOS-2 proper growth (Fig. 2.11).

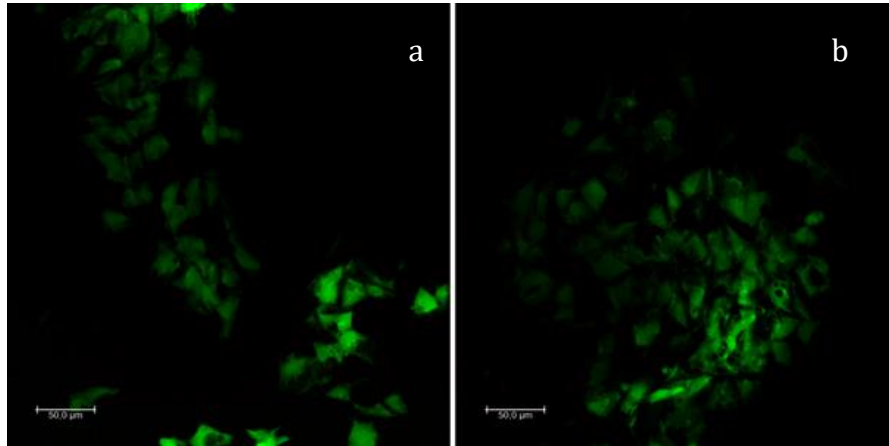


Figure 2.11: Representative CSLM images 400× with FDA staining at 1 day (a) and 7 days (b), respectively

2.3.12. Scanning Electron Microscopy (SEM) investigation

These results were confirmed by the SEM images after 24 h and 7 days as reported in Fig. 2.12 (a) and 2.12 (b), respectively.

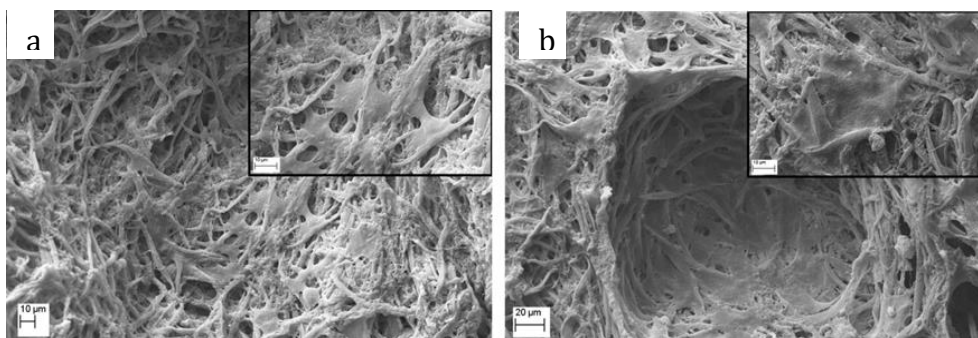


Figure 2.12: Representative SEM images of SAOS-2 cells cultured wool fibril sponges: for 1 day (a) and 7 days (b) 1000x; inset: 3000x

After 24 h, the cells were widely spread on the cortical cell network of the wool fibril sponges showing the typical morphology of the SAOS-2 cell line (Fig. 2.12 (a) and inset). At day 7, the wool fibril sponges resulted completely

coated by the cells; in particular, the cells were found even in the pores (Fig. 2.12 (b) and inset).

In summary, the wool fibril sponges made of keratin contain cellular-binding motifs that mimic the sites of cell attachment found in the native extracellular matrix components, which facilitate better growth via providing proliferation signals to the cells, and minimise apoptotic cell death [231].

2.3.13. Ageing of wool fibril sponges vs commercial collagen sponges

Keratin extracted from wool is biodegradable *in vitro* (by trypsin) and *in vivo* (by subcutaneous embedding in mice) [105].

Commercial collagen sponges have been taken as the reference polymeric material, to compare the ageing behavior of wool fibril sponges.

Collagen, the prevalent protein naturally produced by fibroblasts, provides strength and structural stability to tissues throughout the body including skin, blood vessels, tendon, cartilage and bone.

Along with hydroxyapatite, collagen is one of the two major components of bone [232].

Gingostat sponge-like material (Fig. 2.13) is used in dental surgical procedures as a resorbable material for placement in the area of dental implants and bone defects reconstruction. Gingostat sponges are made of native collagen and show haemostatic properties (keratin too).



Figure 2.13: Gingistat collagen sponges [233]

Figure 2.14 shows collagen and wool fibril sponges respectively.



Figure 2.14: Visual appearance of collagen sponge (left) and wool fibril sponge (right)

Collagen and wool fibril sponge were immersed into the Ringer's solution (ageing reference solution for bone biomaterials) at 37 °C [234-236].

The degradation rate of collagen sponges was significantly higher compared to the wool fibril sponge degradation rate.

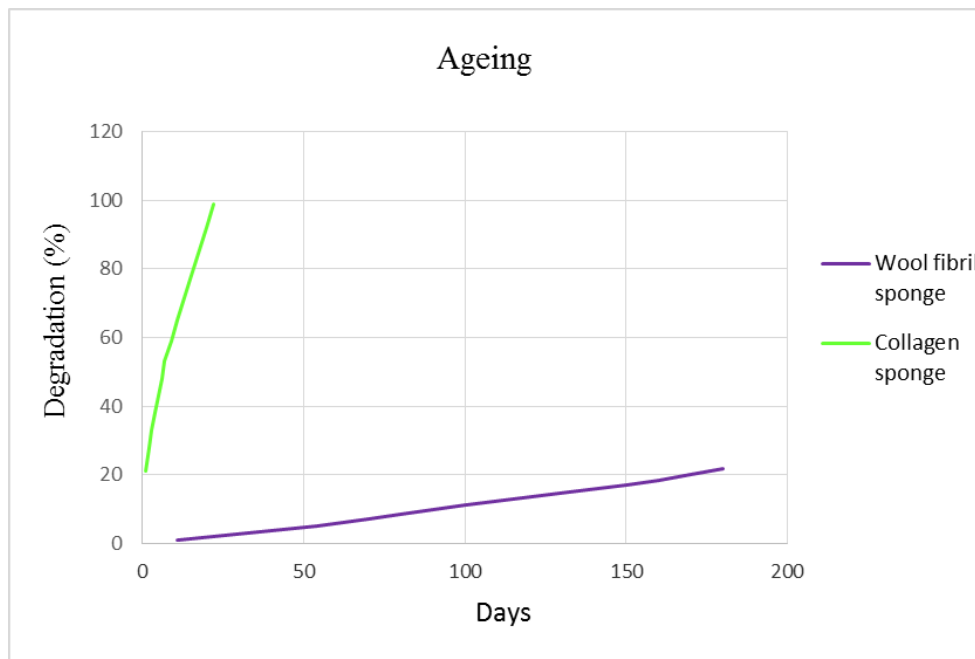


Figure 2.15: Degradation rate of the commercial collagen sponge (GINGISTAT) vs wool fibril sponge.

The collagen sponge degraded completely in 22 days compared to the wool fibril sponge that, after 180 days, showed a degradation rate of 22 % only (Fig. 2.15).

The longer degradation rate show that wool fibril sponges can be a promising material for long term support of bone formation *in vivo*.

2.4. Conclusions

In this part of the research work, novel 3D keratin bio-composite sponges have been produced from wool fibrils, with highly interconnected micro and macro-porosity, tailored to match the natural bone tissue features.

Mechanical properties of the wool fibril sponges come out in favour of promising applications as bio-absorbable scaffold for bone tissue engineering, since they are easy to handle and resilient in wet conditions.

The wool fibril sponges contain cellular-binding motifs that mimic the sites of cell attachment found in the native extra-cellular matrix components, which facilitate better growth providing proliferation signals to the cells, and minimise apoptotic cell death demonstrated by biocompatibility-cell viability assay with SAOS-2.

Finally, ageing tests revealed that wool fibril sponges, characterized by an exceptional amount of crosslinks that stabilize the keratin structure, are surpassingly stable, showing longer degradation rate compared to commercial collagen sponges, suggesting promising applications for long term support of bone formation *in vivo*.

Chapter 3

Wool fibrils sponges and Pulsed Electromagnetic Field (PEMF)

3.1. Aim of the work

The aim of the work of this experimental part is the evaluation of the effects exerted by the wool fibril sponges structure joined to the pulsed electromagnetic field stimulus, on the proliferation and differentiation of SAOS-2 cells, cultured in both proliferative and osteogenic media.

3.2. Bone remodeling

Bone formation can be divided into two different steps: modeling and remodeling [237].

Modeling consists in bone formation occurring during development and allows individual bones to grow in size and to shift in space.

Remodeling is mainly a local, lifelong homeostatic process involving tissue renewal, where old bone, the matrix included, is resorbed by osteoclasts. Subsequently there is a deposition of new bone by osteoblasts. It is mainly a local process. Remodeling replaces the matrix but it leaves the shape, internal architecture, and mineral content unchanged. In healthy young adults, the total bone mass remains constant, indicating that the rates of bone formation and resorption are equal.

This physiological process is fundamental for bone health [238]. It repairs the damage resulting from repeated stresses by fixing small cracks or deformities and prevents accumulation of an excess of old bone which can lose during time its mechanical performances.

Factors influencing bone remodeling

The remodeling process is regulated by all the following factors [239]:

- genetic factors - genes determine bone's response to factors influencing bone remodeling;
- mechanical factors - mechanical stimulus influences the gene expression during ossification stages;
- vascular factors - vascularization is essential for normal bone development (supplying blood cells, oxygen, minerals, ions, glucose, hormones and growth factors);
- nutritional factors - excess of salt, caffeine, alcohol and nicotine, reduce the calcium intake resulting in increased bone resorption.
- hormonal factors - the endocrine system produces hormones regulating bone remodeling;
- other factors - growth factors and cytokines regulate bone remodeling.

Bone mechanotransduction

Mechanical stimulus is one of the important regulators of bone remodeling, since it can influence the physiological processes at molecular, cellular, or systemic level. This conversion of mechanical stimuli into biochemical responses is referred to mechanotransduction [240].

Mechanical forces can cause a number of short or long-term biochemical processes inside a cell, such as gene induction, protein synthesis, cell proliferation, apoptosis, and cell differentiation to maintain proper physiological conditions. Anomalous mechanical forces alter cellular functions, leading to pathologies [241].

The relationship between mechanical stimulus and bone remodeling was first suggested by Wolff in 1892 in his famous law: "*Bone remodels in response to the mechanical stresses it experiences so as to produce an anatomical structure best able to resist the applied stress*" [242]. In addition, Frost proposed that there is a certain physiological threshold and when stress is below it, bone resorption occurs; on the contrary, bone formation occurs above the threshold.

Both osteoblasts and osteoclasts are capable of directly sensing the mechanical stimulus and regulating their biochemical activity accordingly [243-244].

A global bone strain moves the extracellular fluid through the lacuno-canalicular network (Fig. 3.1); hence the gene expression of the cells is mechanically regulated by the extracellular fluid flow shear stress.

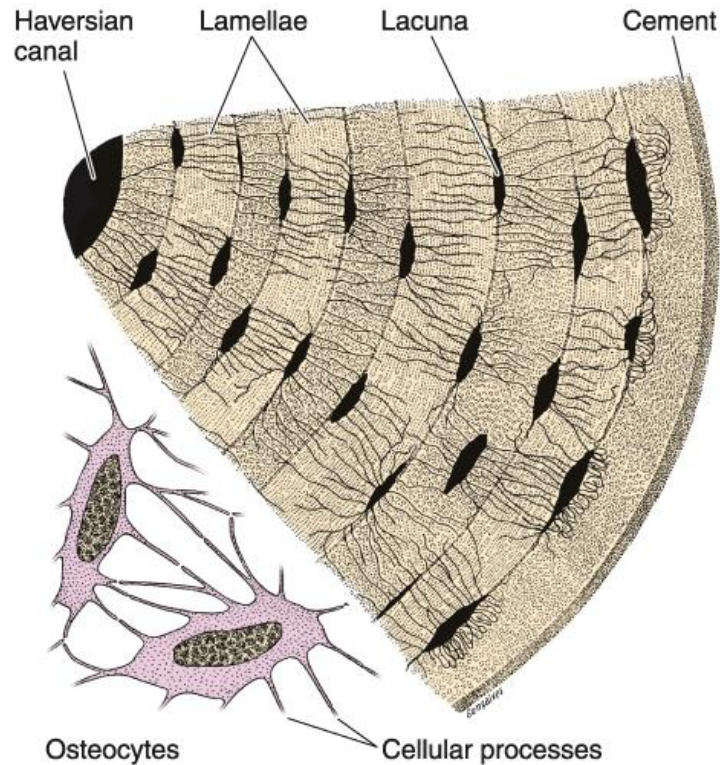


Figure 3.1: Schematic drawing of two osteocytes and part of a haversian system. Collagen fibers of contiguous lamellae are sectioned at different angles [245]

The osteocytes are embedded in a mineralized bone matrix: this 3D network of lacunae, containing cellular bodies and canaliculi is permeable to bone extracellular fluid [246-247]. A global bone deformation moves the extracellular fluid through the lacuno-canalicular porosity, in such a way that osteocytes are submitted to a fluid flow shear stress [248-255]. When the bone is loaded, the extracellular fluid is squeezed, so fluid flow shear stress is produced onto the membrane of the osteocytes.

This shear stress can modulate the gene expression of the bone cells more efficiently than other mechanical forces (i.e. hydrostatic compression and substrate deformation) [256-257]. *In vitro* mechanical stimulation influences the level of alkaline phosphate, cAMP, intracellular calcium, nitric oxide, PGE₂, c-fos, COX-2, osteopontin and osteocalcin [258-261].

The structural environment, inside and outside cells, gives the instructions to modulate the gene expression. [262-273].

The bone cells adhere to extracellular matrix by focal adhesion integrins and to themselves by adherent junction cadherins [274-275]. Integrins and cadherins are the mechanical bonds of the mechanotransduction system.

The action of the shear stress on stretch-activated ion channels, voltage-sensitive calcium channels, cytoskeleton, and other architectural subjects, is

translated into biochemical information targeting specific genes by load-bearing mechanosomes: the genes are those of *c-fos*, *COX-2* and bone matrix proteins (Fig. 3.2) [275-276].

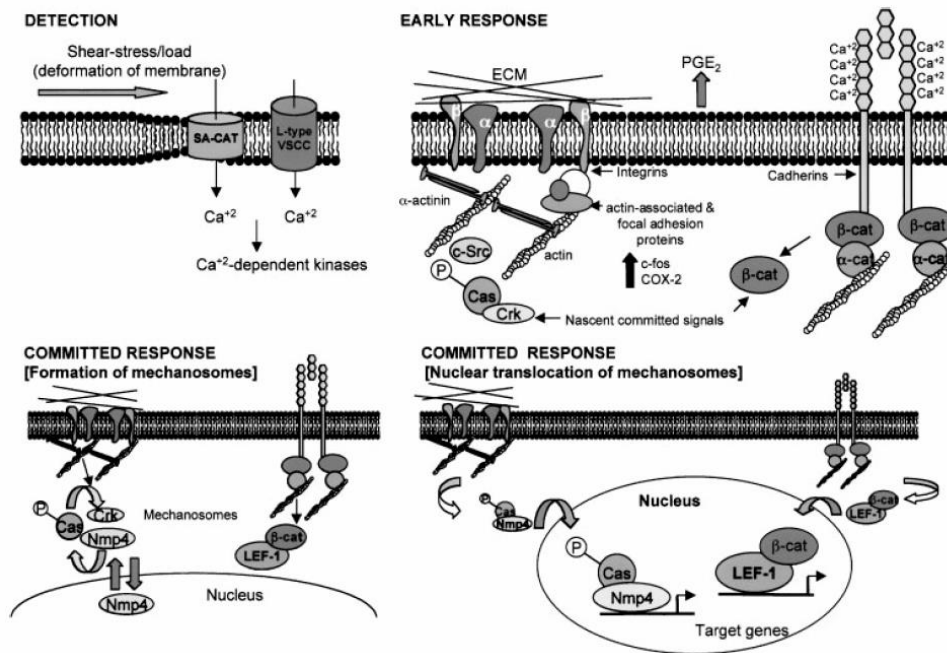


Figure 3.2: Translation of physical stimulation into biochemical signals and gene expression [275]

Bone remodeling by electromagnetic stimulus

Electromagnetic fields regulate, in connective tissue cells, the DNA synthesis and the expression of genes for extracellular matrix proteins. *In vitro* studies have shown the effects of an electromagnetic stimulation on the metabolism of bone cells in terms of increased proliferation and increased type-1 collagen synthesis [277-278].

In vivo studies have drawn attention to the ability of applied electromagnetic fields to heal bone defects, osteotomies, fresh fractures and fracture non-unions [279-281].

Numerous observations suggest that cell responsiveness to the electromagnetic fields is accompanied by increases in cytosolic calcium concentration and might involve calcium/calmodulin pathway (Fig. 3.3) [282-283].

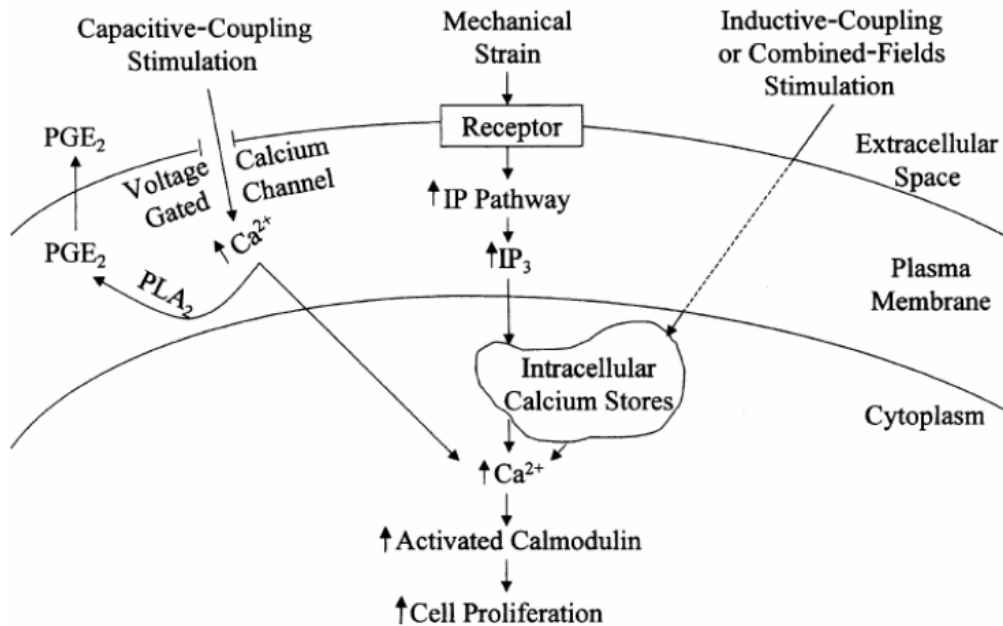


Figure 3.3: Translation of electromagnetic and mechanical stimulation into biochemical signals [283]

The electromagnetic stimulation increases the calcium influx [284] and the inhibition of voltage-gated calcium channels, with channel blockers, abolishes the proliferation response of the bone cells [285]. Studies based on signal transduction inhibitors explain the electromagnetic modulation of cellular metabolism by means of calcium translocation through voltage-gated calcium channels and by means of intercellular calcium release, leading to increase in cytosolic calcium, activated calmodulin, and prostaglandin secretion (Fig. 3.3) [286-287].

According to Pavalko's diffusion-controlled/solid-state signaling model (fig. 3.2), the increase of the cytosolic calcium concentration is a starting point of signaling pathways targeting specific genes of the bone matrix [275].

Pulsed electromagnetic fields are clinically successful in promoting healing of bone defects, suggesting that a modulation of growth factor and morphogenic protein production may be involved [288-293].

3.3. Models and numerical dosimetry inside an electromagnetic bioreactor

The following brief introduction describes the currents induced by the Pulsed Electromagnetic Field into the bioreactor, calculated by numerical dosimetry.

A numerical dosimetry inside the electromagnetic bioreactor is a very useful tool to evaluate the specific and effective physical stimulus transduced by the cells *in vitro*, not only by describing the local time-dependent magnetic field, but also by discussing the local hydrostatic forces (perpendicular to the cell membranes) and the local shear forces (parallel to the cell membranes), both caused by the magnetic field to evaluate in detail forces that have a role in the tensegrity-mechanotransduction theory of Ingber [294].

Previous work carried out by Mognaschi *et al.* [295] proposed a model for the theoretical link between the electromagnetically induced mechanical forces and the biological mechanism of the cell tensegrity.

Figure 3.4 shows an electromagnetic bioreactor, based on two solenoids (i.e. air-cored Helmholtz coils) connected in series and powered by a pulse generator. The solenoids have a quasi-rectangular shape and their planes are parallel with a distance of 10 cm, so that the cell cultures can be placed 5 cm away from each solenoid plane. The setup is based on the theory of the Helmholtz coils, that is, in order to optimize the spatial homogeneity of the magnetic field, especially in the central region where the cells are stimulated, the two coils should be supplied by the same current (i.e. with same magnitude and direction) and their dimensions and distance should be comparable (in particular, the coils diameter and distance should be equal if the coils have a circular shape).

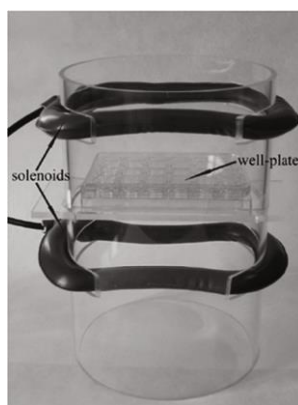


Figure 3.4: Electromagnetic bioreactor. Solenoids of the electromagnetic bioreactor with a culture well-plate in the central region [295]

Figure 3.5 shows the electric measurement simultaneously performed, of two coils powered via a Burndy connector, of which two terminals are used for

delivering current to the coils. The pulse generator fed the two 1000-turns coils in series by a nearly square-wave voltage (frequency equal to 75 Hz), whereas the resulting current in the coils' wire ranged from 0 to about 319 mA in 1.36 ms (under a finite element viewpoint, this current was equivalent to 0–319 A in 1.36 ms flowing in each winding).

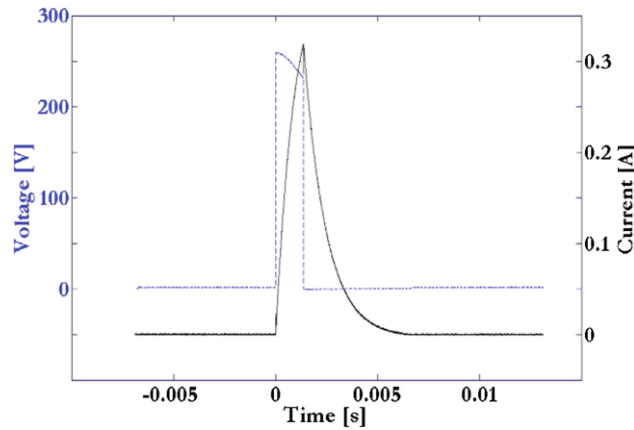


Figure 3.5: Electric measurements. Measurements of current (black continuous line) and voltage (blue dashed line) [295]

This current generates a time varying and homogeneous magnetic induction (frequency = 75 Hz), according to the Faraday-Neumann-Lenz and the Lorentz laws [296].

This induced field, inside the cylindrical culture well-plate, generates a concentric and planar distribution of induced electric currents with corresponding induced distribution of radial mechanical forces: in the range 0–1.36 ms the magnetic induction was arising, the currents clockwise, and the radial mechanical forces inwardly directed (i.e. compression); whereas, on the contrary, during the temporal range 1.36–6 ms, the magnetic induction was decreasing, the currents anticlockwise, and the radial mechanical forces outwardly directed (traction) (Fig. 3.6).

The preceding analytical solution was numerically confirmed and the forces were comparable to those applied in the study of cellular mechanics [297]; so, the seeded cells were also stimulated with time varying mechanical forces acting onto their plasma membrane at the frequency of 75 Hz.

Thanks to this model it was possible to state that inside this electromagnetic bioreactor, as shown in figure 3.6, the magnetic induction was able to produce time varying mechanical forces acting perpendicularly or tangentially onto the cell membrane; as a consequence, these forces were able to modulate the cell tensesgrity via tensile and compressive deformations [294].

It is known that fluid tension (i.e. traction) and compression affect the cell tensesgrity of osteoblasts.

This study has performed a detailed numerical dosimetry inside our extremely-low-frequency electromagnetic bioreactor which has been successfully used in *in vitro* biotechnology and tissue engineering researches

[298-305] and has been applied to the experimental work carried out in this thesis.

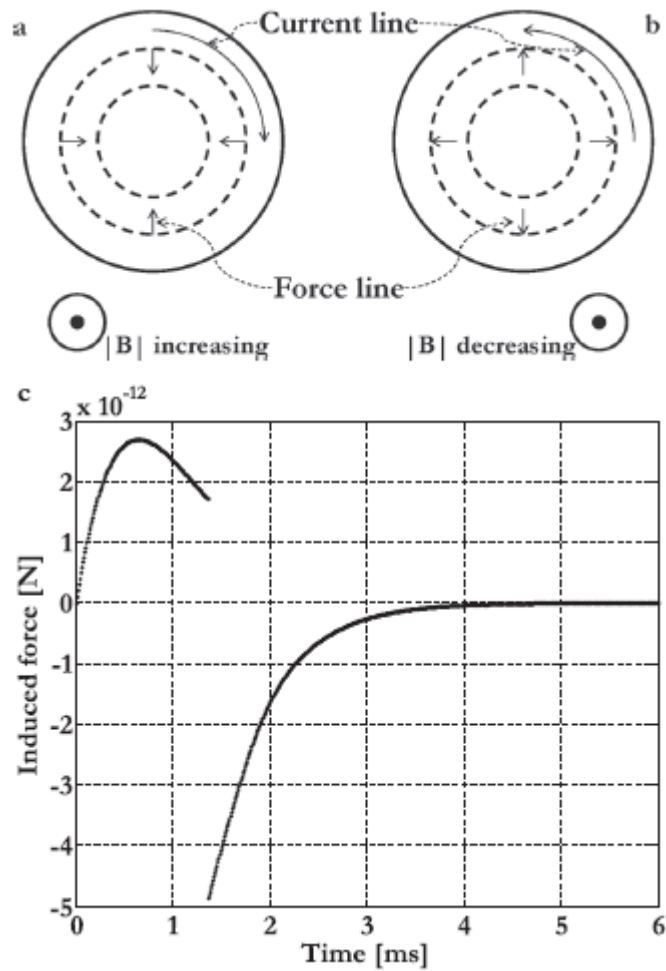


Figure 3.6: Induced electric currents and induced mechanical forces. Induced electric currents (the actual current direction is shown) and induced mechanical forces inside the culture wells during the temporal ranges 0–1.36 ms (a) and 1.36–6 ms (b). Temporal pattern of the induced force inside the culture wells during the time range 0–6 ms (sign convention: compression force > 0 N, traction force < 0 N) (c) [295]

3.4. Materials and methods

All methods previously described will not be described again in this paragraph. Please see paragraph 2.2.

Electromagnetic bioreactor apparatus

The electromagnetic bioreactor consisted of a supporting structure custom-designed in a tube of polymethylmethacrylate; the windowed tube had a well-plate and two solenoids (Helmoltz coils), the planes of which were parallel [298]. In this experimental setup, the magnetic field and the induced electric field were perpendicular and parallel to the scaffold surfaces, respectively. The cell surfaces were 5 cm away from the solenoid plane, and the solenoids were powered by a Biostim SPT pulse generator (Igea, Carpi, Italy), which generated PEMF. Given the position of the solenoids and the characteristics of the pulse generator, the electromagnetic stimulation had the following parameters: magnetic field intensity equal to 2 ± 0.2 mT, induced electric tension amplitude equal to $5 - 1$ mV, signal frequency of 75 ± 2 Hz, and pulse duration of 1.3 ms [300].

The magnetic field was measured with a Hall Effect transverse gaussmeter probe (Sypris Solutions, Louisville, KY) and gaussmeter (Laboratorio Elettrofisico, Milan, Italy), the induced electric tension was measured with a standard coil probe, and the temporal pattern of the electromagnetic signal was evaluated by a digital oscilloscope (LeCroy, Chestnut Ridge, NY).

In clinical settings the PEMF parameters were similar, but a period of 30–40 min represented the exposure time for tissues or organs. The PEMF biological effect was directly evaluated on SAOS-2 cells and the exposure time was determined experimentally. In our experimental settings, the electromagnetic bioreactor was placed into a standard cell culture incubator in a 37 °C, 5% CO₂ environment.

3.4.1. Characterization methods

Confocal Laser Scanning Microscope (CLSM) analysis was performed after 24 h from cell seeding on the wool keratin sponges. All the other experiments were performed after 21 days of culture in proliferative medium (PM), with and without PEMF, and in osteogenic medium (OM), with and without PEMF.

Cell culture

The human osteosarcoma cell line SAOS-2 was obtained from the American Type Culture Collection (HTB85, ATCC, Manassas, VA, USA). The cells were cultured in McCoy's 5A modified medium with 0.4% L-glutamine and HEPES (Cambrex Bio Science, Baltimore, Maryland), supplemented with 15% foetal bovine serum, 1% sodium pyruvate, 1% antibiotics and 0.2% amphotericin B.

The cells were cultured at 37 °C with 5% CO₂, routinely trypsinized after confluency, counted and seeded onto keratin sponges. Before seeding keratin scaffolds were sterilised at 180 °C for 3 h, then equilibrated for 24 h in physiological solution and for three days in culture medium.

Cells were cultured on scaffold for 1, 3 and 7 days changing the culture medium two times per week.

For osteogenic differentiation analysis, dexamethasone and β-glycerophosphate (both osteogenic factors) were added to the previously indicated medium at the concentration of 10⁻⁸ M and 10 mM, respectively. Ascorbic acid, another osteogenic supplement, is a component of the McCoy's 5A modified medium. Before cell seeding, scaffolds were sterilized at 180 °C for 3 hours, then washed twice in PBS for 10 min and incubated O.N. in cell culture medium. The cells were cultured at 37 °C, 5% CO₂, routinely trypsinized after confluence, counted, and seeded at a density of 4×10⁵ cells/scaffolds in 48-well plates.

Cytoskeleton organization

After 24 hours culture, cell-seeded scaffolds were washed with phosphate-buffered saline (PBS, pH 7.4), fixed with 4% (w/v) paraformaldehyde solution for 30 min at 4 °C, and permeabilized with 0.1% Triton X-100. In order to visualize the f-actin cytoskeleton organization, cells were then stained with Tetramethylrhodamine B isothiocyanate (TRITC) phalloidin conjugate solution (10 µg/ml, EX/EM maxima ~ 540/575) in PBS for 40 min at RT. Following extensive washes in PBS, nuclei were counterstained with Hoechst 33342 (2 µg/ml). Finally, samples were observed with a confocal fluorescence microscope (Leica TCS SPII Microsystems, Bensheim, Germany).

Phosphate determination

A commercially available kit system (Phosphate Colorimetric Assay Kit) was used to quantify inorganic phosphate levels. The cell-seeded scaffolds were washed with TBS, and chilled on ice in cold TBS for 15 min. Samples were then sonicate cells for 50 s 3 times at high setup (50 KHz and 250 W) in pulsed mode (30 s sonication – 10 s break – 10 s sonication). The samples were then centrifuged for 15 min at 4 °C at top speed using a cold microcentrifuge to remove any insoluble material. Supernatant was collected and transferred to a clean tube. The supernatant was diluted 1:10 with distilled water. At the end of reaction, absorbance reading was performed at 655 nm with a microplate reader (BioRad Laboratories). Samples were run in triplicate and compared against the standard solution calibration curve. The amount of phosphate from samples was expressed as pmol/(cellsxwell).

Calcium quantification (calcium-cresolphthalein complexone method)

On day 21 of culture, the calcium deposition from PEMF stimulated and unstimulated samples cultured either in PM or OM was determined by the calcein detection and calcium cresolphthalein complexone methods.

The calcium content of each sample was assayed to quantify the amount of mineralized matrix present and was measured using a Calcium Fast kit (Mercury SpA, Naples, Italy) according to the manufacturer's instructions. The colorimetric end point assay measures the amount of purple-colored calcium-cresolphthalein complexone complex formed when cresolphthalein complexone binds to free calcium in an alkaline solution. Briefly, an aliquot (1 ml) of 1 N HCl was added to each sample and incubated for 24 h at RT to release calcium into solution. The sample supernatant was diluted 1/10 with the Assay Working Solution previously prepared by mixing equal parts of calcium-binding reagent and calcium buffer reagent provided by the kKit. Ca²⁺ standards in concentrations ranging from 0 to 10 mg/ml were prepared from dilutions of a 100 mg/ml stock solution of Ca²⁺. The absorbance reading was performed at 595 nm with a microplate reader (BioRad Laboratories) using 100 µl of standard or sample placed into individual wells of a 96-well plate. Samples were run in triplicate and compared against the standard solution calibration curve.

EDX

Energy-dispersive x-ray spectroscopy (EDX) was performed to assess the presence of calcium element in the scaffolds in the different culture conditions.

ELISA

On day 21 of culture, in order to evaluate the amount of extracellular matrix proteins produced by PEMF stimulated and unstimulated samples cultured either in PM or OM, an ELISA assay was performed. The samples were washed extensively with sterile PBS to remove culture medium and then incubated for 24 h at 37 °C with 1 ml of sterile sample buffer (20 mM Tris-HCl, 4 M GuHCl, 10 mM EDTA, 0.066% (w/v) sodium dodecyl sulphate (SDS), pH 8.0). At the end of the incubation period, the total protein concentration was evaluated with the BCA Protein Assay Kit (Pierce Biotechnology Inc., Rockford, Illinois). Calibration curves to measure COL-I, COL-III, DEC, OP, OC, OSN, FN, BMP-2 and ALP were performed as previously described [306]. The amount of extracellular matrix constituents from samples was expressed as pg/(cellsxwell).

Alkaline Phosphatase (ALP) activity

On day 21 of culture, the alkaline phosphatase (ALP) activity from PEMF stimulated and unstimulated samples cultured either in PM or OM was evaluated by a colorimetric end point assay. The assay measures the conversion of the colorless substrate p-nitrophenol phosphate (PNPP) by the enzyme ALP to the yellow product p-nitrophenol, where the rate of the color change corresponds to the amount of enzyme present in the solution. An aliquot (1 ml)

of 0.3 M PNPP (dissolved in glycine buffer, pH 10.5) was added to each sample at 37 °C. After incubation, the reaction was stopped by the addition of 100 ml 5 M NaOH. Standards of PNPP in concentrations ranging from 0 to 50 mM were freshly prepared from dilutions of a 500 mM stock solution and incubated for 10 min with 7 U of ALP previously dissolved in 500 ml of water. The absorbance reading was performed at 405 nm with a microplate reader (BioRad Laboratories, Hercules, California) using 100 ml of standard or sample placed into individual wells of a 96-well plate. Samples were run in triplicate and compared against a calibration curve of p-nitrophenol standards. The enzyme activity was expressed as μ moles of p-nitrophenol produced per minute per μ g of enzyme.

Statistical Analysis

Each test was repeated three time at least in the same experimental conditions. Differences between groups were tested by the one-way analysis of variance. The Tukey's test was used to correct for multiple comparisons and statistical relevance was established at two-tailed $p \leq 0.05$. All calculations were generated using the GraphPad Prism 5.0 software (GraphPad Inc., San Diego, California).

3.5. Results and discussion

3.5.1. 3-(4,5-dimethylthiazole-2yl)-2,5-diphenyl tetrazolium bromide (MTT) test

PEMF dose screening

In order to evaluate the best operative conditions for PEMF application, a set of experiments was performed.

Hence, SAOS-2 cells were submitted to PEMF treatments consisting in different dose and time of application: 1 h only on the first day, 4 hours only on the first day, 1 h every day or 4 h every day of culture.

Cell viability in different PEMF treatment conditions was analyzed by MTT test.

PEMF Treatments Legend:

1h Fd : 1 hour First day

4hFd : 4 hours First day

1h Ad : 1 hours All days

4h Ad : 4 hours All days

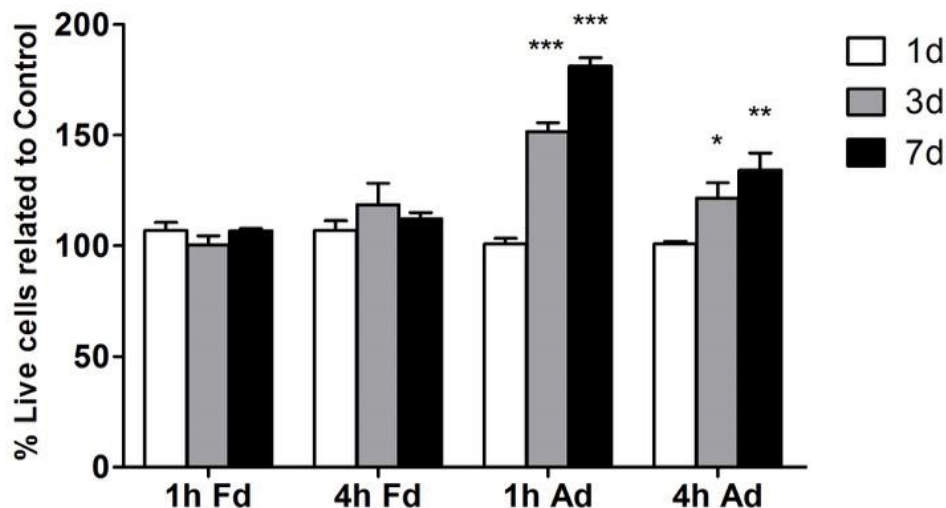


Figure 3.7: Viability of SAOS-2 cells cultured on wool fibril sponges expressed as % of live cells treated with different PEMF applications related to control (untreated). Results are presented as an average \pm standard deviation (ns $p > 0,05$, * $p < 0,05$ ** $p < 0,01$; *** $p < 0,001$)

After one day culture no differences in cell viability has been detected. On day 3, significant differences have been observed in cell viability of cell treated with PEMF for 1 hour or 4 hours every day. After 7 days culture higher

significant positive results have been obtained when cells are exposed to PEMF one hour everyday (Fig. 3.8).

For this reason, this PEMF dose have been selected to perform the subsequent experiments.

Cell viability in response to PEMF stimulus

In this step of the experimental work, SAOS-2 cells have been cultured in both proliferative and osteoinductive media and the PEMF stimulus on proliferation in both culture conditions (PM and OM) was analyzed.

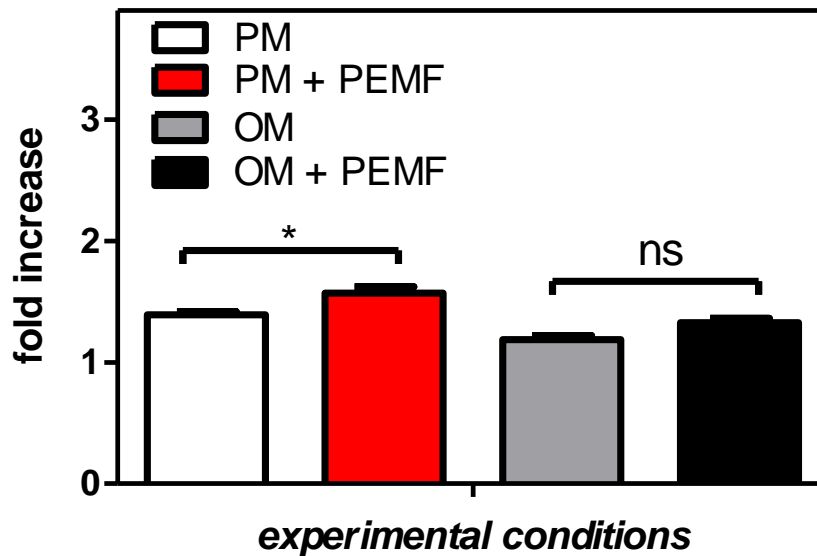


Figure 3.8: Viability is expressed as fold increase related to adherent cells at 21 days from seeding. Results are presented as an average \pm standard deviation (ns $p > 0.05$; $*p < 0.05$)

Figure 3.8 shows an efficient and significant increase in proliferation given by PEMF application when SAOS-2 cells are cultured in proliferative conditions, corroborating previous data [300].

Electromagnetic exposure increased Ca^{2+} currents due to overexpression of voltage-gated Ca^{2+} channels; this is an occurrence that may be well correlated with proliferative events [307].

3.5.2. Cytoskeleton organization

SAOS-2 cells morphology and organization have been evaluated. In figure 3.9 cells cultured on wool fibril sponges can be seen, showing their typical morphology with the cytoskeleton organization in evidence.

Figure 3.9 (a') is an orthogonal view of the CLSM image showing that cells are organized in different planes demonstrating their presence and growth not only on the sponge surface but in its inner part too.

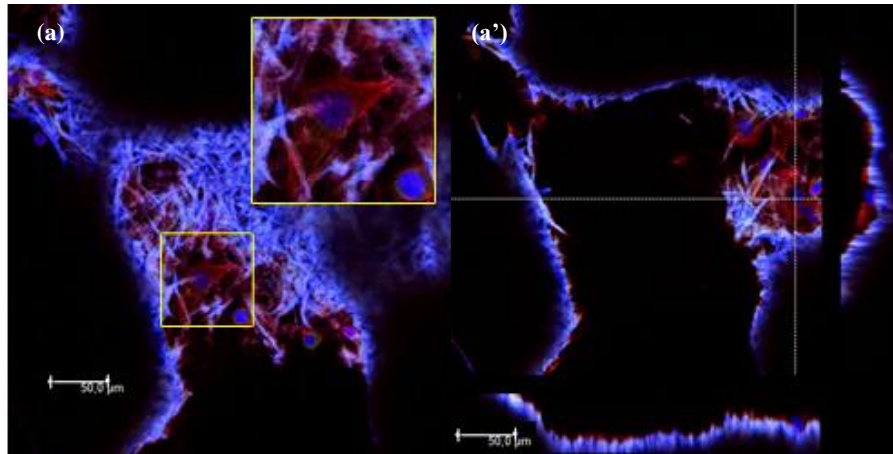


Figure 3.9: Morphological analysis of osteoblast-like cells seeded on keratin scaffold after 24 h of culture (PM). The cytoskeleton organization was observed by F-actin staining with Phalloidin-TRITC (red); Cells nuclei were counterstained with Hoechst 33342 (2 $\mu\text{g}/\text{mL}$, blue) and observed by Confocal Laser Scanning Microscopy (CLSM) (a). Magnified area of cells is shown in inset. Orthogonal view of CLSM image is shown (a'). Scale bar = 50 μm

3.5.3. Fluorescein diacetate (FDA) assay

A viability test of SAOS-2 cells cultured in different conditions was carried out.

Figure 3.10 shows representative CLSM images of SAOS-2 cells stained with the FDA assay at 21 days culture.

In every condition, stained cells showed the typical SAOS-2 cells morphology indicating that wool fibrils sponges do not affect the SAOS-2 proper growth and differentiation (Fig. 3.10).

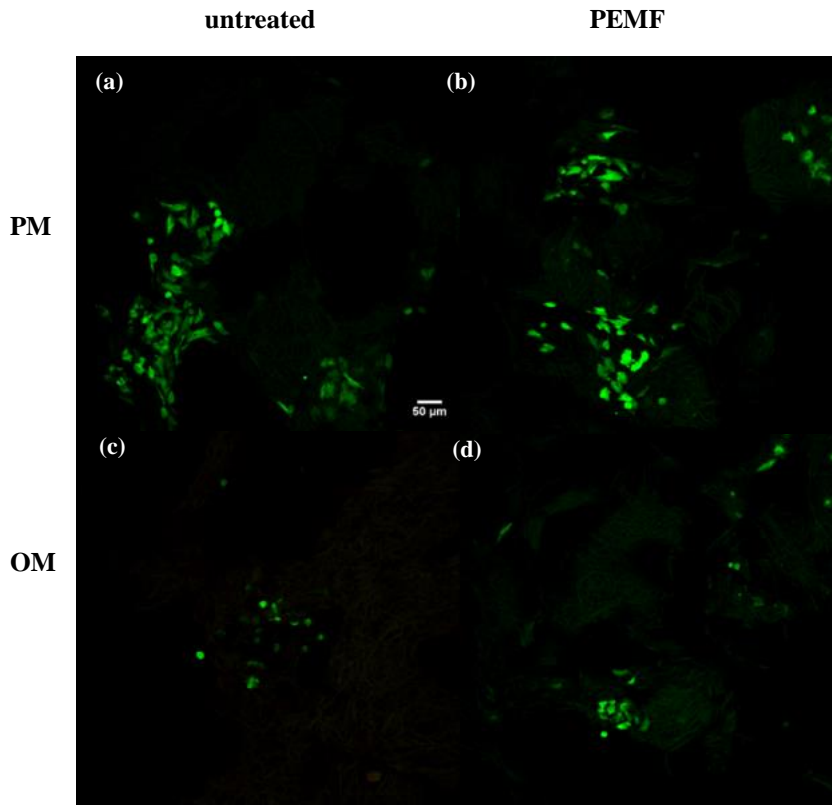


Figure 3.10: Representative CLSM images (20X) with FDA staining at 21 days of culture

3.5.4. Phosphate determination

Bone tissue performs many functions other than locomotion, including calcium and phosphate storage, sheltering of bone marrow, support and protection of soft tissues.

The inorganic material of bone consists predominantly of phosphate and calcium ions; however, significant amounts of bicarbonate, sodium, potassium, citrate, magnesium, carbonate, fluorite, zinc, barium, and strontium are also present [308-309].

The typical stiffness and resistance of bone tissue is due to deposition of hydroxyapatite crystals, which are represented by the chemical formula $\text{Ca}_{10}(\text{PO}_4)_6(\text{OH})_2$, on collagen and other matrix proteins scaffolds, *via* nucleation of calcium and phosphate ions inside the matrix vesicles [310].

Phosphate ions are released into the vesicles by degradation of phosphate-containing compounds by the ALP secreted by osteoblasts. Then, the phosphate and calcium ions inside the vesicles nucleate, forming the hydroxyapatite crystals [311].

Osteogenic differentiation can be followed by the analysis of phosphate deposition, since the final stage of the *in vitro* differentiation process results in

a high expression of osteocalcin and osteopontin in the late stage of differentiation process, followed by calcium and phosphate deposition [312-313].

Figure 3.11 shows a significant increase in phosphate deposition when SAOS-2 cells are stimulated by PEMF mechanical stimuli while they are induced to differentiate by an osteoinductive culture medium.

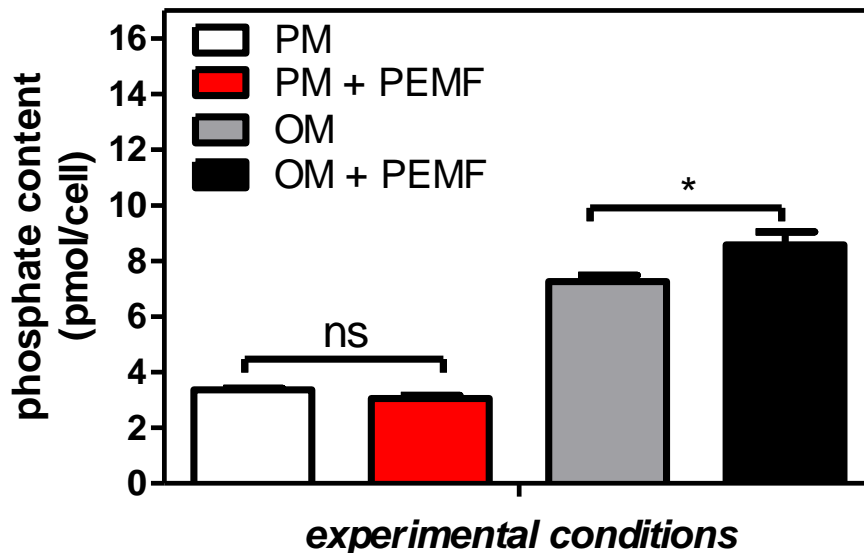


Figure 3.11: Quantification of phosphate content. Phosphate measured in cell seeded-scaffold showing quantity (pmol)/(cell). Results are presented as an average \pm standard deviation (ns $p > 0.05$; * $p < 0.05$).

This result suggests that PEMF-mediated mechanotransduction inducing phosphate deposition, occurs for differentiated cells by biochemical osteogenic factors (OM culture medium).

3.5.5. Calcium quantification

Similarly, also calcium deposition is a marker of osteogenic differentiation.

In order to examine the effect of PEMF stimulation on the mineral metabolism of osteoblast-like cells, the total content of calcium was determined in PEMF-stimulated cultures and in control cultures, in proliferative and osteogenic conditions (Fig. 3.12).

The stimulated cultures showed a significant increase of calcium content compared to controls, indicating an enhanced mineral formation by osteoblast-like cells.

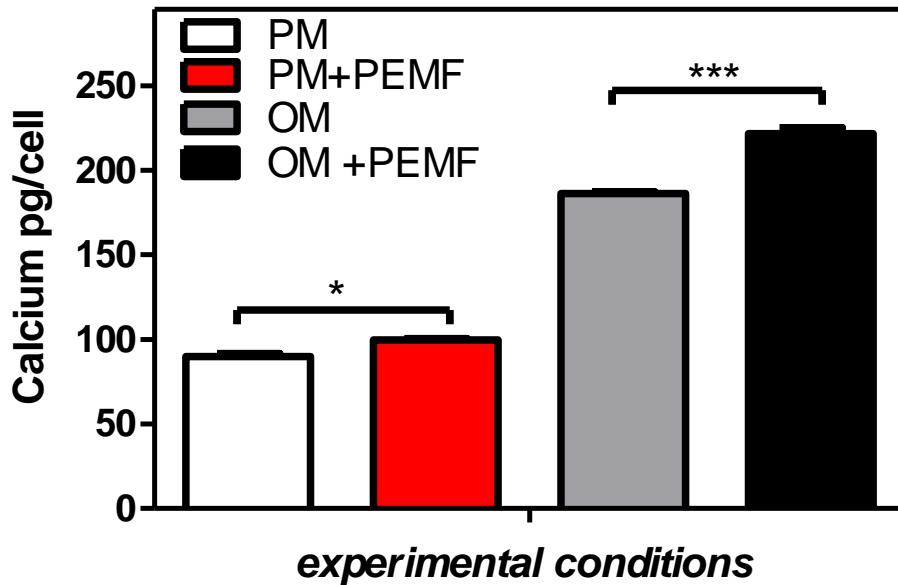


Figure 3.12: Quantification of calcium content. Results are expressed as (pg)/(cell) and are presented as an average \pm standard deviation (* $p < 0.05$; *** $p < 0.001$)

The calcium deposition increase was highly significant and more marked in SAOS-2 cells cultured in osteogenic conditions, compared to proliferative conditions. Nevertheless, also in proliferative conditions a significant increase in calcium deposition has been observed.

The increase in mineralization was consistent with the rise in the alkaline phosphatase expression in response to an electromagnetic wave exposure, as reported in other studies [314-315].

3.5.6. SEM and EDX

SEM micrographs of wool fibril sponges with SAOS-2 cells cultured in proliferative and osteogenic media are shown in figure 3.13. Pictures show the typical surface morphology of the SAOS-2 cells stuck to the wool fibril sponges; cells are evenly deposited on the sponge surface and also embedded into the fibril substrate.

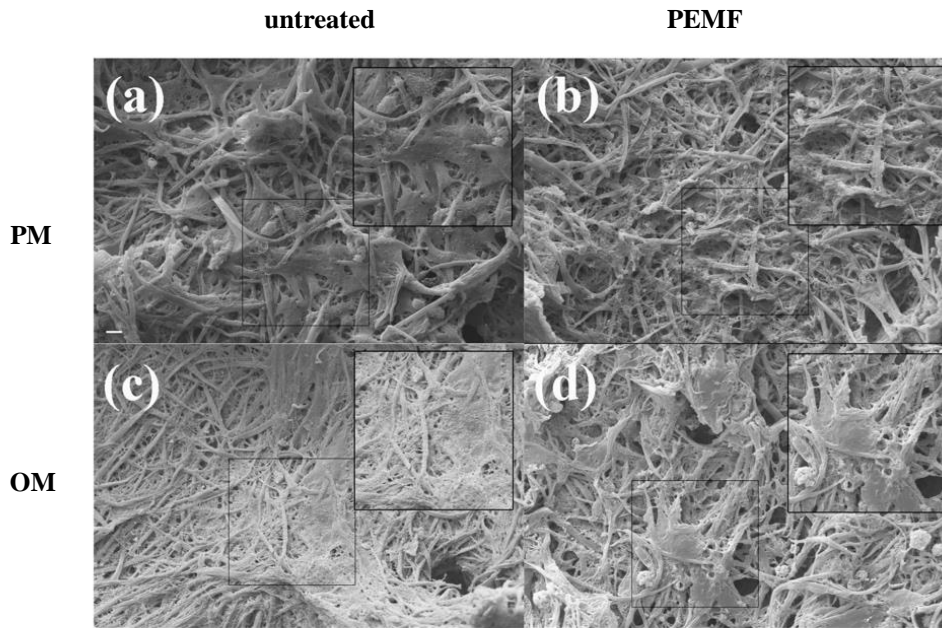


Figure 3.13: Representative SEM images of osteoblast-like cells incubated for 21 days on each experimental conditions. Magnification 1Kx; Scale bars = 10 μm . Magnified areas of cells are shown in insets

SEM investigation at high magnifications revealed areas of mineral deposition that were interspersed among the osteoblast-like cells both in PEMF and non-PEMF stimulated cultures in osteogenic culture conditions (Fig. 3.13 c and d).

EDX microanalysis

As expected, the semi-quantitative Energy Dispersive X-ray analysis confirmed the data on calcium deposition obtained *via* colorimetric assay. Figures 3.14, 3.15, and 3.16 show the EDX spectra of the wool fibril sponges surfaces without cells, with SAOS-2 cells and with SAOS-2 cells stimulated by PEMF, in proliferative conditions.

Table 3.1 reports the calcium amount of the same samples, calculated with the limits of such a methodology: in all these conditions the calcium amount seemed to be negligible.

Table 3.1: Calcium amount onto the wool fibril sponges surfaces without cells, with SAOS-2 cells and with SAOS-2 cells stimulated by PEMF in proliferative conditions.

PM	
	Calcium (% weight)
Without cells	0.49
With cells	0.33
With cells + PEMF	0.41

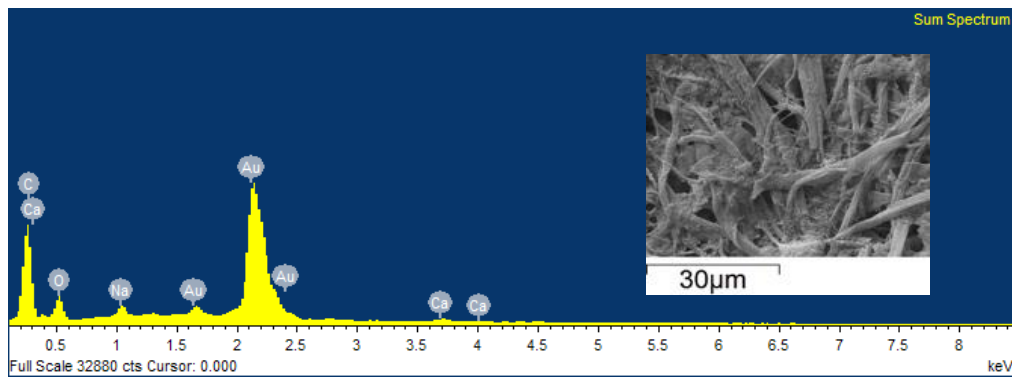


Figure 3.14: EDX analysis of scaffolds bathed for 21 days in proliferative medium without SAOS-2 cells (scale bar = 30 µm; magnification 5000x)

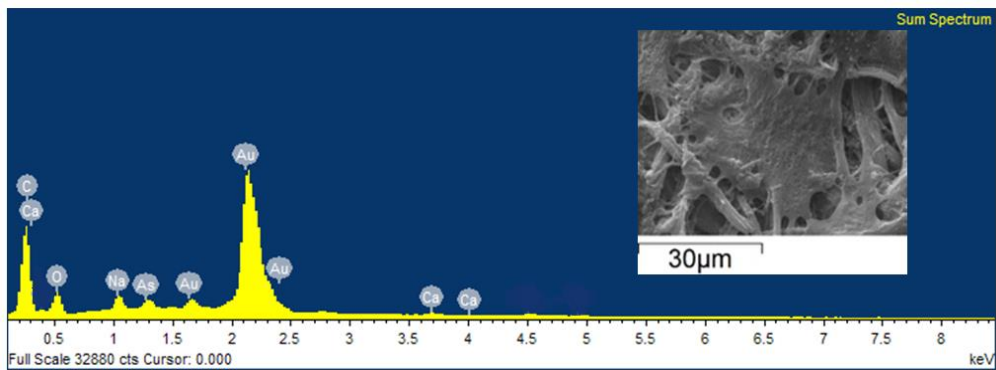


Figure 3.15: EDX analysis of scaffolds cultured for 21 days in proliferative medium with SAOS-2 cells (scale bar = 30 µm; magnification 5000x)

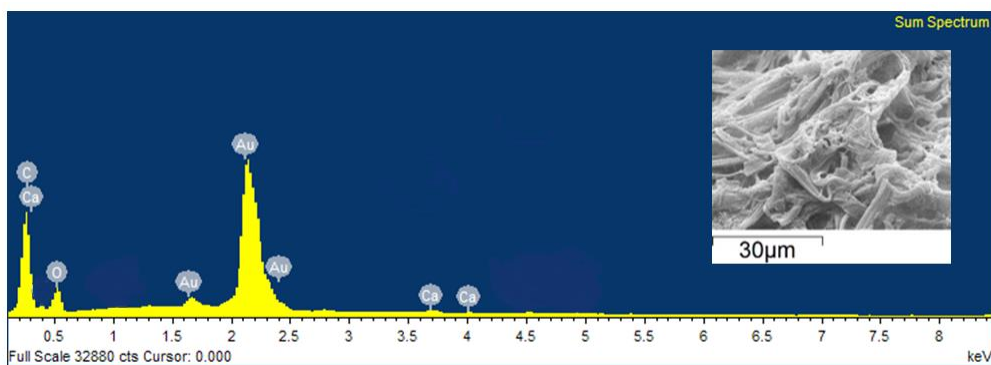


Figure 3.16: EDX analysis of scaffolds cultured for 21 days in proliferative medium with SAOS-2 cells + PEMF (scale bar = 30 µm; magnification 5000x)

Figures 3.17, 3.18, and 3.19 show the EDX spectra of the wool fibril sponges surfaces without cells, with SAOS-2 cells and with SAOS-2 cells stimulated by PEMF, in osteogenic conditions.

Observation of mineralizing cell cultures at different magnifications revealed areas of globular mineral deposition (mineral spherules) among the osteoblast-like cells (Fig. 3.18), especially in PEMF-stimulated cultures (Fig. 3.19). Small mineral nodules with an approximate diameter of 10 nm were found as early indicators of newly formed biomineral in direct contact to the cell surface.

Table 3.2 shows that mineral spherules were rich in calcium and the calcium amount increased in scaffolds cultured for 21 days in osteogenic medium with SAOS-2 cells + PEMF.

Table 3.2: Calcium amount produced by SAOS-2 cells in osteogenic conditions

OM	
	Calcium (% weight)
Without cells	0.7
With cells	1.6
With cells + PEMF	9.2

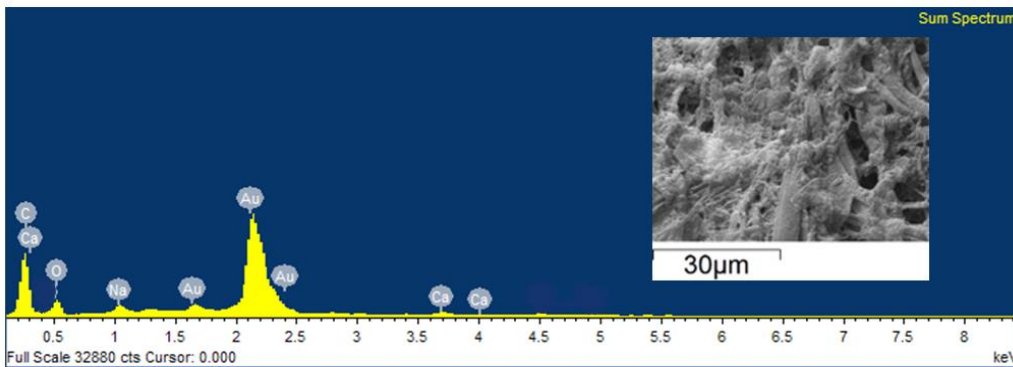


Figure 3.17: EDX analysis of scaffolds cultured for 21 days in osteogenic medium without SAOS-2 cells (scale bar = 30 µm; magnification 5000x)

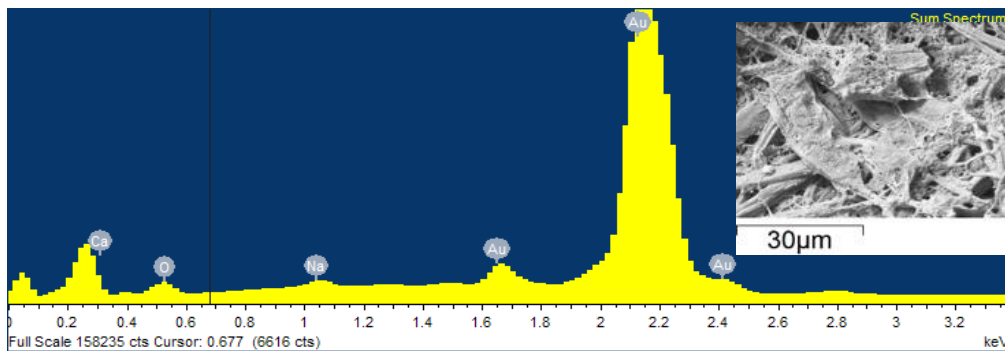


Figure 3.18: EDX analysis of scaffolds cultured for 21 days in osteogenic medium with SAOS-2 cells (scale bar = 30 µm; magnification 5000x)

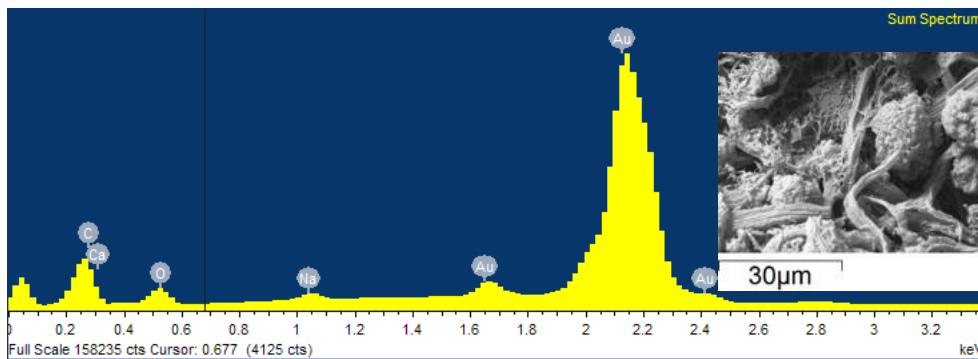


Figure 3.19: EDX analysis of scaffolds cultured for 21 days in osteogenic medium with SAOS-2 cells + PEMF (scale bar = 30 μm; magnification 5000x)

3.5.7. Protein Matrix analysis

To evaluate the amount of the ECM constituents produced by SAOS-2 cell in unstimulated or PEMF-stimulated conditions, an ECM protein extraction was performed on day 21 after culture in PM or OM.

At the end of the culture period, the detection of bone proteins showed some differences.

As expected, osteogenic medium conditions resulted in higher ECM proteins deposition in comparison with the proliferative culture system.

PEMF was applied to both OM and PM cultured cells and in both cases stimulation in ECM proteins production was detected.

In proliferative conditions the PEMF stimulation resulted in a significant increase of all proteins analyzed except BMP-2.

Protein deposition was particularly enhanced for osteopontin, which was 2.35 fold bigger compared with unstimulated cells in PM (Tab. 3.3).

Osteopontin is an extracellular glycosylated bone phosphoprotein secreted at the early stages of the osteogenesis before the onset of mineralization. Osteopontin binds calcium, it is likely to be involved in the regulation of the hydroxyapatite crystals growth [316-318] and, through specific interaction with the vitronectin receptor, it promotes the attachment of cells to the matrix [319-320].

Table 3.3: ELISA Analysis of Bone Extracellular Matrix Protein Production after 21 days of culture expressed as pg/(cellxscaffold). In comparison to unstimulated samples, a *p* value <0.05 was considered statistically significant (*).

	PM	PM+PEMF	PEMF/PM	OM	OM+PEMF	PEMF/OM
ALP	2.3 ± 0.02	2.6 ± 0.01	1.13*	9.4 ± 0.16	11.3 ± 0.47	1.2*
BMP2 (bone sialoprotein)	0	0	0	0.04 ± 0.01	0.07 ± 0.01	1.75*
decorin	6.6 ± 0.9	11 ± 2	1.66*	37 ± 0.5	41.2 ± 0.2	1.11*
fibronectin	1.1 ± 0.03	1.6 ± 0.1	1.45*	4.8 ± 0.07	6.2 ± 0.03	1.29*
osteocalcin	0.9 ± 0.01	1.2 ± 0.01	1.33*	2.8 ± 0.04	4.01 ± 0.05	1.43*
osteonectin	0.3 ± 0.05	0.4 ± 0.01	1.33*	1.3 ± 0.1	1.95 ± 0.05	1.5*
osteopontin	0.2 ± 0.02	0.47 ± 0.04	2.35*	2.6 ± 0.07	2.96 ± 0.01	1.13*
type I collagen	4.0 ± 1.1	6.7 ± 0.2	1.67*	12.1 ± 0.4	14.8 ± 0.2	1.22*
type III collagen	10.4 ± 1.5	14 ± 1.4	1.34*	38.3 ± 4.0	51.8 ± 7.1	1.35*

In osteogenic conditions the PEMF stimulation gives rise to higher amount of EMC proteins analyzed, also BMP-2, compared to unstimulated conditions. In this case BMP-2 amount is notably increased (1.75 fold) compared to unstimulated cells while in proliferative conditions BMP-2 was not produced.

Osteocalcin level in PEMF stimulated cells in OM is very high, indicating that at this time of culture the cells represent mature osteoblasts.

These positive results are due to time varying and homogeneous magnetic induction (75 Hz frequency), according to the Faraday-Neumann-Lenz and Lorentz laws [296], generated by the PEMF application.

This induced field, results in a concentric and planar distribution of induced electric currents with corresponding induced distribution of radial mechanical forces, so, the seeded cells were also stimulated with time varying mechanical forces acting onto their plasma membrane at the frequency of 75 Hz.

The magnetic induction was able to produce time varying mechanical forces acting perpendicularly or tangentially onto the cell membrane; as a consequence, these forces were able to modulate the cell tensesgrity via tensile and compressive deformations [294] (i.e. traction and compression) affecting the cell tensesgrity of osteoblasts.

3.5.8. Alkaline Phosphatase (ALP) activity

Finally, the osteogenic differentiation can be also analyzed by monitoring the alkaline phosphatase (ALP) activity.

Intracellular ALP showed the highest activity in the early differentiation stages. For this reason ALP is an early biomarker of osteoblast differentiation [321].

In vitro osteogenic differentiation has been divided into three stages [313]. The first stage consists in a peak in the number of cells followed by early cell differentiation, which is characterized by the transcription and protein expression of alkaline phosphatase (ALP) [322]. After this initial peak, ALP activity starts declining [323]. Figure 3.20 shows the absence of significant effect of PEMF on the ALP activity when SAOS-2 cells were in proliferative conditions. Nevertheless, in osteogenic medium, PEMF application resulted in a decrease of the ALP activity.

This data suggest that PEMF stimulated an earlier differentiation compared to cells not submitted to PEMF stimulation in osteogenic conditions, showing a perfect synergy between biochemical and mechanical stimuli in acceleration of the differentiation process.

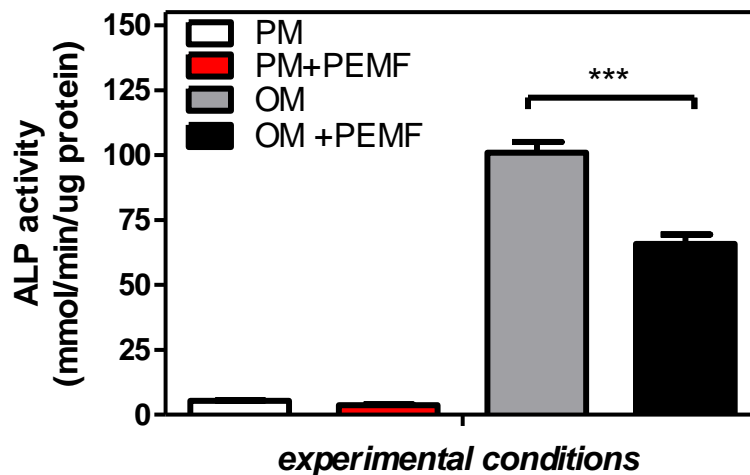


Figure 3.20: ALP activity of osteoblast-like cells seeded onto the different scaffolds and cultured in osteogenic medium (OM). ALP activity was determined colorimetrically, corrected for the protein content measured with the BCA Protein Assay Kit and expressed as millimoles of p-nitrophenol produced per min per μg of protein. Bars express the mean values \pm std of results from three experiments; *** $p < 0.001$

3.5.9. Compression behavior

Wool fibril sponges submitted to repeated compression cycles carried out in the dry state, showed a permanent deformation that was not evidenced in the same sponges when compressed in wet conditions.

Because their application is forecast to be made in wet conditions (body fluid conditions), the compression behavior of the sponges after 21 days

immersion in culture medium was evaluated in wet conditions too. The compression behavior of samples cut from the wool fibril sponges submitted to 10 repeated compression cycles in the wet state, after 21 days immersion in PM without cells, with and without PEMF application, is reported in Fig. 3.21 and 3.22 respectively. Fig. 3.23 and 3.24 show the behavior of the sponges immersed 21 days in osteogenic culture medium (OM). The same framework of experiments is reported in Fig. 3.25, 3.26, 3.27 and 3.28 for sponges immersed with SAOS-2 cells 21 days in PM and OM respectively.

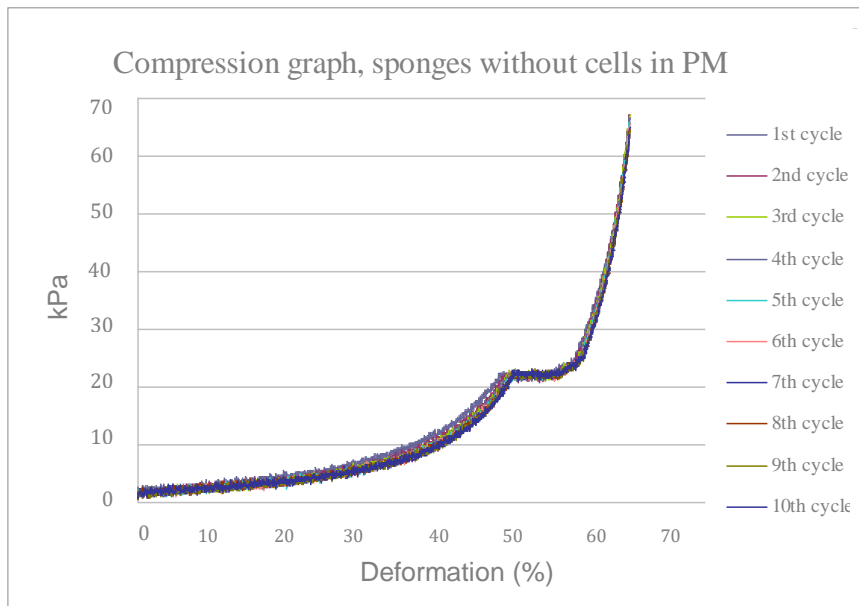


Figure 3.21: Compression behavior of the wool fibril sponges in the wet state after 21 day culture in PM without cells

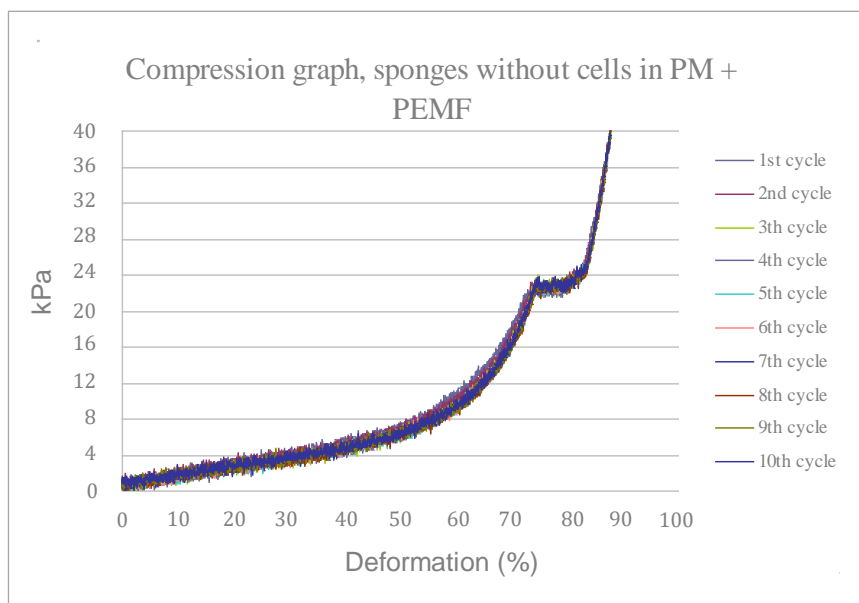


Figure 3.22: Compression behavior of the wool fibril sponges in the wet state after 21 day culture in PM without cells with PEMF application

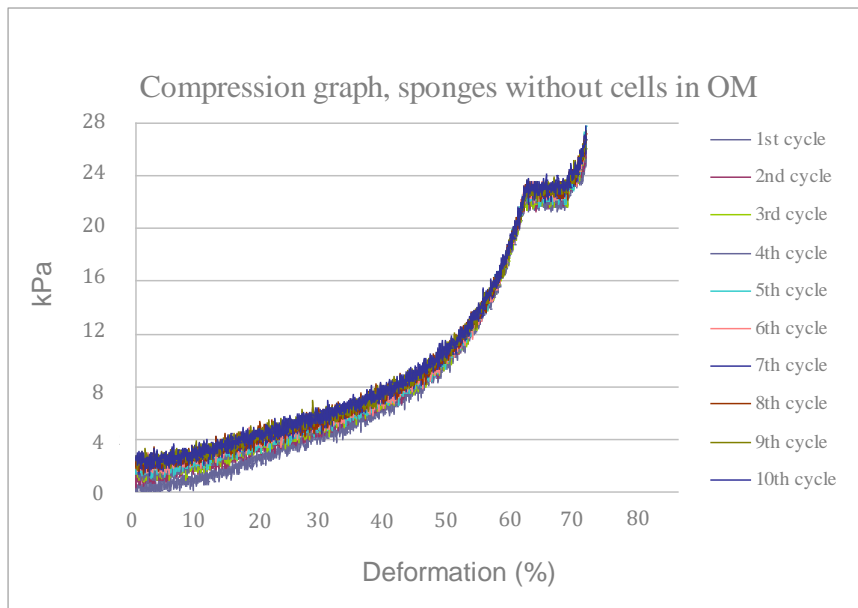


Figure 3.23: Compression behavior of the wool fibril sponges in the wet state after 21 day culture in OM without cells

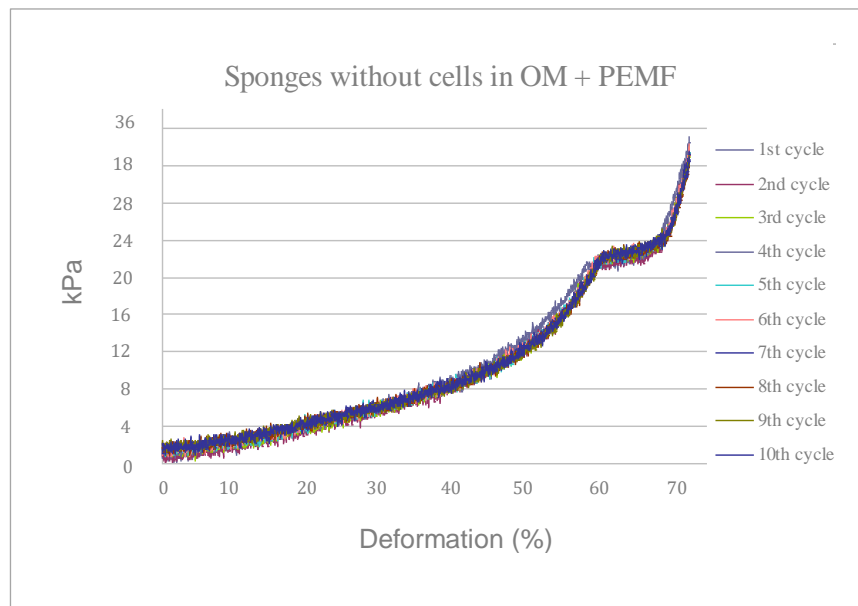


Figure 3.24: Compression behavior of the wool fibril sponges in the wet state after 21 day culture in OM without cells with PEMF application

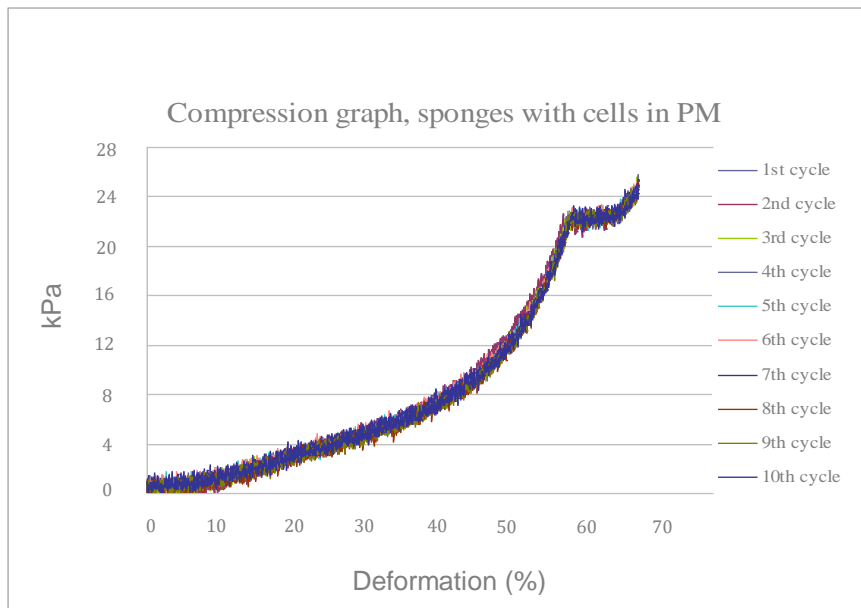


Figure 3.25: Compression behavior of the wool fibril sponges in the wet state after 21 day culture in PM with cells

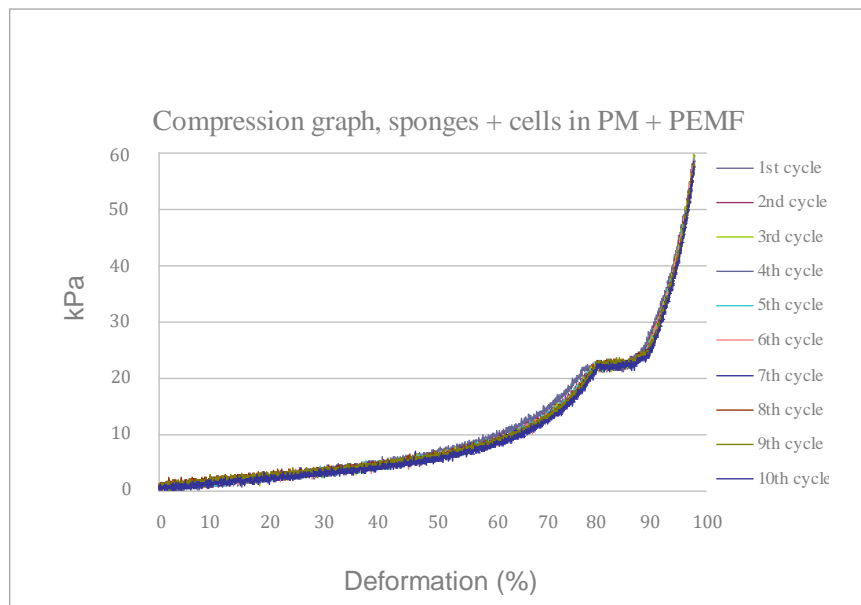


Figure 3.26: Compression behavior of the wool fibril sponges in the wet state after 21 day culture in PM with cells with PEMF application

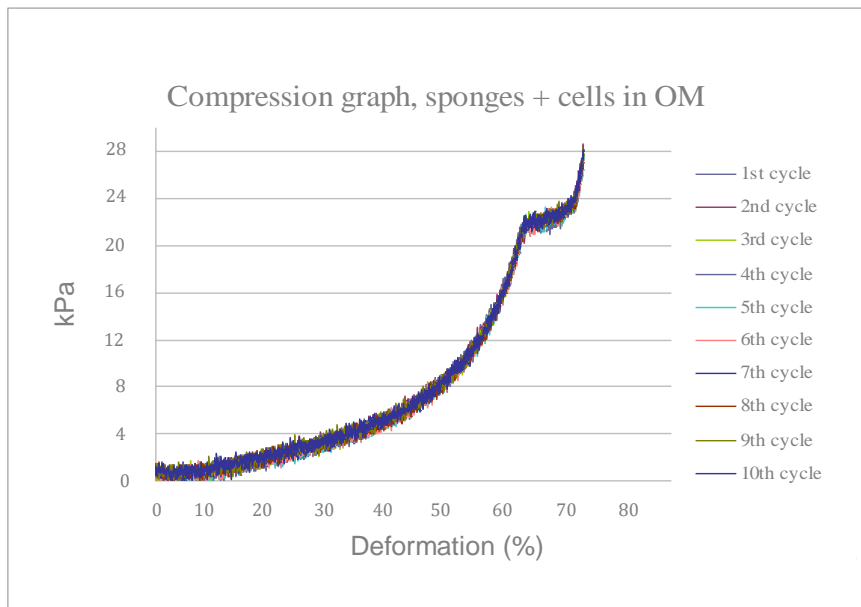


Figure 3.27: Compression behavior of the wool fibril sponges in the wet state after 21 day culture in OM with cells

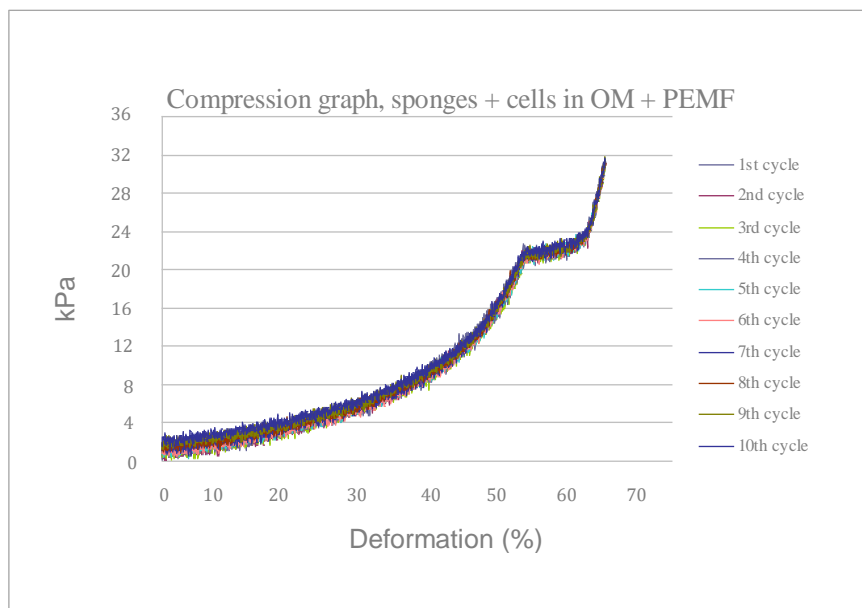


Figure 3.28: Compression behavior of the wool fibril sponges in the wet state after 21 day culture in OM with cells with PEMF application

As a general comment, after 21 days culture in osteogenic and proliferative medium, the resilience behavior was still observed: traces are almost overlapping each other and no permanent deformation can be detected.

All compression traces display a horizontal line in the load range 22 – 24 kPa, which is most likely due to reversible crushing deformation of the pore structure of the sponges. In other words, water filled the macro- and micro-pores and also penetrated into the amorphous keratin domains, resulting in increased elasticity of the whole structure.

Nevertheless, for compression loads higher than 24 kPa, the structure of the wool fibre assembly would not represent a sponge anymore.

Thus, the compression moduli of the sponges have been compared in the load ranges 2-8 kPa and 10-22 kPa, in order to represent the slope changes of the compression trace in those ranges. Results of the compression moduli calculated in the selected ranges are reported in Table 3.4.

Table 3.4: Compression moduli in the selected ranges

	Compression range (kPa)	Average Modulus (kPa)
Without cells in PM	2-8	18.0 ± 5.2
	10-22	11.1 ± 8.3
Without cells in PM+PEMF	2-8	14.1 ± 2.2
	10-22	85.2 ± 8.1
Without cells in OM	2-8	21.3 ± 3.1
	10-22	80.4 ± 7.4
Without cells in OM+PEMF	2-8	22.1 ± 3.1
	10-22	54.4 ± 4.6
With cells in PM	2-8	24.2 ± 2.2
	10-22	102.6 ± 9.1
With cells in PM+PEMF	2-8	16.2 ± 2.7
	10-22	58.3 ± 9.2
With cells in OM	2-8	27.4 ± 30.1
	10-22	90.5 ± 90.2
With cells in OM+PEMF	2-8	25.1 ± 3.3
	10-22	59.3 ± 8.1

No significant differences in the mechanical behavior between sponges with cells or without cells, in PM and OM media, with and without PEMF application have been detected. The presence of SAOS-2 cells did not influence neither the compression moduli nor the resilience of the sponges in wet conditions.

As expected, the wool fibril sponges show high chemical and physical stability after 21 day culture, despite the fact that they consist of proteins, hence biodegradable polymers.

3.6. Conclusions

The aim of the work of this experimental part was the evaluation of the effects exerted by the wool fibril sponges structure joined to the pulsed electromagnetic field stimuli, on the proliferation and differentiation of SAOS-2 cells, cultured in both proliferative and osteogenic media.

The integrated bio-engineering approach of applying bio-mechanical stimuli from pulsed electromagnetic field (PEMF), in addition to the 3D architectural feature given by the 3D scaffolds showed to be a successful solution.

In fact, PEMF stimulated an earlier differentiation in osteogenic conditions, showing a perfect synergy between biochemical and mechanical stimuli in acceleration of the differentiation process.

Finally, the wool fibril sponges showed high chemical and physical stability after 21 day culture, despite the fact that they consist of proteins, hence biodegradable polymers.

Chapter 4

Keratin fibrils 3D sponges, keratin hydrogels and 2D keratin fibrils films in stem cell attachment

4.1. Aim of the work

Since a stem cell-based approach is an attractive alternative to current treatment techniques in tissue engineering, the aim of this experimental part was to examine the attachment and growth of stem cells on different 2-D and 3-D keratin-based scaffolds.

4.2. Materials and methods

All methods previously described will not be described again in this paragraph. Please see 2.2.

4.2.1. Preparation of keratin hydrogels

Botany wool, 20.3 μm mean fibre diameter, in the form of top (the fibre sliver obtained from raw wool by scouring, carding, and combing processes) was supplied by The Woolmark Co., Italy. All analytical grade chemicals were purchased from Sigma-Aldrich, except otherwise specified.

Wool fibres were cut into snippets of some millimetres and bathed in the reducing solution (26 mg/ml) containing Tris/HCl (550 mM; pH 8.6), DTT (140 mM), ethylenediaminetetraacetic acid (5 mM) and urea (8 M) and shaken for 4 hours in linitest apparatus.

The resulted keratin solution has been filtered on a 120 mesh sieve and dialyzed against water with a cellulose dialysis tube (cut of 12 KDa) changing water every h for two days. The resulting water solution was lyophilized obtaining the keratin powder.

The powder has been re-suspended in the extraction buffer with a concentration of 140 mg/ml at room temperature, the solution has been dialyzed against water, as described above, obtaining the hydrogels, subsequently cut into cylinders fitting the well plates dimension, as for sponges. Keratin hydrogel were sterilized with ethanol.

4.2.2. Preparation of 2D keratin fibrils films

Botany wool, 20.3 μm mean fiber diameter, in the form of tops (the sliver obtained from raw wool by scouring, carding, and combing processes) was supplied by The Woolmark Co., Italy. All chemicals were of analytical grade and purchased from Sigma-Aldrich, except otherwise specified.

Wool fibres were cut into snippets of some millimetres and bathed in 0.1 N NaOH with liquor ratio 1:50 (8 g in 400 ml), at 60 °C for 24 h.

The snippets were then rinsed with distilled water until neutral pH on a stainless steel sieve (120 mesh), bathed into 100 ml of deionised water and subjected to ultrasonic treatment for 30 min with a Sonics Vibracell 750, equipped with a stainless steel 1/2 inch “solid” probe, tuning the ultrasonic power to 600 W at the frequency of 20 kHz, with control temperature set at 50 °C.

This treatment produces a suspension of cortical cells and fiber fragments in an aqueous protein matrix. Coarse fiber fragments were removed by filtration with a stainless steel sieve (120 mesh). The permeate cell suspension was concentrated by Rotavapor at 50 °C, to a final concentration of dry solid of about 10 g/l, then finally cast into films in 2 polyethylene moulds of 10 cm \times 10 cm in standard atmosphere (20 °C and 65% RH). The overall yield based on the initial wool mass was 10% wt [92].

4.2.3. Characterization methods

Isolation, expansion, and culture of BM-MSCs

The design of this study was approved by the Institutional Review Board of the Fondazione IRCCS Policlinico San Matteo and the University of Pavia (2011). BM aspirates were harvested from healthy paediatric hematopoietic stem cell donors after obtaining written informed consent. Thirty milliliters of BM from each donor was assigned to BM-MSC generation; heparin was added as an anticoagulant. Mononuclear cells were isolated from BM aspirates (30 ml) by

Ficoll density gradient centrifugation (density, 1.077 g/ml; Lymphoprep, Nycomed Pharma, Oslo, Norway) and plated in non-coated 75- to 175-cm² polystyrene culture flasks (Corning Costar, Celbio, Milan, Italy) at a density of $16 \cdot 10^4$ cells/cm².

Cells were cultured in Mesencult medium (Stem Cell Technologies, Vancouver, Canada) supplemented with 2 mM L-glutamine, 50 µg/mL gentamycin, and 10% fetal calf serum. Cultures were maintained at 37 °C in a humidified atmosphere containing 5% CO₂. After 48 h, non adherent cells were discarded and culture medium was replaced twice a week. After reaching 80% confluence as a minimum, the cells were harvested and replated for expansion at a density of 4000 cells/cm² until the fifth passage. The colony-forming unit fibroblast assay (CFUF) was performed as described previously [324] CFU-F formation was examined after 12 days of incubation in a humidified atmosphere (37 °C, 5% CO₂); the clonogenic efficiency was calculated as the number of colonies per 10⁶ BM mononuclear cells seeded. According to the International Society for Cellular Therapy on the nomenclature of mesenchymal progenitors, the cells cultured for this study were defined as multipotent stromal cells. To phenotypically characterize BM-MSCs and to define their purity, FACS analysis was performed as previously described [324].

After reaching 80% confluence at a minimum, the cells were harvested and replated for expansion at a density of $2.5 \cdot 10^4$ cells/cm². The cells were cultured at 37 °C, 5% CO₂, and three fifths of the medium was renewed every 3 days.

Water swelling

For the moisture regain determination (water uptake), films previously dried in a ventilate oven at 105 °C to constant mass were stored in standard conditions (using a conditioned room at 20 °C and 65% RH) for 24 h.

The water uptake was determined as the ratio between the amount of water absorbed and the weight of dried film versus time. For swelling ratio determination, films were cut into square pieces (10x10 mm) and soaked in distilled water at room temperature until a constant size was achieved.

Measures were performed with a stereomicroscope at 20x magnification. Typically, complete equilibration was obtained in 2 h. The swelling ratio was calculated according to the following equation: $[(V_{wet} - V_{dry}) / V_{dry}] \times 100$, where V_{dry} and V_{wet} are the volumes of the dry and the wet sponges, respectively.

Compression behavior

Compression properties of the keratin hydrogels were determined in conditioned standard atmosphere at 20 °C, 65% RH with an Instron 5500 R Series IX dynamometer, according to the CNR standard developed for the evaluation of wool mattresses. Six samples (8 mm diameter, 3.6 mm thickness) were submitted to 10 compression cycles (maximum load of 5 N) at the constant deformation rate of 10 mm/min, in order to evaluate also the

resilience. Every compression cycle was stopped on reaching 3.6 mm stroke, starting from the top of the hydrogel.

Samples were measured for compression modulus and deformation, reporting the average and the standard deviation of the results.

Statistical Analysis

Each test was repeated three times at least in the same experimental conditions. Differences between groups were tested by the one-way analysis of variance. The Tukey's test was used to correct for multiple comparisons and statistical relevance was established at two-tailed $p \leq 0.05$. All calculations were generated using the GraphPad Prism 5.0 software (GraphPad Inc., San Diego, California).

4.3. Results and discussion

4.3.1. Morphological characterization

Wool fibril sponges and films, and keratin hydrogels were cut and shaped to the appropriate size of the well-plate. Sponges were bright yellow due to the thermal stabilization process, films were chalky opaque white and homogeneous, while keratin hydrogel were semi-transparent (because of the high water content of 97 %), as shown in Figure 4.1.

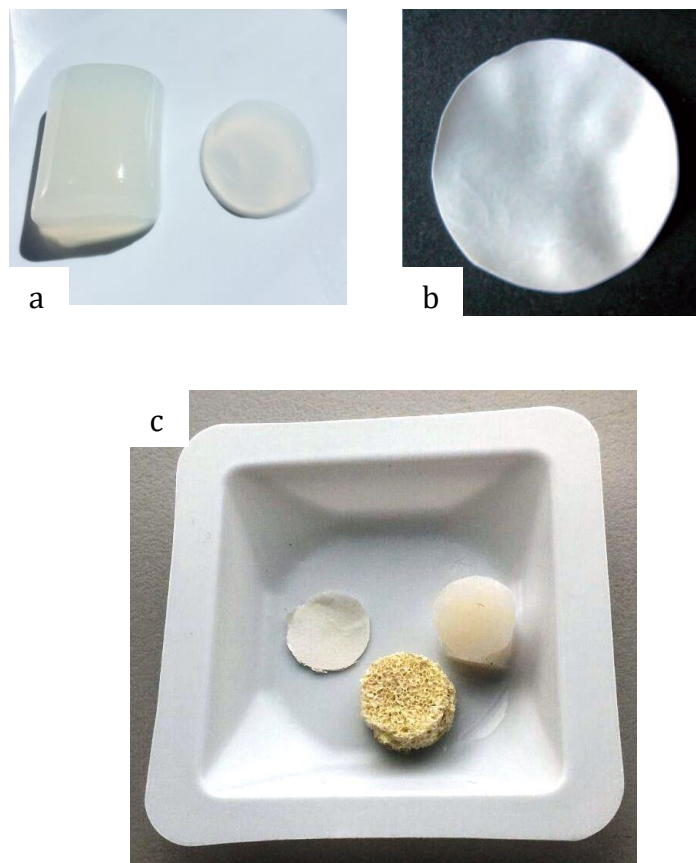


Figure 4.1: Visual appearance of keratin hydrogel before cut (a), wool fibril film before cut (b), wool fibril film, sponges and keratin hydrogel after cut (c)

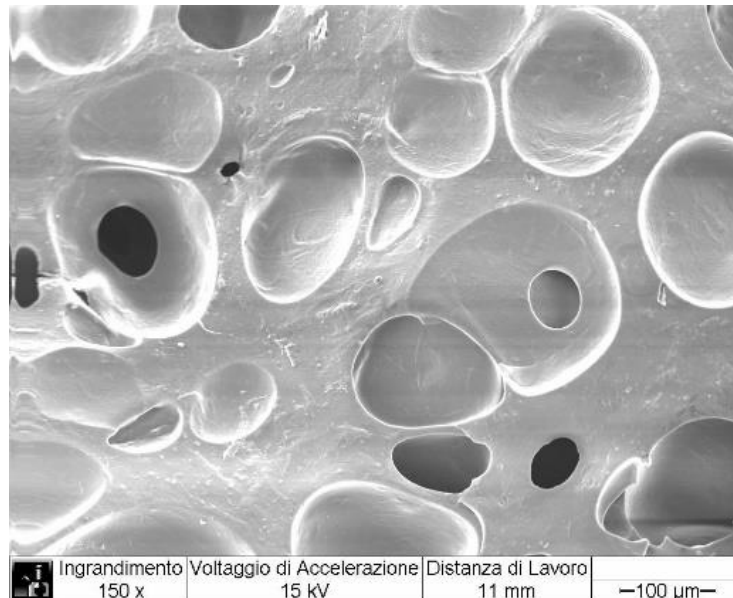


Figure 4.2: SEM cross-section of the keratin hydrogel (150x)

Figure 4.2 shows the frozen cross-section of the keratin hydrogels, where pores with the order of magnitude ranging from 50 to 200 μm are clearly visible. Pores, which are partially interconnected, resulted from water evaporation during preparative sputtering in high vacuum conditions before SEM investigation.

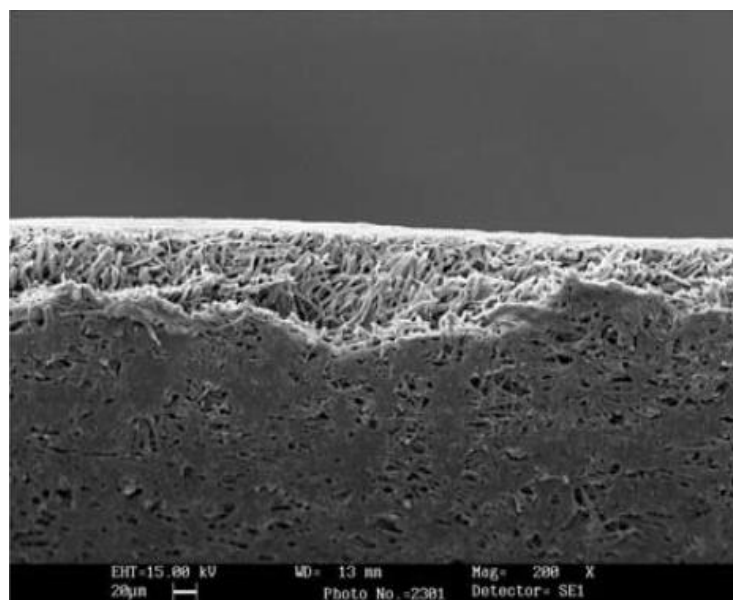


Figure 4.3: Cross-section of the wool fibril (200x)

Figure 4.3 shows the very particular cross-section of the wool fibril films obtained by removing the non-fibrous keratin matrix before casting of the water-wool fibrils suspension.

In this way, the residual layer of cross-linked protein matrix attached to the surface of the fibrils (wool cortical cells), sticks the cells to each other in the contact points, resulting in a porous solid, strong, and flexible film of randomly oriented fibrils. The internal feature of the film is a network structure shown in SEM pictures obtained by fragile fracture (Fig. 4.3) in liquid nitrogen. Removal of the water-soluble protein matrix allows the formation of the porous structure, which is mechanically superior, less fragile and different from the compact structure of films made by casting the whole protein matrix-fibrils suspension [92].

4.3.2. Amino acid composition

HPLC investigation was carried out to study the protein composition of the wool fibril films and keratin hydrogels, compared to the original wool. In table 4.1 the amino acid composition of the keratins extracts is reported.

Table 4.1: Amino acid composition of the keratin hydrogel and wool fibril films compared with the original wool (*p< 0.001)

Amino acid	Wool (mol %)	Wool fibril film (mol %)	Keratin gel (mol %)
CYA	0.19	0.21	0.2
ASP	9.29	8.59	8.44
SER	11.67	6.61	9.91
GLU	15.59	12.20	14.02
GLY	7.23	6.39	7.82
HIS	0.52	0.82	0.55
ARG	5.86	6.41	6.24
THR	6.79	5.60	6.15
ALA	5.65	6.50	6.21
PRO	3.12	7.40	6.25
LANT	0.43*	6.45*	0.42
½ CYS	9.55*	2.31*	9.41
TYR	2.49	2.69	3.43
VAL	5.48	6.35	5.41
MET	0.37	0.41	0.42
LYS	3.99	5.70	2.91
ILE	2.86	4.80	3,1
LEU	7.11	8.65	7
PHE	1.82	1.90	2,2

Cysteine, which is not found in natural keratins but is present as a result of the preparative reductive-extraction of keratins from the samples to be submitted to HPLC, is conventionally reported as ½ cystine (mol%), since this last is the amino acid that is really found in keratins.

The main difference in the amino acid composition of the wool fibril films and the keratin hydrogel, compared with the original wool, is the loss of cystine and the formation of lanthionine.

Lanthionine, which is responsible for the thioether (-S-) interchain bonds, is formed from cystine disulphide bonds (-S-S-) during the alkali treatment made to prepare the wool fibril films.

As expected, the keratin hydrogel show the same cystine content and the same negligible amount of lanthionine of the pristine wool. In conclusion, the amino acid composition of the keratin hydrogel is more similar to that of the original pristine wool than the fibril film.

4.3.3. SDS-PAGE

Since the reductive extraction process used for the hydrogel preparation is the same used for the SDS-PAGE of the wool fibres, obviously the molecular weight distribution of the film is the same of the pristine wool (Fig. 4.4).

As for wool fibrils sponges, films were insoluble in the SDS-PAGE buffer because lanthionine (thioether) formation prevents solubilisation in reducing agents.

This unsuccessful result in the molecular weight determination is consistent with thioether formation, although the presence of more non-reducible cross-linked species other than the thioether linkage could not be excluded [227].

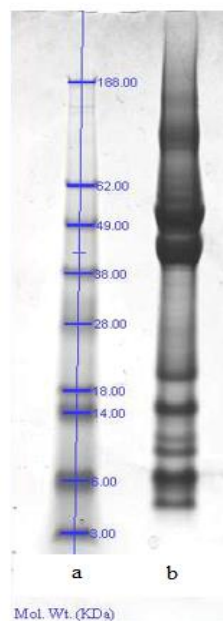


Figure 4.4: SDS-PAGE patterns of keratin hydrogel (b); molecular marker (a)

4.3.4. PH of the water extract

This test has been carried out in order to exclude the presence of alkali traces that could negatively affect the pH of the culture media.

All water extracts were neutral, confirming the absence of alkali residues that could be released by the samples.

4.3.5. Thermal analysis (DSC)

The DSC traces of the wool fibril film and sponge compared to the reference wool fibers are reported in figure 4.5.

As a general comment, the large first-order transitions below 100 °C are due to water evaporation, while the bimodal endothermic peaks between 200 and 300 °C are related to denaturation of the crystalline protein domains; finally, the uneven peaks at temperatures higher than 300 °C are due to the degradation of other histological components [226].

More in detail, the trace of the reference wool, displayed the typical features of the fine crimped Merino fibres, characterised by the large endotherm due to water evaporation with temperature peak at around 60 °C, and a characteristic thermal events taking place in the temperature range 230–255 °C [226], with a bimodal endothermic peak, namely the presence of a shoulder in the higher temperature side of the trace.

This behavior has been mainly explained by two principal theories: one attributes the doublet to differences in the thermal denaturation of the α -form crystallites with respect to the degradation of other histological components, namely the matrix; the other attributes the bimodal trace to differences in the transition enthalpy of the α -helical material in the domains of *ortho*- and *para*-cortical cells, that are typically arranged in two distinct sides of the cortex in this kind of wool.

In other words, *para*-cortical cells, which contain a higher amount of high sulphur matrix, seem to be more thermally stable than *ortho*-cortical cells.

When the *ortho*- and *para*- domains are arranged in a bilateral manner (assembled in two different sides of the fibre) the DSC trace is bimodal [228] while, when the *ortho*- and *para*-cortical cells are randomly arranged as in the film and sponge, the denaturation peak is single.

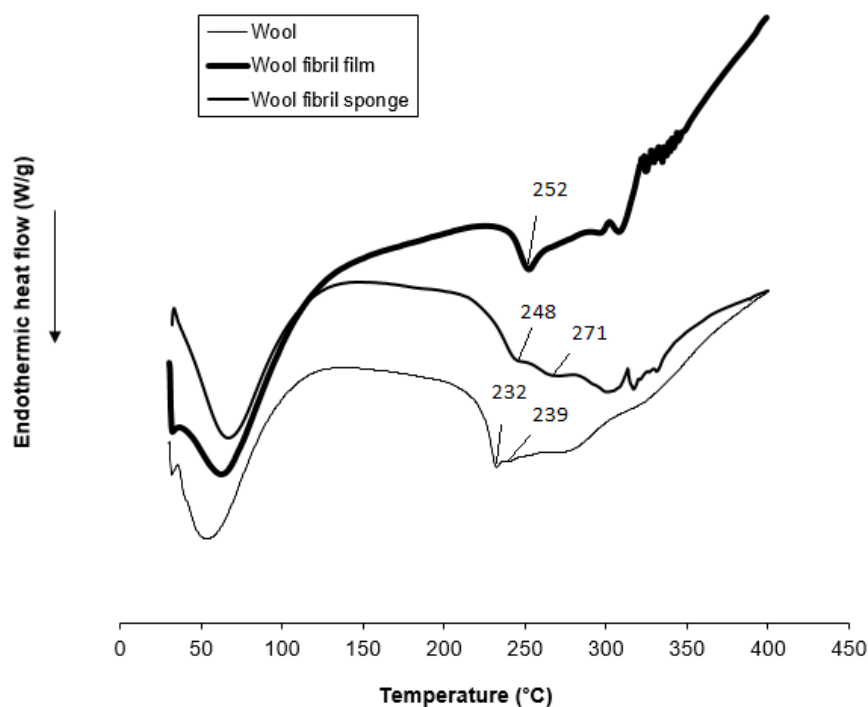


Figure 4.5: DSC thermograms of the wool fibril film and the keratin hydrogel compared with the original wool fibers

Indeed, denaturation of the wool fibrils film occurred with a single peak but shifted to a higher temperature (252 °C), and this could be due to the presence of lanthionine cross-links in the residual high-sulfur matrix surrounding the intermediate filaments, which cannot be regarded as belonging to *ortho* or *para*-domains any longer.

Moreover, the denaturation of the wool fibril sponge occurred with two peaks at 248 and 271 °C; the peak at 248 °C has the same interpretation given for the film, while the peak at higher temperature probably corresponds to denaturation of the highly crosslinked protein fraction resulting from the thermal stabilization carried out at 180 °C for 2 h, which should increase the number of isopeptide and other interchain linkages especially in the matrix proteins.

The denaturation/degradation of the keratin hydrogel occurred at lower temperature (105 °C) (Fig. 4.6) compared to wool reference, wool fibril sponges and films. Keratin hydrogel is composed by keratin macromolecules (reduced keratin) with newly formed cystine crosslinks diluted in a swollen structure incorporating high amount of water. In the presence of water, denaturation/degradation of keratin occurs at very low

temperature, as shown in figure 4.6 where only one peak is visible, that corresponds to simultaneous water evaporation and protein degradation.

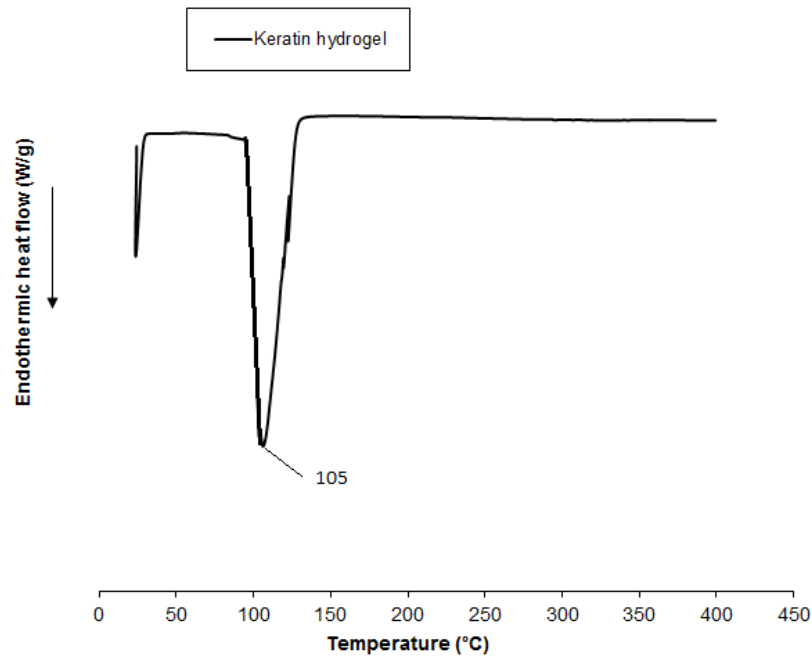


Figure 4.6: DSC thermograms of the wool fibril film and the keratin hydrogel

4.3.6. Water swelling

The keratin film significantly swelled in water, more than films of reduced keratin from literature [102]. Soaking the bio-composite film for 2 h in water caused a volume swelling of 42%, due to 27% thickness and 12% surface increases [91]. This difference is more likely due to the presence of still structured cortical cells (fibrils) with an inner, low crosslinked, more hydrophilic assembly of intermediate filament proteins.

4.3.7. Tensile behavior

Tensile test were obviously carried out for films only; results are shown in table 4.2. Tensile properties of the wool fibrils sponges are reported in paragraph 2.3.8.

Table 4.2: Tensile properties of wool fibril film

Tensile strenght (MPa)	Elongation at break (%)	Young modulus (MPa)
11.36 ± 2.42	3.18 ± 0.19	451.33 ± 57.32

According to literature, films from reduced keratin are too fragile to be used alone, so that cross-linking or blending with other polymers is needed to improve mechanical properties [102].

The porous wool fibril film showed tensile strength close to that of cross-linked keratin films [102] and higher than those of compact bio-composite films [92].

The excellent performance are due to the internal feature of the film, which is the network structure described in 4.1.1 made of randomly oriented fibrils, stuck to each other in the contact points by the protein matrix, characterised by the strength and flexibility which resemble the core of the wool fibre.

In fact, only the plain partial removal of the protein fraction gives rise to resistant films that are easy to handle, in opposition to the typical properties of pure keratin material, which often has to be processed with the addition of other polymers, or cross-linked, or plasticized.

4.3.8. Compression behavior

The hydrogel was submitted to ten repeated compression cycles, in order to measure the resilience performances too.

The compression properties of the gel are similar to those of the wool fibril sponges.

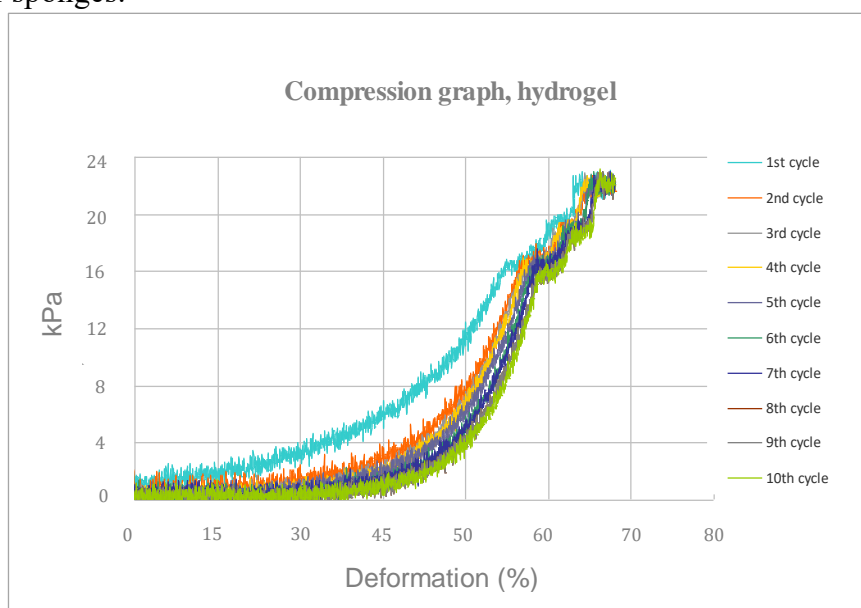


Figure 4.7: Compression behavior of the keratin hydrogel

The first cycle compression squeezed away the major part of the non-bounded water, resulting in a permanent deformation (30.2 %) of the hydrogel structure.

Smaller additional permanent deformations have been observed after the first cycle of compression (40.2 % after the tenth cycle).

The hydrogel compression moduli from the first to the tenth cycle increased from 12.1 kPa to 34 kPa (SD = 2.2 and 5.3 kPa respectively) in the load range from 2 kPa to 8 kPa (first slope) and from 50 kPa to 110 kPa (SD = 3.1 and 5.2 kPa respectively) in the load range from 6 kPa to 16 kPa (second slope). The third slope was not taken into account.

Thanks to the very high amount of water present in the keratin hydrogel, the structure is quite resilient, especially after the second compression cycle.

4.3.9. Cell viability

Human bone marrow mesenchymal stem cells were cultured on the different keratin-based materials, in order to evaluate the cell viability.

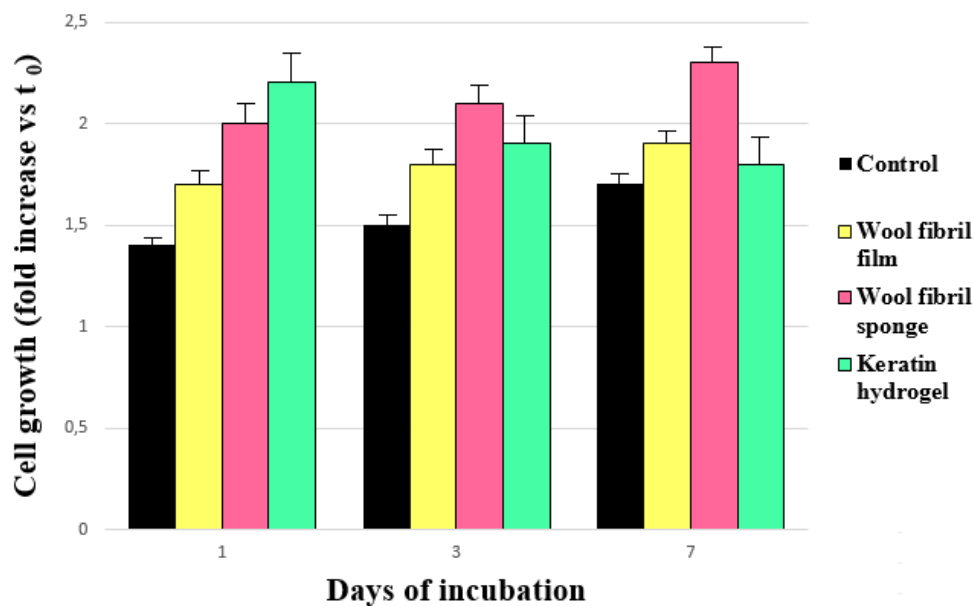


Figure 4.8: Human bone marrow mesenchymal stem cells growth. Cells were seeded on the top of tissue culture well plate (ctrl), films, sponges and hydrogels, and the viability was assessed at different times of incubation by MTT assay. Cell growth was expressed as fold increase related to seeded cell (time 0=T₀).

All keratin materials showed to be a better support for stem cell growth compared to the plastic control (Fig. 4.8). This because keratin is naturally biocompatible and possesses cell motifs binding residues of leucine-aspartic acid-valine (LDV), glutamic acid-aspartic acid-serine (EDS) and arginine-glycine- aspartic acid (RGD) supporting cellular attachment [53-54].

Stem cells proliferation after 1 day was found to be 1.7, 2 and 2.2 fold bigger when cells were cultured onto the film, the sponge and the hydrogel respectively.

Hence, after one-day culture, keratin hydrogel showed the best performance. On day 3 and 7, cells cultured on films and sponges showed additional increase in cell growth.

The hydrogel disappointing data on day 3 and 7 was probably due to the intrinsic low stability of hydrogels structure in culture media that results in stem cells loss during time.

Biological *in vitro* characterization of hydrogels is not an easy task; for instance, keratin hydrogels have been tested *in vivo* by-passing the *in vitro* experimentation [56].

These preliminary results suggest that keratin materials have good supportive properties for stem cells. The 3-D structure of wool fibril sponges and the hydrogels resulted in a peak of proliferation after the first day, suggesting that this two are the best systems for cell attachment compared to wool fibril films.

In addition, the low *in vitro* performances of the hydrogel could be not so bad *in vivo*, where the hydrogel structure degradation will result in cell delivery rather than cell lost; for this reason this material should be deeply investigated for cell delivery applications.

4.3.10. Ageing of the wool fibril films and the keratin hydrogels

The degradation rate of the wool fibril film and the keratin hydrogel were compared with the wool fibril and the collagen sponges by ageing in the Ringer's solution. Results are shown in figure 4.9.

As previously reported, a commercial collagen sponge degraded completely in 22 days while the wool fibril sponge, after 180 days, showed a degradation of 22 % only.

Fast degradation of the hydrogel was probably due to sterilization in ethanol, which may denature proteins making them more susceptible to degradation. In addition, water does not allow the formation of additional crosslink produced after casting and/or thermal stabilization as for wool fibril sponge, film and collagen sponge.

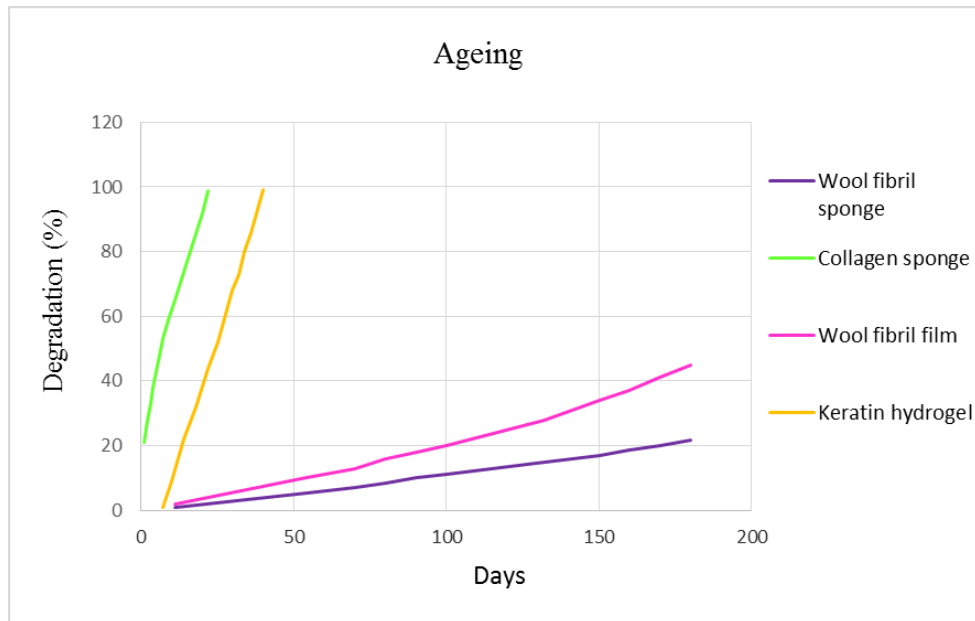


Figure 4.9: Degradation rate comparison of wool fibril film, sponge, keratin hydrogel and collagen sponge

The wool fibril film showed 45 % degradation after 180 days. Compared to the wool fibril sponge, the film seemed less durable, probably because it was not submitted to the thermal stabilization treatment carried out on the sponge to improve crosslinking.

The longer degradation rate suggests that wool fibril sponges can be a promising candidate for long term support of bone formation *in vivo*.

4.4. Conclusions

Since a stem cell-based approach is an attractive alternative to current treatment techniques in tissue engineering, 2D wool fibril films and 3D keratin hydrogels have been produced in addition to the wool fibril sponges. The attachment and growth of stem cells on different 2D and 3D keratin-based scaffolds have been evaluated.

All keratin materials showed to be a better support for stem cell growth compared to plastic control. Keratin is naturally biocompatible and possesses cell motifs binding residues of leucine-aspartic acid-valine (LDV), glutamic acid-aspartic acid-serine (EDS) and arginine-glycine-aspartic acid (RGD) supporting cellular attachment. Stem cells proliferation after 1 day was found to be good in particular for cells grown on sponges and hydrogels. On day 3 and 7, cells cultured on hydrogel did not show an additional growth increase, probably due to the intrinsic low stability of the hydrogels structure in culture media that resulted in stem cells loss during time. The 3-D structure of wool fibril sponges and hydrogels resulted in a peak of proliferation after the first day, suggesting that these two 3D scaffolds are superior for cell attachment compared to 2D wool fibril films. Moreover, the low *in vitro* properties of the hydrogel on day 3 and 7 could be not so bad *in vivo*, where the hydrogel structure degradation will result in cell delivery rather than cell lost; for this reason, this material could be deeply investigated as a cell delivery system.

Finally, ageing test revealed that wool fibril sponges, characterized by an exceptional amount of crosslinks that stabilize the keratin structure, are surpassingly stable, showing longer degradation rate compared to all other protein materials (including commercial collagen), suggesting promising applications for long term support of bone formation *in vivo*.

Chapter 5

Conclusions

Novel 3D keratin bio-composite sponges have been produced from wool fibrils, with highly interconnected micro and macro-porosity, tailored to match the natural bone tissue features.

Mechanical properties of the wool fibril sponges come out in favour of promising applications as resorbable scaffold for bone tissue engineering, since they are easy to handle and resilient in wet conditions.

The wool fibril sponges contain cellular-binding motifs that mimic the sites of cell attachment found in the native extra-cellular matrix components, which facilitate better growth providing proliferation signals to the cells and minimise apoptotic cell death, demonstrated by biocompatibility-cell viability assay with SAOS-2.

The integrated bio-engineering approach of applying bio-mechanical stimulus from pulsed electromagnetic field (PEMF), in addition to 3D architectural stimulus given by 3D scaffolds, showed to be a successful solution. In fact, PEMF stimulated an earlier differentiation in osteogenic conditions, showing a perfect synergy between biochemical and mechanical stimuli in acceleration of the differentiation process. In addition to the wool fibril sponges, 2D wool fibril films and 3D keratin hydrogels have been produced.

All keratin materials show to be a better support on stem cell growth compared to plastic control. Keratin is naturally biocompatible and possesses cell motifs binding residues of leucine-aspartic acid-valine (LDV), glutamic acid-aspartic acid-serine (EDS) and arginine-glycine-aspartic acid (RGD) supporting cellular attachment.

Stem cells proliferation after 1 day is found to be good in particular for cells grown on sponges and hydrogels. On day 3 and 7, cells cultured on hydrogel did not show an additional increase in cell growth, probably due to the intrinsic low stability of the hydrogels structure in culture media that results in stem cells loss during time.

The 3D structure of wool fibril sponges and hydrogels resulted in a peak of proliferation after the first day, suggesting that these two 3D scaffolds are superior for cell attachment compared to 2D wool fibril films. Moreover, the low *in vitro* properties of the hydrogel on day 3 and 7 could be not so bad *in vivo*, where the hydrogel structure degradation will result in cell delivery rather than cell lost; for this reason this material could be deeply investigated as cell delivery system.

Finally, ageing test revealed that wool fibril sponges, characterized by an exceptional amount of crosslinks that stabilize the keratin structure, are surpassingly stable, showing longer degradation rate compared to all other protein materials (including commercial collagen), suggesting promising applications for long term support of bone formation *in vivo*.

References

- [1] Sheikh, Z. Najeeb, S., Khurshid, Z., Verma, V., Rashid H., Glogauer M., 2015. Biodegradable Materials for Bone Repair and Tissue Engineering Applications. *Materials*, 8, 5744-5794.
- [2] Athanasiou, K.A., Zhu, C., Lanctot, D.R., Agrawal, C.M., Wang, X., 2000. Fundamentals of biomechanics in tissue engineering of bone. *Tissue Eng.*, 6, 361–381
- [3] Driessens, F.C., van Dijk, J.W., Borggreven, J.M., 1978. Biological calcium phosphates and their role in the physiology of bone and dental tissues I Composition and solubility of calcium phosphates. *Calcif. Tissue Res.*, 26 127–137.
- [4] Yaszemski, M.J., Payne, R.G., Hayes, W.C., Langer, R., Mikos, A.G., 1996. Evolution of bone transplantation: Molecular, cellular and tissue strategies to engineer human bone. *Biomaterials* 17, 175–185
- [5] . Hench L. L, Polak, J. M., 2002. Third generation biomedical materials *Science* 295 (5557), 1014 -1017
- [6] Kretlow, J. D., and Mikos, A. G., 2007. Review: mineralization of synthetic polymer scaffolds for bonetissue engineering. *Tissue Eng.* 13, 927-938.
- [7] Liu, C. Z., Czernuszka, J. T., 2007. Development of biodegradable scaffolds for tissue engineering: a perspective on emerging technology. *Mater. Sci. Technol.* 23, 379-392.
- [8] Eglin, D., Alini, M., 2008. Degradable polymeric materials for osteosynthesis: Tutorial. *Eur. Cell Mater.*, 16, 80–91
- [9] Christensen, F.B., Dalstra, M., Sejling, F., Overgaard, S., Bunger, C., 2000. Titanium-alloy enhances bone-pedicle screw fixation: Mechanical and histomorphometrical results of titanium-alloy versus stainless steel. *Eur. Spine J.* 9, 97–103.
- [10] Eppley, B.L., Sadove, A.M., 1995. A comparison of resorbable and metallic fixation in healing of calvarial bone grafts. *Plast. Reconstr. Surg.* 96, 316–322.
- [11] Marti, C., Imhoff, A.B., Bahrs, C., Romero, J., 1997. Metallic versus bioabsorbable interference screw for fixation of bone-patellar tendon-bone autograft in arthroscopic anterior cruciate ligament reconstruction. A preliminary report. *Knee Surg. Sports Traumatol. Arthrosc.* 5, 217–221.
- [12] Alexander, R., Theodos, L., 1993. Fracture of the bone-grafted mandible secondary to stress shielding: Report of a case and review of the literature. *J. Oral Maxillofac. Surg.* 51 695–697.
- [13] Sumner, D.R., 2015. Long-term implant fixation and stress-shielding in total hip replacement. *J. Biomech.* 48 797–800.
- [14] Chanlalit, C., Shukla, D.R., Fitzsimmons, J.S., An, K.N., O'Driscoll, S.W., 2012. Stress shielding around radial head prostheses. *J. Hand Surg.* 37, 2118–2125.
- [15] Haase, K., Rouhi, G., 2013. Prediction of stress shielding around an orthopedic screw: Using stress and strain energy density as mechanical stimuli. *Comput. Biol. Med.* 43, 1748–1757
- [16] Bauer, T. W., Muschler, G. F., 2000. Bone graft materials. An overview of the basic science. *Clin. Orthop. Relat. Res.* 371, 10-27
- [17] Rabie, A.B., Chay, S.H., Wong, A.M., 2000. Healing of autogenous intramembranous bone in the presence and absence of homologous demineralized intramembranous bone. *Am. J. Orthod. Dentofac. Orthop.* 117 288–297.
- [18] Gamradt, S.C., Lieberman, J.R., 2003. Bone graft for revision hip arthroplasty: Biology and future applications. *Clin. Orthop. Relat. Res.* 417, 183–194.
- [19] Skaggs, D.L., Samuelson, M.A., Hale, J.M., Kay, R.M., Tolo, V.T. 2000. Complications of posterior iliac crest bone grafting in spine surgery in children. *Spine* 25, 2400–2402
- [20] Summers, B.N., Eisenstein, S.M., 1989. Donor site pain from the ilium. A complication of lumbar spine fusion. *J. Bone Joint Surg. Br.* 71(4) 677-680.
- [21] Ge, Z., Jin, Z., Cao, T., 2008. Manufacture of degradable polymeric scaffolds for bone regeneration. *Biomed Mater.* 3(2), 1-11.

- [22] Li, Z., Kawashita, M., 2011. *J. Artif Organs*. Current progress in inorganic artificial biomaterials. 14 163-170
- [23] Schaschke, C., Audic, J.L. 2014. Editorial: Biodegradable materials. *Int. J. Mol. Sci.* 15, 21468–21475
- [24] Yeung, K.W., Wong, K.H., 2012. Biodegradable metallic materials for orthopaedic implantations: A review. *Technol. Health Care* 20, 345–362.
- [25] LeGeros, R.Z., 1993. Biodegradation and bioresorption of calcium phosphate ceramics. *Clin. Mater.* 14, 65–88.
- [26] Tevlin, R., McArdle, A., Atashroo, D., Walmsley, G.G., Senarath-Yapa, K., Zielins, E.R., Paik, K.J., Longaker, M.T., Wan, D.C., 2014. Biomaterials for craniofacial bone engineering, *J. Dent. Res.* 93, 1187–1195.
- [27] Freed, L.E., Vunjak-Novakovic, G., Biron, R.J., Eagles, D.B., Lesnoy, D.C., Barlow, S.K., Langer, R., 1994. Biodegradable polymer scaffolds for tissue engineering. *Nat. Biotechnol.* 12, 689–693.
- [28] Griffith, L.G., Naughton, G., 2002. Tissue engineering-Current challenges and expanding opportunities. *Science* 295, 1009–1014
- [29] Burg, K.J., Porter, S., Kellam, J.F., 2000. Biomaterial developments for bone tissue engineering, *Biomaterials* 21, 2347–2359.
- [30] Sheikh, Z., Sima, C., Glogauer, M., 2015. Bone replacement materials and techniques used for achieving vertical alveolar bone augmentation. *Materials* 8, 2953–2993.
- [31] Blokhuis, T.H., 2014. Bioresorbable bone graft substitutes in Malick, K., Woodhead Publishing Series in Biomaterials, pp 80–92.
- [32] Zijdeveld, S.A., Zerbo, I.R., van den Bergh, J.P., Schulten E.A., ten Bruggenkate, C.M., 2005. Maxillary sinus floor augmentation using a beta-tricalcium phosphate (Cerasorb) alone compared to autogenous bone grafts. *Int J Oral Maxillofac Implants.* 20, 432-440.
- [33] Jell, G., Stevens, M. M., 2006. Gene activation by bioactive glasses. *J Mater Sci Mater Med* 17, 997–1002.
- [34] Tsigkou, O., Hench L.L., Boccaccini A.R., Polak J.M., Stevens M.M., 2007. Enhanced differentiation and mineralization of human fetal osteoblasts on PDLLA containing Bioglass composite films in the absence of osteogenic supplements. *J. Biomed. Mater. Res. A* 80, 837-951.
- [35] Oonishi, H., Kushitani S, Iwaki H. 1995. Comparative bone formation in several kinds of bioceramic granules, in Wilson, J., Hench, L.L., Greenspan, D. (eds.), *Bioceramics*, vol. 8, Proceedings of the 8th International Symposium on Ceramics in Medicine, Elsevier Science Ltd., Tokyo, pp. 137-144.
- [36] Stevens, M. M., 2008. Biomaterials for bone tissue engineering, *Materialstoday*, 11, 18-25.
- [37] He, W., Benson, R. 2014. Polymeric Biomaterials, in: Ebnesajjad, S., Modjarrad, K. (Eds), *Handbook of Polymer Applications in Medicine and Medical Devices*, Elsevier/William Andrew, Oxford, pp. 55–76.
- [38] Rouse, J.G., Van Dyke, M.E., 2010. A Review of Keratin-Based Biomaterials for Biomedical Applications. *Materials* 3(2), 999-1014.
- [39] Nair, L.S., Laurencin, T. C., 2007. Biodegradable polymers as biomaterials. *Prog. Polym. Sci.* 32, 762–798.
- [40] Chu, T.M.G., Warden, S. J., Turner C. H., Stewart, R. L., 2007. Segmental bone regeneration using a load-bearing biodegradable carrier of bone morphogenetic protein-2. *Biomaterials* 28, 459–467.
- [41] Kasten, P., Vogel, J., Geiger, F., Niemeyer, P., Luginbühl R., Szalay, K., 2008. The effect of platelet-rich plasma on healing in critical-size long-bone defects, *Biomaterials*, 29, 3983–3992.
- [42] Reichert, J. C., Saifzadeh, S., Wullschlegel, M.E., Epari, D.R., Schütz M.A., Duda, G.N., Schell, H., van Griensven, M., Redl, H., Hutmacher, D.W., 2009. The challenge of establishing preclinical models for segmental bone defect research. *Biomaterials*, 30, 2149–2163.
- [43] Zhou, J., Lin, H., Fang, T., Li, X., Dai W., Uemura, T., Dong, J., 2010. The repair of large segmental bone defects in the rabbit with vascularized tissue engineered bone. *Biomaterials* 31, 1171–1179.
- [44] Zadpoor, A.A., 2015. Bone tissue regeneration: the role of scaffold geometry, *Biomater. Sci.* 3, 231-245.
- [45] Karageorgiou V., Kaplan, D., 2005. Porosity of 3D biomaterial scaffolds and osteogenesis. *Biomaterials* 26, 5474–5491.
- [46] Gamsjäger, E., Bidan, C., Fischer, F., Fratzl P., Dunlop, J., 2013. Modelling the role of surface stress on the kinetics of tissue growth in confined geometries. *Acta Biomater.* 9, 5531–5543.
- [47] Ripamonti, U., L. Roden, 2010. Biomimetics for the induction of bone formation, 7(4) 467-479.
- [48] Stevens, M.M., Marini, R.P., Schaefer, D., Aronson, J., Langer, R., Shastri, V.P., 2005. *Proc. Natl. Acad. Sci. USA* 102(2) 11450-11455.

- [49] Stevens, M.M., Qanadilo, H.F., Langer, R., Prasad Shastri, V., 2004. A rapid-curing alginate gel system: utility in periosteum-derived cartilage tissue engineering. *Biomaterials* 25, 887-894.
- [50] Cushing, M. C., Anseth, K. S., 2007. Materials science. Hydrogel cell cultures. *Science* 316, 1133-1134.
- [51] Lutolf, M.P., Weber, F.E., Schmoek, H.G., Schense, J.C., Kohler, T., Müller, R., Hubbell, J.A., 2003. Repair of bone defects using synthetic mimetics of collagenous extracellular matrices. *Nat. Biotechnol.* 21, 513-518.
- [52] Wang, B., Yang, W., McKittrick, J., Meyers, M.A., 2016. Keratin: Structure, mechanical properties, occurrence in biological organisms, and efforts at bioinspiration. *Prog. Mater. Sci.* 76, 229-318.
- [53] Tachibana, A., Furuta, Y., Takeshima, H., Tanabe, T., Yamauchi, K., 2002. Fabrication of wool keratin sponge scaffolds for long-term cell cultivation. *J. Biotechnol.* 93, 165-170.
- [54] Verma, V., Verma, P., Ray, P., Ray, A.R., 2008. Preparation of scaffolds from human hair proteins for tissue-engineering applications. *Biomed. Mater.* 3, 1-12.
- [55] Rahmany, M.B., Van Dyke, M., 2013. Biomimetic approaches to modulate cellular adhesion in biomaterials: A review. *Acta Biomaterialia* 9(3) 5431-543.
- [56] Bahawdory Rahmany, M., 2013. Mechanistic investigation of a hemostatic keratin biomaterial, A Dissertation Submitted to the Graduate Faculty of Wake Forest University Graduate School of Arts and Science, Winston-Salem, North Carolina <http://hdl.handle.net/10339/38556>
- [57] Aboushwareb, T., Eberli, D., Ward, C., Broda, C., Atala, J.H, Van Dyke, M., 2009. A keratin biomaterial gel hemostat derived from human hair: evaluation in a rabbit model of lethal liver injury. *J. Biomed. Mater. Res. B* 90B(1) 45-54.
- [58] Richter, J.R., De Guzman, R.C., Van Dyke, M.E., 2011. Mechanisms of hepatocyte attachment to keratin biomaterials. *Biomaterials* 32(30) 7555-7561.
- [59] Wang, J., Hao, S., Luo, T., Yang, Q., Wang, B., 2016. Development of feather keratin nanoparticles and investigation of their hemostatic efficacy. *Mater. Sci. Eng. C* 68, 768-773.
- [60] Nunez, F., Trach, S., Burnett, L., Handa, R., Van Dyke, M., Callahan, M., Smith, T., 2011. *Microcirculation* 18(8), 663-669.
- [61] Barone, J.R., Shmidt, W.F., Christina, F., Liebner, E., 2005. Thermally processed keratin films, *J. Appl. Polym. Sci.* 97, 1644-1651.
- [62] Fraser, R.D.B., Parry, D.A.D., 2011. The structural basis of the filament-matrix texture in the avian/reptilian group of hard b-keratins. *J. Struct. Biol.* 173(2) 391-405.
- [63] Gillespie, J.M., 1990. The proteins of hair and other hard α -keratins, in: Goldman R.D., Steinert P.M. (Eds), *Cellular and molecular biology of intermediate filaments*, Springer, US, pp. 95-128.
- [64] Fraser, R.D.B., MacRae, T.P., Rogers, G.E., 1972. *Keratins: their composition, structure and biosynthesis*, Thomas, Springfield.
- [65] Crewther, W.G., Fraser, R.D.B., Lennox, F.G., Lindley, H., 1965. The chemistry of keratins, *Adv. Protein Chem.* 20, 191-346.
- [66] MacLaren, J.A., 1987. Maximum extraction of wool proteins by thiol-urea solutions. *Text. Res. Inst.* 57, 87-92.
- [67] Fuji, T., Takayama, S., Ito, Y., 2013. A novel purification procedure for keratin-associated proteins and keratin from human hair. *J. Biol. Macromol.* 13(3) 92-106.
- [68] Gennadios, A., 2002. *Protein-Based Films and Coatings*, CRC Press, London.
- [69] Nakamura, A., Arimoto, M., Takeuchi, K., Fujii, T., 2002. A rapid extraction procedure of human hair proteins and identification of phosphorylated species, *Biol. Pharm. Bull.* 25(5) 569-572.
- [70] Alexander, P., Earland, C., 1950. Structure of wool fibres; isolation of an alpha and beta-protein in wool. *Nature* 166(4218), 396-397.
- [71] Thompson, E.O.P., O'Donnel, I.J., 1959. Studies on oxidised wool. I. A comparison of the completeness of oxidation with peracetic acid and performic acids. *Aust. J. Biol. Sci.* 12 282-293.
- [72] Lewis, D.M., Rippon, J.A., 2013. *The coloration of wool and other keratin fibres*, John Wiley, Bradford.
- [73] Wolfram, L.J., 2003. Human hair: A unique physicochemical composite. *J. Am. acad. Dermatol.* 48(6) 106-114.
- [74] Earland, C., Knight, C., 1955. Studies on the structure of keratin: I. The analysis of fractions isolated from wool oxidized with peracetic acid. *Biochim. Biophys. Acta*, 17, 457-461.
- [75] Lee, H., Noh, K., Lee, S.C., Kwon, I., Han, D., Lee, I., and Hwang, Y., 2014. Human Hair Keratin and Its-Based Biomaterials for Biomedical Applications *Tissue Eng. Regen. Med.* 11(4), 255-265.
- [76] Zhang, Q., Shan, G., Cao, P., He, J., Linc, Z., Huang, Y., Ao, N., 2015. Mechanical and biological properties of oxidized horn keratin. *Mat. Sci. Eng. C* 47, 123-134.

- [77] Ayutthaya, S.I.N., Tanpichai, S., Wootthikanokkhan, J., 2015. Keratin Extracted from Chicken Feather Waste: Extraction, Preparation, and Structural Characterization of the Keratin and Keratin/Biopolymer Films and Electrospuns. *J. Poly. Environ.* 23(4), 506-516.
- [78] Park, M., Shin, H.K., Kim, B., Kim, M.J., Kim, I., Park, B., Kim, H., 2015. Effect of discarded keratin-based biocomposite hydrogels on the wound healing process in vivo. *Mat. Sci. Eng. C* 55, 88–94.
- [79] Zoccola, M., Montarsolo, A., Mossotti, R., Patrucco, A., Tonin, C., 2015. Green Hydrolysis as an Emerging Technology to Turn Wool Waste into Organic Nitrogen Fertilizer. *Waste and Biomass Valorization* 6, 891-897.
- [80] Villa, A.L.V., Aragão, M.R.S., dos Santos, E.P., Mazotto, A.M., Zingali, R.B., de Souza, E.P. and Vermelho, A.B., 2013. Feather keratin hydrolysates obtained from microbial keratinases: effect on hair fiber. *BMC Biotechnol.* 13(15) 1-11.
- [81] Eslahi, N., Dadashian, F., Nejad, N.H., 2013. An investigation on keratin extraction from wool and feather waste by enzymatic hydrolysis. *Prep. Biochem. Biotech.* 43(7) 624-648.
- [82] Mokrejs, P., Svoboda, P., Hrnčirik, J., Janacova, D., Vasek, V., 2011. Processing poultry feathers into keratin hydrolysate through alkaline-enzymatic hydrolysis. *Waste Manag Res.* 29(3) 260-267.
- [83] Mukesh Kumar, D.J., Lavanya, S., Priya, P., Immaculate Nancy Rebecca, A., Balakumaran, M.D., Kalaichelvan, P.T., 2012. Production of Feather Protein Concentrate from Feathers by In vitro Enzymatic Treatment, its Biochemical Characterization and Antioxidant Nature. *Middle-East J.* 11 (7) 881-886.
- [84] Mokrejs, P., Krejci, O., Svoboda, P., Rasayan, V.V., 2011. Modeling technological conditions for breakdown of waste sheep wool. *J. chem.* 4(4) 728-735.
- [85] Mokrejs, P., Krejci, O., Svoboda P., 2011. Producing keratin hydrolysates from sheep wool *OJC* 27(4) 1303-1309.
- [86] Tonin, C., Zoccola, M., Aluigi, A., Varesano, A., Montarsolo, A., Vineis, C., Zimbardi, F., 2006. Study on the conversion of wool keratin by steam explosion. *Biomacromolecules* 7(12), 3499-3504.
- [87] Zhang, Y., Zhao, W., Yang, R., 2015. Steam flash explosion assisted dissolution of keratin from feathers. *ACS Sustain. Chem. Eng.* 3(9), 2036-2042.
- [88] Zoccola, M., Aluigi, A., Patrucco, A., Vineis, C., Forlini, F., Locatelli, P., Sacchi, M.C., Tonin, C., 2012. Microwave-assisted chemical-free hydrolysis of wool keratin. *Text. Res. J.* 82(19) 2006-2018.
- [89] Bhavsar, P., Zoccola, M., Patrucco, A., Montarsolo, A., Rovero, G., Tonin, C., in press. Comparative study on the effects of superheated water of superheated water and high temperature alkaline hydrolysis on wool keratin. *Text. Res. J.*
- [90] Chen, J., Ding, S., Ji, Y., Ding, J., Yang, X., Zou, M., 2015. Microwave-enhanced hydrolysis of poultry feather to produce amino acid. *Chem. Eng. Process.* 87, 104–109.
- [91] Patrucco, A., Zoccola, M., Consonni, R., Tonin, C., 2013. Wool cortical cell-based porous films, *Text. Res. J.* 83(15), 1563-1573.
- [92] Patrucco, A., Aluigi, A., Vineis, C., Tonin, C., 2011. Bio-composite keratin films from wool fibrillation. *J. Biobased. Mater. Bio.* 5(1), 124-131.
- [93] Sionkowska, A., Skopinska-Wisniewska, J., Planecka, A., Kozłowska, J., 2010. The influence of UV irradiation on the properties of chitosan films containing keratin. *Polym. Degrad. Stabil.* 95(12) 2486–2491.
- [94] Moore, G.R.P., Martelli, S.M., Gandolfo, C., do Amaral Sobral, P.J., Laurindo, J.B., 2006. Influence of the glycerol concentration on some physical properties of feather keratin films, *Food Hydrocolloids*, 20(7), 975–982.
- [95] Fujii, T., Ogiwara, D., Arimoto, M., 2004. Convenient procedures for human hair protein films and properties of alkaline phosphatase incorporated in the film, *Biol. Pharm. Bull.* 27, 89–93.
- [96] Poole, A.J., Church, J.S., 2015. The effects of physical and chemical treatments on Na2S produced feather keratin films, *Int. J. Biol. Macromol.* 73, 99–108.
- [97] Tonin, C., Aluigi, A., Vineis, C., Varesano, A., Montarsolo, A., Ferrero, F., 2007. Thermal and structural characterization of poly(ethylene-oxide)/keratin blend films. *J. Therm. Anal. Calorim.* 89(2), 601-608.
- [98] Kawano, Y., Okamoto, S., 1975. Film and gel of keratin, *Kagaku to Seibutsu* 13(5), 291-292.
- [99] Okamoto, S., 1977. On the formation of films from some proteins, *Nippon Shokuhin Kogyo Gakkaishi* 24(1), 40-50.
- [100] Katoh, K., Shibayama, M., Tanabe, T., Yamauchi, K., 2004. Preparation and physicochemical properties of compression-molded keratin films, *Biomaterials* 25(12), 2265-72.
- [101] Buchko, C.J., Chen, L.C., Shen, Y.D.C., Martin, 1999. Processing and microstructural characterization of porous biocompatible protein polymer thin films, *Polymer* 40, 7397-7407.

- [102] Tanabe, T., Okitsu, N., Yamauchi, K., 2004. Fabrication and characterization of chemically crosslinked keratin films, *Mater. Sci. Eng. C* 24(3), 441-446.
- [103] Fujii, T., Ide, Y., 2004. Preparation of Translucent and Flexible Human Hair Protein Films and Their Properties. *Biol. Pharma Bull.* 27(9), 1433-1436.
- [104] Reichl, S., 2009. Films based on human hair keratin as substrates for cell culture and tissue engineering. *Biomaterials* 30(36), 6854-6866.
- [105] Yamauchi, K., Yamauchi, A., Kusunoki, T., Kohda, A., Konishi, Y., 1996. Preparation of stable aqueous solution of keratins and physiochemical and biodegradational properties of films, *J. Biomed. Mater. Res.* 31(4), 439-444.
- [106] Tanabe, T., Okitsu, N., Tachibana, A., Yamauchi, K., 2002. Preparation and characterization of keratin-chitosan composite film. *Biomaterials* 23(3), 817-825.
- [107] Yamauchi, K., Hojo, H., Yamamoto, Y., Tanabe, T., 2003. Enhanced cell adhesion on RGDS-carrying keratin film. *Mat. Sci. Eng. C* 23(4), 467-472.
- [108] L.S. Reichl, C.C. Müller-Goymann, 2011. Keratin film made of human hair as a nail plate model for studying drug permeation. *Eur. J. Pharm. Biopharm.* 78(3), 432-440.
- [109] Selmin, F., Cilurzo, F., Aluigi, A., Franzè, S., Minghetti, P., 2012. Regenerated keratin membrane to match the in vitro drug diffusion through human epidermis, *Resul. Pharma Sci.* 2(0), 72-78.
- [110] Lee, K.Y., Ha, W.S., 1999. DSC studies on bound water in silk fibroin/Scarboxymethyl kerateine blend films, *Polymer* 40(14), 4131-4134.
- [111] Lee, K.Y., Kong, S.J., Park, W.H., Kwon, I.C., 1998. Effect of surface properties on the antithrombogenicity of silk fibroin/S-carboxymethyl kerateine blend films. *J. Biomater. Sci. Polym. Ed.* 9, 905-914.
- [112] Lee, K., 2001. Characterization of silk fibroin/S-carboxymethyl kerateine surfaces: evaluation of biocompatibility by contact angle measurements. *Fib. Polym.* 2(2), 71-74.
- [113] Vasconcelos, A., Freddi, G., Cavaco-Paulo, A., 2008. Biodegradable materials based on silk fibroin and keratin. *Biomacromolecules* 9(4), 1299-1305.
- [114] Tanase, C.E., Spiridon, I., 2014. PLA/chitosan/keratin composites for biomedical applications. *Mat. Sci. Eng. C*, 40, 242-247.
- [115] Aluigi, A., Vineis, C., Ceria, A., Tonin, C., 2008. Composite biomaterials from fibre wastes: characterization of wool-cellulose acetate blends, *Compos. Part A-Appl. S.*, 39(1), 126-132.
- [116] Fortunati, E., Aluigi, A., Armentano, I., Morena, F., Emiliani, C., Martino, S., Santulli, C., Torre, L., Kenny, J.M., Puglia, D., 2015. Keratins extracted from merino wool and brown alpaca fibres: thermal, mechanical and biological properties of PLLA based biocomposites, *Mat. Sci. Eng. C*, 47(1), 394-406.
- [117] Thilagar, S., Jothi, N.A., Omar, A.R.S., Ganabgadi, S., 2009. Effect of keratin-gelatin and bFGF-gelatin composite film as a sandwich layer for fullthickness skin mesh graft in experimental dogs. *J. Biomed. Mater. Res. B* 88B, 12-16.
- [118] Vasconcelos, A., Pêgo, A.P., Henriques, L., Lamghari, M., Cavaco-Paulo, A., 2010. Protein matrices for improved wound healing: elastase Inhibition by a synthetic peptide model, *Biomacromolecules* 11, 2213-2220.
- [119] Ramanathan, G., Raja, M.D., Barge, S., Sivagnanam, U.T., 2015. Preparation and characterization of keratin-based biosheet from bovine horn waste as wound dressing material. *S. Singaravelu Mater. Lett.*, 152, 90-93.
- [120] Cui, L., Gong, J., Fan, X., Wang, P., Qiu, Y., 2012. Transglutaminase-modified wool keratin film and its potential application in tissue engineering. *Eng. Life Sci.* 13(2), 149-155.
- [121] Chen, Y.H., Dong, W.R., Chen, Q.Y., Zhao, B.L., Zou, Z.Z., Xiao, Y.Q., Hu, G.D., Qiu, X.X., 2007. Biological dressing with human hair keratin collagen sponge-poly 2-hydroxyethyl methacrylate composite promotes burn wound healing in SD rats, *Nan Fang Yi Ke Da Xue Xue Bao* 27, 1621-1626.
- [122] Chen, Y.H., Dong, W.R., Xiao, Y.Q., Zhao, B.L., Hu, G.D., An, L.B., 2006. Preparation and bioactivity of human hair keratin-collagen sponge, a new type of dermal analogue. *Nan Fang Yi Ke Da Xue Xue Bao* 26, 131-138.
- [123] Singaravelu, S., Ramanathan, G., Raja, M.D., Nagiah, N., Padmapriya, P., Kaveri, K., Sivagnanam, U.T., 2016. Biomimetic interconnected porous keratin-fibrin-gelatin 3D sponge for tissue engineering application, *Int. J. Biol. Macromol.* 86, 810-809.
- [124] Tan, H.B., Wang, F.Y., Ding, W., Zhang, Y., Ding, J., Cai, D.X., Yu, K.F., Yang, J., Yang, L., Xu, Y.Q., 2015. Fabrication and evaluation of porous Keratin/chitosan (KCS) scaffolds for effectively accelerating wound healing, *Biomed. Environ. Sci.* 28(3), 178-189.
- [125] Kirubanandan, S., Babu, U.D., 2012. Macroporous keratin scaffold – a novel biomaterial for biomedical applications. *Int. J. Pharm. Chem. Sci.* 1(4) 1447, 1447-1454.
- [126] Katoh, K., Tanabe, T., Yamauchi, K., 2004. Novel approach to fabricate keratin sponge scaffolds with controlled pore size and porosity. *Biomaterials* 25, 4255-4262.

- [127] Tachibana, A., Kaneko, S., Tanabe, T., Yamauchi, K., 2005. Rapid fabrication of keratin-hydroxyapatite hybrid sponges toward osteoblast cultivation and differentiation. *Biomaterials* 26(3), 297-302.
- [128] Kurimoto, A., Tanabe, T., Tachibana, A., Yamauchi, K., 2003. Keratin sponge: Immobilization of lysozyme. *J. Biosci. Bioeng.* 96(3), 307-309.
- [129] Hamasaki, S., Tachibana, A., Tada, D., Yamauchi, K., Tanabe, T., 2008. Fabrication of highly porous keratin sponges by freeze-drying in the presence of calcium alginate beads, *Mat. Sci. Eng. C* 28(8), 1250-1254.
- [130] Yamauchi, K., Maniwa, M., Mori, T., 1998. Cultivation of fibroblast cells on keratin-coated substrata. *J. Biomat. Sci. Polym. E.* 9, 259-270.
- [131] Tachibana, A., Nishikawa, Y., Nishino, M., Kaneko, S., Tanabe, T., Yamauchi, K., 2006. Modified keratin sponge: binding of bone morphogenetic protein-2 and osteoblast differentiation. *Journal Biosci. Bioeng.* 102(5), 425-429.
- [132] Kakkar, P., Verma, S., Manjubala, I., Madhan, B., 2014. Development of keratin-chitosan-gelatin composite scaffold for soft tissue engineering. *Mat. Sci. Eng. C* 45, 343-347.
- [133] Gupta, P., Nayak, K.K., 2016. Optimization of keratin/alginate scaffold using RSM and its characterization for tissue engineering. *Int. J. Biol. Macromol.* 85, 141-149.
- [134] Nayak, K.K., Gupta, P., 2015. In vitro biocompatibility study of keratin/agar scaffold for tissue engineering. *Int. J. Biol. Macromol.* 81, 1-10.
- [135] Kowalczewski, C.J., Tombyln, S., Wasnick, D.C., Hughes, M.R., Ellenburg, M.D., Callahan, M.F., Smith, T.L., Van Dyke, M.E., Burnett, L.R., Saul, J.M., 2014. Reduction of ectopic bone growth in critically-sized rat mandible defects by delivery of rhBMP-2 from kerateine biomaterials. *Biomaterials* 35(10), 3220-3228.
- [136] Xu, S., Sang, L., Y. Zhang, X. Wang, X. Li, 2013. Biological evaluation of human hair keratin scaffolds for skin wound repair and regeneration, *Mater. Sci. Eng. C* 33(2), 648-655.
- [137] Park, M., Kim, B.S., Shin, H.K., Park, S.J., Kim, H.Y., 2013. Preparation and characterization of keratin-based biocomposite hydrogels prepared by electron beam irradiation. *Mat. Sci. Eng. C* 33(8), 5051-5057.
- [138] Silva, R., Fabry, B., Boccaccini, A.R., 2014. Fibrous protein-based hydrogels for cell encapsulation, *Biomaterials* 35(25), 6727-6738.
- [139] Ozaki, Y., Takagi, Y., Mori, H., Hara, M., 2014. Porous hydrogel of wool keratin prepared by a novel method: An extraction with guanidine/2-mercaptoethanol solution followed by a dialysis. *Mat. Sci. Eng. C* 42, 146-154.
- [140] Blanchard, C.R. Timmons, S.F., Smith, R.A., 2000. Keratin-based hydrogel for biomedical applications and method of production, US Patent 6159496.
- [141] Nakata, R., Osumi, Y., Miyagawa, S., Tachibana, A., Tanabe, T., 2015. Preparation of keratin and chemically modified keratin hydrogels and their evaluation as cell substrate with drug releasing ability. *J. Biosci. Bioeng.* 120(1), 111-116.
- [142] Burnett, L.R., Rahmany, M.B., Richter, J.R., Aboushwareb, T.A., Eberli, D., Ward, C.L., Orlando, G., Hantgan, R.R., Van Dyke, M.E., 2013. Hemostatic properties and the role of cell receptor recognition in human hair keratin protein hydrogels. *Biomater.* 34(11), 2632-2640.
- [143] Peyton, C.C., Keys, T., Tombyln, S., Burmeister, D., Beumer, J.H., Holleran, J.L., Sirintrapun, J., Washburn, S., Hodges, S.J., 2012. Halofuginone infused keratin hydrogel attenuates adhesions in a rodent cecal abrasion model. *J Sur Res* 178(2), 545-552.
- [144] Branham, K.E., English, J.P., Cowsar, D.R., 2005. Keratin based hydrogel sheets prepared from fabric for biomedical and other applications and method of production. WO/2005/124011.
- [145] Than, M.P., Smith, R.A., Cassidy, S., Kelly, R., Marsh, C., Maderai, A., Kirsner, R.S., 2013. Use of a keratin-based hydrogel in the management of recessive dystrophic epidermolysis bullosa. *J. Dermatol. Treat.* 24(4), 290-291.
- [146] Thirupathi Kumara Raja, S., Thiruselvi, T., Sailakshmi, G., Ganesh, S., Gnanamani, A., 2013. Rejoining of cut wounds by engineered gelatin-keratin glue, *Biochim. Biophys. Acta* 1830(8), 4030-403
- [147] Saul, J.M., Ellenburg, M.D., de Guzman, R.C., Van Dyke, M., 2011. Keratin hydrogels support the sustained release of bioactive ciprofloxacin, *J. Biomed. Mater. Res A* 98(4), 544-553.
- [148] Apel, P.J., Garrett, J.P., Sierpinski, P., Ma, J., Atala, A., Smith, T.L., Koman, L.A., Van Dyke, M.E., 2008. Peripheral nerve regeneration using a keratin-based scaffold: long-term functional and histological outcomes in a mouse model. *J. Hand. Surg.* 33(9), 1541-1547.
- [149] Sierpinski, P., Garrett, J., Ma, J., Apel, P., Klorig, D., Smith, T., Koman, L.A., Atala, A., Van Dyke, M., 2008. The use of keratin biomaterials derived from human hair for the promotion of rapid regeneration of peripheral nerves, *Biomaterials* 29(1), 118-128.

- [150] Sierpinski, P., Garrett, J., Ma, J., Apel, P., Klorig, D., Smith, T., Koman, L.A., Atala, A., Van Dyke, M., 2008. The use of keratin biomaterials derived from human hair for the promotion of rapid regeneration of peripheral nerves, *Biomaterials* 29(1), 118-128.
- [151] Lin, Y.C., Ramadan, M., Van Dyke, M., Kokai, L.E., Philips, B.J., Rubin, J.P., Marra, K.G., 2012. Keratin gel filler for peripheral nerve repair in a rodent sciatic nerve injury model. *Plast. Reconstr. Surg.* 129(1), 67-78.
- [152] Pace, L.A., Plate, J.F., Smith, T.L., Van Dyke, M.E., 2013. The effect of human hair keratin hydrogel on early cellular response to sciatic nerve injury in a rat model. *Biomaterials* 34(24), 5907–5914.
- [153] Lin, Y., Marra, K.G., 2012. Injectable systems and implantable conduits for peripheral nerve repair. *Biomed. Mater.* 7(2), 1-9.
- [154] Kongprathet, T., Wanichwecharungruang, S., 2015. Sustaining guest molecules on bio-surfaces by grafting the surfaces with cyclodextrins. *Carbohydr. Polym.* 119, 110–117.
- [155] Poole, A.J., Church J.S. and Huson, M.G., 2009. Environmentally sustainable fibers from regenerated protein, *Biomacromolecules* 10, 1–8.
- [156] Aluigi, A., Corbellini, A., Rombaldoni, F., Zoccola, M., Canetti, M., 2013. Morphological and structural investigation of wool-derived keratin nanofibres crosslinked by thermal treatment. *Int. J. Biol. Macromol.* 57, 30–37.
- [157] Park, M., Shin, H.K., Panthi, G., Rabbani, M.M., Alam, A., Choi, J., Chung, H., Hong, S., Kim, H., 2015. Novel preparation and characterization of human hair-based nanofibers using electrospinning process. *Int. J. Biol. Macromol.* 76, 45–48.
- [158] Zoccola, M., Aluigi, A., Vineis, C., Tonin, C., Ferrero, F., Piacentino, M.G., 2008. Study on cast membranes and electrospun nanofibers made from keratin/fibroin blends. *Biomacromolecules* 9, 2819–2825.
- [159] Li, J., Li, Y., Li, L., Mak, A.F.T., Ko, F., Qin, L., 2009. Preparation and biodegradation of electrospun PLLA/keratin nonwoven fibrous membrane. *Polym. Degrad. Stabil.* 94(10), 1800-1807.
- [160] Pham, Q.P., Sharma, U., Mikos, A.G., 2006. Electrospinning of polymeric nanofibers for tissue engineering applications: a review. *Tissue Eng.* 12(5), 1197-211.
- [161] Yuan, J. Xing, Z., Park, S.W., Geng, J., Kang, I., Yuan, J. , Shen, J., Meng, W., Shim, K., Han, I., Kim, J., 2009. Fabrication of PHBV/Keratin Composite Nanofibrous Mats for Biomedical Applications, *Macromol. Res.* 17, 850-855.
- [162] Aluigi, A., Varesano, A., Montarsolo, A., Vineis, C., Ferrero, F., Mazzuchetti, G., Tonin, C., 2007. Electrospinning of keratin/poly(ethylene oxide)blend nanofibers. *J. Appl. Polym. Sci.* 104(2), 863-870.
- [163] Aluigi, A., Vineis, C., Varesano, A., Mazzuchetti, G., Ferrero, F., Tonin, C., 2008. Structure and properties of keratin/PEO blend nanofibres. *Eur. Polym. J.* 44(8), 2465-2475.
- [164] Varesano, A., Aluigi, A., Vineis, C., Tonin, C., 2008. Study on the shear viscosity behavior of keratin/PEO blends for nanofibre electrospinning. *J. Polym. Sci. B* 46(12), 1193-201.
- [165] Aluigi, A., Tonetti, C., Vineis, C., Tonin, C., Mazzuchetti, G., 2011. Adsorption of copper(II) ions by keratin/PA6 blend nanofibres, *Eur. Polym. J.* 47(9), 1756-1764.
- [166] Zhao, X., Lui, Y.S., Choo, C.K.C., Sow, W.T., Huang, C.L., Ng, K.W., Tan, L.P., Loo, J.S.C., 2015. Calcium phosphate coated keratin–PCL scaffolds for potential bone tissue regeneration. *Mat. Sci. Eng. C* 49, 746–753.
- [167] Choi, J., Panthi, G., Liu, Y., Kim, J., Chae, S., Lee, C., Park, M., Kim, H., 2015. Keratin/poly (vinyl alcohol) blended nanofibers with high optical transmittance, *Polymer* 58, 146–152.
- [168] Zoccola, M., Montarsolo, A., Aluigi, A., Varesano, A., Vineis, C., Tonin, C., 2007. Electrospinning of polyamide 6/modified-keratin blends, *E-Polymers* 27, 1433-1436).
- [169] Isarankura, N.A.S., Tanpichai, S., Sangkhun, W., Wootthikanokkhan, J., 2016. Effect of clay content on morphology and processability of electrospun keratin/poly(lactic acid) nanofiber, *Int. J. Biol. Macromol.* 85, 585–595.
- [170] Xing, Z.C., Yuan, J., Chae, W.P., Kang, I.K., 2011. Keratin nanofibers as a biomaterial. *International Conference on Nanotechnology and Biosensors IPCBEE* 2, 120-124.
- [171] Katoh, K., Shibayama, M., Tanabe, T., Yamauchi, K., 2004. Preparation and properties of keratin poly(vinyl alcohol) blend fiber, *J. Appl. Polym. Sci.* 91, 756–762.
- [172] Yamauhi, K., Khoda, A., 1997. Keratin microcapsules Novel proteinous microcapsules from wool keratins. *Colloid Surf. B Biointerfaces* 9, 117-119.
- [173] Saravanan, S., Sameera, D.K., Moorthi, A., Selvamurugan, N., 2013. Chitosan scaffolds containing chicken feather keratin nanoparticles for bone tissue engineering, *Int. J. Biol. Macromol.* 62, 481–486.
- [174] Li, J., Li, Y., Li, L., Mak, A.F.T., Ko, F., Qin, L., 2009. Fabrication and degradation of poly(L-lactic acid) scaffolds with wool keratin, *Compos. Part B-Engineering* 40(7), 664–667.

- [175] Kakkar, P., Madhan, B., 2016. Fabrication of keratin-silica hydrogel for biomedical applications, *Mat, Sci. Eng. C* 66, 178–184.
- [176] Aluigi, A., Zoccola, M., Vineis, C., Tonin, C., Ferrero, F., Canetti, M., 2007. Study on the structure and properties of wool keratin regenerated from formic acid, *Int. J. Biol. Macromol.* 41(3), 266–273.
- [177] Enoch, S., Leaper, D.J., 2008. Basic science of wound healing. *Surgery (Oxford)*, 26(2), 31–37.
- [178] Mayet, N., Choonara, Y.E., Kumar, P., Tomar, L.K., Tyagi, C., Du Toit, L.C., Pillay, V., 2014. A comprehensive review of advanced biopolymeric wound healing systems. *J. of Pharm. Sci.* 103(8), 2211–2230.
- [179] Boateng, J., Catanzano, O., 2015. Advanced therapeutic dressings for effective wound healing-a review. *J. Pharm. Sci.* 104(11), 3653–3680.
- [180] Pechter, P.M., Gil, J., Valdes, J., Tomic-Canic, M., Pastar, I., Stojadinovic, O., Kirsner, R.S., Davis, S.C., 2012. Keratin dressings speed epithelialization of deep partial-thickness wounds. *Wound Repair Regen.* 20(2), 236-242.
- [181] Tang, L., Sierra, J.O., Kelly, R., Kirsner, R.S., Li, J., 2012. Wool-derived keratin stimulates human keratinocyte migration and types IV and VII collagen expression. *Exp. Dermatol.* 6, 458-460.
- [182] Blanchard, C.R., Smith, R.A., Siller-Jackson, A., 1999. Keratinous protein material for wound healing applications and method. US Patent 6274163.
- [183] Van Dyke, M., Blanchard, C.R., Siller-Jackson A., 2000. Soluble keratin peptides, EP patent 1265570 B1.
- [184] Blanchard, C., Siller-Jackson, A.J., Smith, R.A., Blanchard, C.R., Timmons, S.F., 2001. Absorbent keratin wound dressing. US Patent 6270793.
- [185] Van Dyke, M., 2008. Wound healing compositions containing keratin biomaterials. EP patent 2146738 A2.
- [186] Loan, F., Cassidy, S., Marsh, C., Simcock, J., 2016. Keratin-based products for effective wound care management in superficial and partial thickness burns injuries. *Burns*, In Press.
- [187] Hammond, C., Than, M., Walker J., 2010. From the laboratory to the leg: patient's and nurses perceptions of product application using three different dressing formats. *Wound Pract. Res.* 18, 189–195.
- [188] Than, M.P., Smith, R.A., Hammond, C., Kelly, R., Marsh, C., Maderal, A.D., Kirsner, R.S., 2012. Keratin-based wound care products for treatment of resistant vascular wounds. *J. Clin. Aesthet. Dermatol.* 5(12), 31-35.
- [189] Jin, J., Limburg, S., Joshi, S.K., Landman, R., Park, M., Zhang, Q., Kim, H.T., Kuo, A.C., 2013. Peripheral nerve repair in rats using composite hydrogel-filled aligned nanofiber conduits with incorporated nerve growth factor. *Tissue Eng. Part A*, 19 (19-20), 2138-2146.
- [190] Salgado, A.J., Coutinho, O.P., Reis, R.L., 2004. Bone Tissue Engineering: state of the art and future trends, *Macromol. Biosci.* 4(8), 743-765.
- [191] Fröhlich, M., Grayson, W.L., Wan, L.Q., Marolt, D., Drobic, M., Vunjak-Novakovic, G., 2008. Tissue engineered bone grafts: biological requirements, tissue culture and clinical relevance. *Curr. Stem. Cell. Res. Ther.* 3, 254-264.
- [192] De Guzman, R.C., Saul, J.M., Ellenburg, M.D., Merrill, M.R., Coan, H.B., Smith, T.L., Van Dyke, M.E., 2013. Bone regeneration with BMP-2 delivered from keratose scaffolds. *Biomaterials* 34(6), 1644-1456.
- [193] Dias, G.J., Peplow, P.V., McLaughlin, A., Teixeira, F., Kelly, R.J., 2010. Biocompatibility and osseointegration of reconstituted keratin in an ovine model. *J. Biomed. Mater. Res. Part A* 92(2), 513-520.
- [194] Yin, X.C., Li, F.Y., He, Y.F., Wang, Y., Wang, R.M., 2013. Study on effective extraction of chicken feather keratins and their films for controlling drug release, *Biomater. Sci.* 1, 528-536.
- [195] Tomblyn, S., Pettit Kneller, E.L., Walker, S.J., Ellenburg, M.D., Kowalczewski, C.J., Van Dyke, M., Burnett, L., Saul, J.M., 2015. Keratin hydrogel carrier system for simultaneous delivery of exogenous growth factors and muscle progenitor cells. *J. Biomed. Mater. Res. B Appl. Biomater.* 104(5).
- [196] de Guzman, R.C., Rabbany S.Y., 2016. PEG-Immobilized Keratin for Protein Drug Sequestration and pH-Mediated Delivery. *J. Drug Deliv.* (2016), 1-10.
- [197] Li, Q., Zhu, L., Liu, R., Huang, D., Jin, X., Che, N., Li, Z., Qu, X., Kang, H., Huang, Y., 2012. Biological stimuli responsive drug carriers based on keratin for triggerable drug delivery, *J. Mater. Chem.* 22, 19964-19973.
- [198] Xu, H., Shi, Z., Reddy, N., Yang, Y., 2014. Intrinsically water-stable keratin nanoparticles and their in vivo biodistribution for targeted delivery. *J. Agric Food Chem.* 62(37), 9145-50.

- [199] Han, S., Ham, T.R., Haque, S., Sparks, J.L., Saul, J.M., 2015. Alkylation of human hair keratin for tunable hydrogel erosion and drug delivery in tissue engineering applications. *Acta Biomaterialia*, 23, 201–213.
- [200] Dou, Y., Zhang, B., He, M., Yin, G., Cui, Y., Savina, I.N., 2015. Keratin/polyvinyl alcohol blend films cross-linked by dialdehyde starch and their potential application for drug release. *Polymers* 7, 580-591.
- [201] Ham, T.R., Lee, R.T., Han, S., Haque, S., Vodovotz, Y., Gu, J., Burnett, L.R., Tomblynn, S., Saul, J.M., 2015. Tunable keratin hydrogels for controlled erosion and growth factor delivery, *Biomacromolecules* 17(1), 225-236.
- [202] K.W., Wang, S., Taraballi, F., 2012. Method for encapsulating living cells in a keratin-containing hydrogel. WO2013012397.
- [203] Lv, X.G, Li, Z., Chen, S.Y., Xie, M.K., Huang, J.W., Peng, X.F., Yang, R.X., Wang, H.P., Xu, Y.M., Feng, C., 2016. Structural and functional evaluation of oxygenating keratin/silk fibroin scaffold and initial assessment of their potential for urethral tissue engineering. *Biomaterials* 84, 99–110.
- [204] Noishiki, Y., Ito, H., Miyamoto, T., Inagaki, H., 1982. Application of denatured wool keratin derivatives to an antithrombogenic biomaterial: vascular graft coated with heparinized keratin derivative. *Kobunshi Ronbunshi* 39(4), 221-227.
- [205] Lund, B.S., Burleson, L., James, M., Burris, S., Link, P., Brinkley, M., 2015. Proceedings of the National Conference On Undergraduate Research (NCUR) 2015 Eastern Washington University, Spokane WA.
- [206] Shen, D., Wang, X., Zhang, L., Zhao, X., Li, J., Cheng, K., Zhang, J., 2011. The amelioration of cardiac dysfunction after myocardial infarction by the injection of keratin biomaterials derived from human hair, *Biomaterials* 32(35), 9290-9299.
- [207] Reichl, S., Borrelli, M., Geerling, G., 2011. Keratin films for ocular surface reconstruction. *Biomaterials* 32(13), 3375-3386.
- [208] Borrelli, M., Joepen, N., Reichl, S., Finis, D., Schoppe, M., Geerling, G., Schrader, S., 2015. Keratin films for ocular surface reconstruction: evaluation of biocompatibility in an in-vivo model. *Biomaterials*, 42, 112–120.
- [209] Rahmany, M.B., Hantgan, R.R., Van Dyke, M., 2013. A mechanistic investigation of the effect of keratin-based hemostatic agents on coagulation. *Biomaterials* 34(10), 2492–2500.
- [210] Li, Y., Wang, Y., Ye, J., Yuan, J., Xiao, Y., 2016. Fabrication of poly(ϵ -caprolactone)/keratin nanofibrous mats as a potential scaffold for vascular tissue engineering. *Mat. Sci. Eng. C* 68, 177–183.
- [211] Täuber, A., Müller-Goymann, C.C., 2015. In vitro permeation and penetration of ciclopirox olamine from poloxamer 407-based formulations – comparison of isolated human stratum corneum, bovine hoof plates and keratin films. *International Journal of Pharmaceutics* 89(1–2), 73–82.
- [212] <http://www.scienceimage.csiro.au/library/textile/i/7663/the-structure-of-a-merino-wool-fibre/>
- [213] Fan, J., Yu, W.D., 2011. Fractal analysis of the ortho-cortex and para-cortex of wool fiber. *Adv. Mater. Res.*, 197–198, 86–89.
- [214] Zoccola, M., Aluigi, A., Tonin, C., 2009. Characterisation of keratin biomass from butchery and wool industry wastes. *J. Mol. Struct.* 938(1–3), 35–40.
- [215] Marshall, R.C., de Boos, A., Gillespie, J.M., Marler, J.W., Reis, P.J., Rogan, I.M., White, M.A., Whiteley, K.J., Williams, V.A., 2009. An investigation of the relationship of wool textile properties to fibre protein composition, in: G.H. Crawshaw (Ed), *Proceedings of the 8th international wool textile research conference*, 1, Chistchurch, p. 259.
- [216] Okanović, D., Ristić, M., Kormanjoš, Š., Filipović, S., Živković, B., 2009. Chemical characteristics of poultry slaughterhouse byproducts. *Biotechnology in Animal Husbandry* 25 (1-2), 143-152.
- [217] Rogers, G. E., Reis, P.J., Ward, K.A., Marshall, R.C., (Eds) 1989. *The Biology of Wool and Hair*, Springer, New York.
- [218] M.A. Moharram, T.Z.A. Abdel-Rehim, S.M. Rabie, Infrared study of the effect of heat on wool *J. Appl. Polym. Sci.* 26 (1981) 921–932.
- [219] Vasconcelos, A., Gomes, A.C., Cavaco-Paulo, A., 2012. Novel silk fibroin/elastin wound dressing. *Acta Biomater.* 8, 3049-3060.
- [220] Friedman, M., 2004. Application of the ninhydrin reaction for analysis of amino acid peptides and proteins to agricultural and biomedical sciences. *J. Agric. Food Chem.* 52, 385-406
- [221] Marshall, R.C., 1981. Analysis of the proteins from single wool fibre by two-dimensional polyacrilamide gel electrophoresis. *Text. Res. J.* 51, 106-108.
- [222] EN-ISO 5079, Determination of Breaking Force and Elongation at Break of Individual Fibers, *Int. Stand. Organ.*, 1995.

- [223] O'Donnel, I.J., Thompson, E.O.P., 1964. Reduced wool IV: the isolation of a major component. *Austr J Biol Sci*; 17: 973–979.
- [224] Maclaren, J. A., Milligan, B., 1981. *Wool Science: chemical reactivity of the wool fibre*, N.S.W.: Science Press, Marrickville Australia, pp 5–6.
- [225] Horn, M.J., Jones D.B., Ringel, S.J., 1941. Isolation of a new sulfur-containing amino acid lanthionine from sodium carbonate-treated wool. *J Biol Chem* 138, 141–149.
- [226] Spei, M., Holzem, R., 1987. Thermoanalytical investigations of extended and annealed keratins. *Colloid Polym. Sci.* 265, 965–970.
- [227] Zhang, Q., Schenauer, M.R., McCarter, J.D., Flynn, G.C., 2013. IgG1 thioether bond formation in vivo. *J. Biol. Chem.* 23, 16371–16382.
- [228] Wortmann, F.J., Deutz, H., 1998. Thermal analysis of ortho- and para-cortical cells isolated. *Wool fibers, J. Appl. Polym. Sci.* 68, 1991–1995.
- [229] Vineis, C., Aluigi, A., Tonin, C., 2011. Outstanding traits and thermal behavior for the identification of speciality animal fibres. *Text. Res. J.* 81 (3), 264–272.
- [230] Anderson, H.C., Hsu, H.H.T., Raval, P., Reynold, P.R., Gurley, D.J., Aguilera, M.X., Davis, L.S., Moylan, P.E., 1998. Bone inducing agent in Saos-2 cell extracts and secretion., *Cell Mater.* 8, 89–98.
- [231] Srinivasan, B., Kumar, R., Shanmugam, K., Sivagnam, U.T., Reddy, N.P., Sehgal, P.K., 2010. J. Biomed, Porous keratin scaffold-promising biomaterial for tissue engineering and drug delivery. *J. Biomed. Mater. Res. B Appl. Biomater.* 92B, 5–12.
- [232] O'Brien, F.J., 2011. Biomaterials & scaffolds for tissue engineering, *materialstoday* 14 (3) 88–95.
- [233] <http://www.dentalgreen.it/gingistat.html>
- [234] Ayre, W.N., Denyer, S.P., Evans, S.L., 2014. Ageing and moisture uptake in polymethyl methacrylate (PMMA) bone cements. *J Mech Behav Biomed Mater.* 32(100), 76–88.
- [235] Arnold, J. C., Venditti, N.P., Prediction of the long-term creep behavior of hydroxyapatite-filled polyethylmethacrylate bone cements. *Journal of Materials Science: Materials in Medicine*, 2007, 18(9) 1849–1858.
- [236] Halley, J. L., Turner, I. G., Miles, A. W., 1995. Fracture properties of fully cured acrylic bone cement. *Journal of Materials Science: Materials In Medicine* 6, 635–638.
- [237] Ross, F.P., Christiano, A.M., 2006. Nothing but skin and bone. *J.Clin.Invest.* 116, 1140–1149.
- [238] *Bone Health and Osteoporosis: A Report of the Surgeon General.* 2004. Chapter 2, Rockville.
- [239] Fernández-Tresguerres-Hernández-Gil, I., Alobera-Gracia, M.A., del Canto-Pingarrón, M., Blanco-Jerez, L., 2006. Physiological bases of bone regeneration II. The remodeling process. *Med Oral Patol Oral Cir Bucal.* 11(E), 151–157.
- [240] Huang, H., Kamm, R.D., Lee, R.T., 2004. Cell Mechanics and Mechanotransduction: Pathways, Probes, and Physiology. *Am J Physiol Cell Physiol.* 287(1), 1–11.
- [241] Ingber D.E., 2003. Mechanobiology and diseases of mechanotransduction. *Ann Med* 35(8), 564–577.
- [242] Wolff J., 1892. *Das Gesetz der Transformation der Knochen*, Berlin: Hirschwald.
- [243] Rubin, J., Rubin, C., Jacobs C., 2006. Molecular pathways of mechanical signaling in bone. *Gene.* 367, 1–16.
- [244] Liedert, A., Kaspar, D., Blakytyn, R., Claes, L., Ignatius A., 2006. Signal transduction pathways involved in mechanotransduction in bone cells. *Biochem Biophys Res Commun.* 349(1),1–5.
- [245] http://book.myhistology.com/basic-histo/8.%20Bone_files.html
- [246] Burger, E.H., Klein-Nulend J., 1999. Mechanotransduction in bone-role of the lacuno-canalicular network. *FASEM J.* 13, 101–112.
- [247] Burger, E.H., Klein-Nulend, J., Smit, T., 2003. Strain-derived canalicular fluid flow regulates osteoclast activity in a remodeling osteon-a proposal. *J. Biomech.* 36, 1453–1459.
- [248] Zeng, Y., Cowing, S.C., Weinbaum, S., A., 1994. Fiber matrix for fluid flow and streaming potentials in the canaliculi of an osteon. *Ann Biomed Eng.* 22, 80–292.
- [249] Weinbaum, S., Cowin, S.C., Zeng, Y., 1994. A model for the extitation of osteocytes by mechanical loading-induced bone fluid shear stresses. *J. Biomech.* 27, 339–360.
- [250] Cowin, S.C., Weinbaum, S., Zeng, Y., A., 1995. A case for bone canaliculi as the anatomical site of strain generated potentials. *J. Biomech.* 28, 1281–1297.
- [251] Cowin, S.C., Weinbaum, S., 1998. Strain amplification in the bone mechanosensory system. *Am. J. Med. Csi.* 316, 184–188.
- [252] You, L., Cowin, S.C., Schaffler, M.B., Weinbaum, S., 2001. A model for strain amplification in the actin cytoskeleton of osteocytes due to fluid drag of pericellular matrix. *J. Biomech* 34, 1375–1386.
- [253] Cowin, S.C., 2004. Tissue growth and remodeling. *Annu Rev. Biomed. Eng.* 6, 77–107.

- [254] Han, Y., Cowin, S.C., Schaffler, M.B., Weinbaum, S., 2004. Mechanotransduction and strain amplification in osteocyte cell processes. *Proc. Natl. Acad. Sci. U.S.A.* 101, 16689-16694.
- [255] You, L.D., Weinbaum, S., Cowin, S.C., Schaffler, M.B., 2004. Ultrastructure of the osteocyte process and its pericellular matrix. *Anat Rec. A. Discov Mol. Cell Evol. Biol.* 278, 505-513.
- [256] Klein-Nulend, J., van der Plas, A., Semeins, C.M., Ajubi, N.E., Frangos, J.A., Nijweide, P.J., Burger, E.H., 1995. Sensitivity of osteocytes to biomechanical stress in vitro. *FASEB J*; 9, 441-445.
- [257] Smalt, R., Mitchell, F.T., Howard, R.L., Chambers, T.J., 1997. Induction of NO and prostaglandin E2 in osteoblasts by wall-shear stress but not mechanical strain. *Am J Physiol* 273, 751-758.
- [258] Saunders, M.M., You, J., Trosko, J.E., Yamasaki, H., Li, Z., Donahue, H.J., Jacobs, C.R., 2001. Gap junctions and fluid flow response in MC3T3-E1 cells. *Am J Physiol Cell Physiol* 281, pp. 1917-1925.
- [259] Ajubi, N.E., Klein-Nulend, J., Alblas, M.J., Burger, E.H., Nijweide, P.J., 1999. Signal transduction pathways involved in fluid flow-induced PGE2 production by cultured osteocytes. *Am J Physiol* 276, 171-178.
- [260] Bakker, A.D., Soejima, K., Klein-Nulend, J., Burger, E.H., 2001. The production of nitric oxide and prostaglandin E2 by primary bone cells is shear stress dependent. *J Biomech* 34, 671-677.
- [261] Bancroft, G.N., Sikavitsas, V.L., van den Dolder, J., Sheffield, T.L., Ambrose, C.G., Jansen, J.A., Mikos, A.G., 2002. Fluid flow increases mineralized matrix deposition in 3D perfusion culture of marrow stromal osteoblasts in a dose-dependent manner. *Proc Natl Acad Sci U.S.A.* 99 12600-12605.
- [262] Ingber, D.E., Cellular tensegrity: defining new rules of biological design that govern the cytoskeleton. *J Cell Sci* 1993 104 (3), 613-627.
- [263] Ingber, D.E., Dike, L., Hansen, L., Karp, S., Liley, H., Maniotis, A., McNamee, H., Mooney, D., Plopper, G., Sims, J., 1994. Cellular tensegrity: exploring how mechanical changes in the cytoskeleton regulate cell growth, migration, and tissue pattern during morphogenesis. *Int Rev Cytol* 150, 173-224.
- [264] Stamenovic, D., Fredberg, J.J., Wang, N., Butler, J.P., Ingber, D.E., 1996. A microstructural approach to cytoskeletal mechanics based on tensegrity. *J Theor Biol* 181, 125-136.
- [265] Ingber, D.E., 1997. Tensegrity: the architectural basis of cellular mechanotransduction. *Annu Rev Physiol* 59, 575-599.
- [266] Ingber, D.E., 1997. Integrins, tensegrity, and mechanotransduction. *Gravit Space Biol Bull* 10, 49-55.
- [267] Ingber, D.E., 1998. In search of cellular control: signal transduction in context. *J Cell Biochem Suppl* 30-31, 232-237.
- [268] Chen, C.S., Ingber, D.E., 1999. Tensegrity and mechanoregulation: from skeleton to cytoskeleton. *Osteoarthritis Cartilage* 7, 81-94.
- [269] Ingber, D.E., 2000. Opposing views on tensegrity as a structural framework for understanding cell mechanics. *J Appl Physiol* 89, 1663-1670.
- [270] Wang, N., Naruse, K., Stamenovic, D., Fredberg, J.J., Mijailovich, S.M., Tolic-Norrelykke, I.M., Polte, T., Mannix, R., Ingber, D.E., 2001. Mechanical behavior in living cells consistent with the tensegrity model. *Proc Natl Acad Sci U.S.A.* 98, 7765-7770.
- [271] Ingber, D.E., Tensegrity I. Cell structure and hierarchical systems biology. *J Cell Sci* 2003 116, 1157-1173.
- [272] Ingber, D.E., 2003. Tensegrity II. How structural networks influence cellular information processing networks. *J Cell Sci* 116, 1397-1408.
- [273] Ingber, D.E., 2003. Mechanosensation through integrins: cells act locally but think globally. *Proc Natl Acad Sci U.S.A.* 100, 1472-1474.
- [274] Marie, P.J., 2002. Role of N-cadherin in bone formation. *J Cell Physiol* 190, 297-305.
- [275] Pavalko, F.M., Norvell, S.M., Burr, D.B., Turner, C.H., Duncan, R.L., Bidwell, J.P., 2003. A model for mechanotransduction in bone cells: load-bearing mechanosomes. *J Cell Biochem* 88, 104-112.
- [276] Chen, N.X., Ryder, K.D., Pavalko, F.M., Turner, C.H., Burr, D.B., Qiu, J., Duncan, R.L., 2000. Ca²⁺ regulates fluid shear-induced cytoskeletal reorganization and gene expression in osteoblasts. *Am J Physiol Cell Physiol* 278, 989-997.
- [277] Korestein, R., Somjen, D., Fischler, H., Binderman, I., 1982. Capacitative pulsed electric stimulation of bone cells. Induction of cyclic-AMP changes and DNA synthesis. *Biochim Biophys Acta*, 803. 302-307.
- [278] Farndale, R.W., Murray, J.C., 1985. Pulsed electromagnetic fields promote collagen production in bone marrow fibroblast via athermal mechanism. *Calcif. Tissue Int.* 37, 178-182.

- [279] Brighton, C.T., Hozack, W.J., Brager, M.D., Windsor, R.E., Pollack, S.R., Vreslovic, E.J., Kotwick, J.E. 1985. Fracture healing in the rabbit fibula when subjected to various capacitively coupled electrical fields. *J. Orthop. Res.* 3, 331-340.
- [280] Inoue, N., Ohnishi, I., Chen, D., Deitz, L.W., Schwardt, J.D., Chao, E.Y. Effects of pulsed electromagnetic fields (PEMF) on late-phase osteotomy gap healing in a canine tibial model. *J. Orthop. Res.* 2002, 20, 110-1114.
- [281] Fredericks, D.C., Piehl, D.J., Baker, J.T., Abbott, J., Nepola, J.V., 2003. Effect of pulsed electromagnetic field stimulation on distraction osteogenesis in the rabbit tibial leg lengthening model. *J. Pediatric Orthop.* 23, 478-483.
- [282] Panagopoulos, D.J., Karabarbounis, A., Margaritis, L.H., 2002. Mechanism for action of electromagnetic fields on cells. *Biochem Biophys Res Commun.* 298, 95-102.
- [283] Aaron, R.K., Boyan, B.D., Ciombor, D.M., Schwartz, Z., Simon, B.J., 2004. Stimulation of growth factor synthesis by electric and electromagnetic fields, *Clin Orthop. Relat. Res* 419, 30-37.
- [284] Fitzsimmons, R.J., Ryaby, J.T., Magee, F.P., Baylink, D.J. 1994. Combined magnetic fields increased net calcium flux in bone cells. *Calcif. Tissue Int* 55, 376-380.
- [285] Lorich, D.G., Brighton, C.T., Grupta, R., Corsetti, J.R., Levine, S.E., Gelb, I.D., Seldes, R., Pollack, S.R., 1998. Biochemical pathway mediating the response of bone cells to capacitive coupling. *Clin Orthop Relat Res* 350, 246-256.
- [286] Zhuang, H., Wans, W., Seldes, R.M., Tahernia, A.D, Fan, H., Brighton, C.T., 1997. Electrical stimulation induces the level of TGF- β -1 mRNA in osteoblastic cells by a mechanism involving calcium/calmodulin pathway. *Biochem Biophys Res. Commun* 237, 225-229.
- [287] Brighton, C.T., Wang, W., Seldes, R., Zhang, G, Pollack, S.R., Signal transduction in electrically stimulates bone cells, *J. Bone Joint Surg, Am.* 2001, 83-a, 1514-1523.
- [288] Bodamyali, T., Bhatt, B., Hughes, F.J., Winrow, V.R., Kanczler, J.M., Simon, B., Abbott, J., Blke, D.R., Stevens, C.R., 1998. Pulsed electromagnetic fields simultaneously induce osteogenesis and upregulate transcription of bone morphogenetic proteins 2 and in rat osteoblasts in vitro. *Biochem Biophys. Res. Commun.*, 250, 458-461.
- [289] Aaron, R.L., Ciombor, D.M., Keeping, H., Keeping, H., Wang, S., Capuano, A., Polk, C., 1999. Power frequency fields promote cell differentiation coincident with an increase in transforming growth factor- β -1 expression, *Bioelectromagnetics* 20, 453-458.
- [290] Lohmann, C.H., Schwartz, Z., Liu Y., Guerkov, H., Dean, D.D., Simon, B., Boyan, B.D. 2000. Pulsed electromagnetic field stimulation of MG63 osteoblast-like cells affects differentiation and local factor production. *J. Orthop Res.* 18, 637-646.
- [291] Guerkov, H.H., Lohmann, C.H., Liu, Y, Deann, D.D., Simon, B.J., Heckman, J.D., Schwartz, Z., Boyan, B.D., 2001. Pulsed electromagnetic fields increase growth factor release by nonunion cells. *Clin. Orthop. Relat. Res.*, 265-279.
- [292] Aaron, R.K., Wang, S., Ciombor, D.M., 2002. Upregulation of basal TGF β 1 levels by EFM coincident with chondrogenesis-implications for skeletal repair and tissue engineering. *J. Orthop. Res.* 20, 233-240.
- [293] Lohmann, C.H., Schwartz, Z., Liu, Y., Li, Z., Simon, B.J., Sylvia, V.L., Dean, D.D., Bonewald, L.F., Donahue, H.J., Boyan, B.D., 2003. Pulsed electromagnetic fields affect phenotype and connexin 43 protein expression in MLO-Y4 osteocyte-like cells ROS 17/2.8 osteoblast-like cells. *J. Orthop. Res.* 21(2), 326-334.
- [294] Mammoto, T., Ingber, D.E., 2010. Mechanical control of tissue and organ development. *Development* 137, 1407-1420.
- [295] Mognaschi, M.E., Di Barba, P., Magenes, G., Lenzi, A., Naro, F., Faro, F., Fassina, L., 2014. Field models and numerical dosimetry inside an extremely-low-frequency electromagnetic bioreactor: the theoretical link between the electromagnetically induced mechanical forces and the biological mechanisms of the cell tensegrity SpringerPlus, 3(473), 1-12.
- [296] Feynman, R.P., Leighton, R.B., Sands, M. 1964. *The Feynman lectures on physics.* Addison-Wesley, Reading.
- [297] Diz-Munoz, A., Krieg, M., Bergert, M., Ibarlucea-Benitez, I., Muller, D.J., Paluch, E., Heisenberg, C.P., (2010). Control of directed cell migration in vivo by membrane-to-cortex attachment. *PLoS Biol* 8(11).
- [298] Fassina, L., Visai, L., Benazzo, F., Benedetti, L., Calligaro, A., Cusella De Angelis, M.G., Farina A., Maliardi, V., Magenes, G., 2006. Effects of electromagnetic stimulation on calcified matrix production by SAOS-2 cells over a polyurethane porous scaffold. *Tissue Eng* 12, 1985-1999.
- [299] Fassina, L., Visai, L., Cusella De Angelis, M.G., Benazzo, F., Magenes, G. 2007. Surface modification of a porous polyurethane through a culture of human osteoblasts and an electromagnetic bioreactor. *Technol Health Care* 15, 33-45.

- [300] Fassina, L., Saino, E., Visai, L., Silvani, G., Cusella De Angelis, M.G., Mazzini, G., Benazzo, F., Magenes, G. (2008). Electromagnetic enhancement of a culture of human SAOS-2 osteoblasts seeded onto titanium fiber-mesh scaffolds. *J Biomed Mater Res Part A* 87, 750–759.
- [301] Fassina, L., Saino, E., Sbarra, M.S., Visai, L., Cusella De Angelis, M.G., Mazzini, G., Benazzo, F., Magenes, G., 2009. Ultrasonic and electromagnetic enhancement of a culture of human SAOS-2 osteoblasts seeded onto a titanium plasma-spray surface. *Tissue Eng Part C Methods* 15, 233–242.
- [302] Fassina, L., Saino, E., Sbarra, M.S., Visai, L., Cusella De Angelis, M.G., Magenes, G., Benazzo, F. 2010. In vitro electromagnetically stimulated SAOS-2 osteoblasts inside porous hydroxyapatite. *J Biomed Mater Res Part A* 9, 1272–1279.
- [303] Osera, C., Fassina, L., Amadio, M., Venturini, L., Buoso, E., Magenes G., Govoni, S., Ricevuti, G., Pascale, A. 2011. Cytoprotective response induced by electromagnetic stimulation on SH-SY5Y human neuroblastoma cell line. *Tissue Eng Part A* 17, 2573–2582.
- [304] Ceccarelli, G., Bloise, N., Mantelli, M., Gastaldi, G., Fassina, L., Cusella De Angelis, M.G., Ferrari, D., Imbriani, M., Visai, L. 2013. A comparative analysis of the in vitro effects of pulsed electromagnetic field treatment on osteogenic differentiation of two different mesenchymal cell lineages. *Biores OpenAccess* 2, 283–294.
- [305] Saino, E., Fassina, L., Van Vlierberghe, S., Avanzini, M.A., Dubruel, P., Magenes, G., Visai, L., Benazzo, F. 2011. Effects of electromagnetic stimulation on osteogenic differentiation of human mesenchymal stromal cells seeded onto gelatine cryogel. *Int J Immunopathol Pharmacol* 24, 1–6.
- [306] Saino, E., Grandi, S., Quartarone, E., Maliardi, V., Galli, D., Bloise, N., Fassina, L., De Angelis, M.G., Mustarelli, P., Imbriani, M., Visai, L., 2011 In vitro calcified matrix deposition by human osteoblasts onto a zinc-containing bioactive glass. *Eur. Cell. Mater.* 21(14), 59–72.
- [307] Grassi, C., D'Ascenzo, M., Torsello, A., Martinotti, G., Wolf, F.I., Cittadini, A., Azzena G.B., 2004. *Cell Calcium*, 35, 307–315.
- [308] Buckwalter, J.A., Glimcher, M.J., Cooper R.R., Recker, R., 1996. Bone biology. I: structure, blood supply, cells, matrix, and mineralization. *Instructional Course Lectures*. 45:371–386.
- [309] Downey, P.A., Siegel, M.I., 2006. Bone biology and the clinical implications for osteoporosis. *Physical Therapy* 86(1):77–91.
- [310] Datta, H.K., Ng, W.F., Walker, J.A., Tuck, S.P., Varanasi, S.S. 2008. The cell biology of bone metabolism. *Journal of Clinical Pathology*. 61(5), 577–587.
- [311] Glimcher, M.J., 1998. The nature of the mineral phase in bone, in: Glimcher M. J., editor. *Metabolic Bone Disease*. San Diego, Calif, USA Academic Press; pp. 23–50.
- [312] Hoemann, C.D., El-Gabalawy, H., McKee, M.D., 2009. In vitro osteogenesis assays: influence of the primary cell source on alkaline phosphatase activity and mineralization. *Pathol Biol* 57, 318–323.
- [313] Huang, Z., Nelson, E.R., Smith, R.L., Goodman, S.B. 2007. The sequential expression profiles of growth factors from osteoprogenitors [correction of osteoprogenitors] to osteoblasts in vitro. *Tissue Eng* 13, 2311–2320.
- [314] Sert, C., Mustafa, D., Duz, M.Z., Aksen, F., Kaya, A., 2002. The preventive effect on bone loss of 50-Hz, 1-mT electromagnetic field in ovariectomized rats. *J Bone Miner Metab* 20, 345–349.
- [315] Torricelli, P., Fini, M., Giavaresi, G., Botter, R., Beruto, D., Giardino, R., 2003. Biomimetic PMMA-based bone substitutes: a comparative *in vitro* evaluation of the effects of pulsed electromagnetic field exposure. *J Biomed Mater Res* 64,182–188.
- [316] Kasugai, S., Nagata, T., Sodek, J., 1992. Temporal studies on the tissue compartmentalization of bone sialoprotein (BSP), osteopontin (OPN), and SPARC protein during bone formation *in vitro*. *J Cell Physiol* 152, 467–477.
- [317] Luan, Y., Praul, C.A., Gay, C.V., 2000. Confocal imaging and timing of secretion of matrix proteins by osteoblasts derived from avian long bone. *Comp Biochem Physiol A Mol Integ Physiol* 126, 213–221.
- [318] Gericke, A., Qin, C., Spevak, L., Fujimoto, Y., Butler, W.T., Sorensen, E.S., Boskey, A.L., 2005 Importance of phosphorylation for osteopontin regulation of biomineralization. *Calcif Tissue Int.* 77(1), 45–54.
- [319] Butler, W.T., 1989. The nature and significance of osteopontin. *Connect Tissue Res* 23, 123–136.
- [320] Butler, W.T., 1995. Structural and functional domains of osteopontin. *Ann N.Y. Acad Sci* 760, 6–11.
- [321] Martino, C.F., Belchenko, D., Ferguson, V., Nielsen-Preiss, S., Qi, H.J. 2008. The effects of pulsed electromagnetic fields on the cellular activity of SaOS-2 cells *Bioelectromagnetics*. 29, 125–132.
- [322] Aubin, J.E., 2001. Regulation of osteoblast formation and function. *Rev Endocr Metab Disord* 2: 81–94.

- [323] Quarles, L.D., Yohay, D.A., Lever, L.W., Caton, R., Wenstrup, R.J. 1992. Distinct proliferative and differentiated stages of murine MC3T3-E1 cells in culture: An in vitro model of osteoblast development. *J Bone Miner Res* 7, 683-692.
- [324] Bernardo, M.E., Zaffaroni, N., Novara, F., Cometa, A.M., Avanzini, M.A., Moretta, A., Montagna, D., Maccario, R., Villa, R., Daidone, M.G., Zuffardi, O., Locatelli, F., Human bone marrow derived mesenchymal stem cells do not undergo transformation after long-term in vitro culture and do not exhibit telomere maintenance mechanisms. *Cancer Res.* 2007; 67:9142–9160.